

**LABORATORY ASSESSMENT OF STRENGTHS AND  
DEFORMABILITY OF ROCK MASS**

**Saisuree Thaweeboon**



**A Thesis Submitted in Partial Fulfillment of the Requirements for the  
Degree of Doctor of Philosophy of Engineering in Geotechnology**

**Suranaree University of Technology**

**Academic Year 2014**

การศึกษาจำกัดและการเปลี่ยนแปลงรูปร่างของมวลหิน  
ในห้องปฏิบัติการ



นางสาวสายสุรีย์ ทวีบุญ

วิทยานิพนธ์นี้เป็นส่วนหนึ่งของการศึกษาตามหลักสูตรปริญญาวิศวกรรมศาสตรดุษฎีบัณฑิต  
สาขาวิชาเทคโนโลยีธรณี  
มหาวิทยาลัยเทคโนโลยีสุรนารี  
ปีการศึกษา 2557

**LABORATORY ASSESSMENT OF STRENGTHS AND  
DEFORMABILITY OF ROCK MASS**

Suranaree University of Technology has approved this thesis submitted in  
partial fulfillment of the requirements for the Degree of Doctor of Philosophy.

Thesis Examining Committee

---

(Dr. Decho Phueakphum)

Chairperson

---

(Prof. Dr. Kittitep Fuenkajorn)

Member (Thesis Advisor)

---

(Dr. Prachya Tepnarong)

Member

---

(Dr. Anisong Chitnarin)

Member

---

(Assoc. Prof. Ladda Wannakao)

Member

---

(Prof. Dr. Sukit Limpijumnong)

Vice Rector for Academic Affairs  
and Innovation

---

(Assoc. Prof. Flt. Lt. Dr. Kontorn Chamniprasart)

Dean of Institute of Engineering

สายสุรีย์ ทวีบุญ : การศึกษากำลังกดและการเปลี่ยนแปลงรูปร่างของมวลหินใน  
ห้องปฏิบัติการ (LABORATORY ASSESSMENT OF STRENGTHS AND  
DEFORMABILITY OF ROCK MASS) อาจารย์ที่ปรึกษา : ศาสตราจารย์ ดร.กิตติเทพ  
เฟื่องขจร, 118 หน้า.

วัตถุประสงค์ของการศึกษานี้คือเพื่อหาค่ากำลังกดและการเปลี่ยนแปลงรูปร่างของตัวอย่าง  
หินที่มีรอยแตกในห้องปฏิบัติการ สักยภาพของเกณฑ์การแตกและการเปลี่ยนแปลงรูปร่างถูก  
ประเมินโดยนำมาเปรียบเทียบกับผลการทดสอบ ผลการทดสอบระบุว่า เมื่อจำนวนรอยแตกและขนาด  
ของรอยแตกเพิ่มขึ้น ส่งผลให้ค่ากำลังกดมีค่าลดลง และเมื่อความดันล้อมรอบเพิ่มขึ้น จะทำให้ค่า  
กำลังกดเพิ่มขึ้นแบบเส้นโค้ง โดยเฉพาะอย่างยิ่งสำหรับตัวอย่างหินที่มีสามชุกรอยแตก สำหรับ  
ตัวอย่างหินหนึ่งชุกรอยแตกที่ขนานกับแกนหลัก จะมีค่ากำลังกดสูงกว่าตัวอย่างหินที่มีรอยแตกตั้ง  
ฉากกับแกนหลัก ค่ากำลังกดจะมีค่าต่ำสุดเมื่อรอยแตกทำมุม 45 องศากับแกนหลัก เกณฑ์ของ  
Hoek-Brown, Sheorey, Yudhbir และ Ramamurthy-Arora สามารถนำมาประเมินค่ากำลังกดกับผล  
การทดสอบได้เป็นอย่างดีเหมือนกัน โดยมีค่าสัมประสิทธิ์ความสอดคล้องมากกว่า 0.9 เกณฑ์ของ  
Hoek-Brown ให้ค่าตัวแปร  $s$  ลดลงอย่างมาก เมื่อความถี่ของรอยแตกมีค่าเพิ่มขึ้น แต่ค่าตัวแปร  $m$  จะ  
มีการเปลี่ยนแปลงเพียงเล็กน้อยเท่านั้น เมื่อพิจารณาสัมประสิทธิ์การเปลี่ยนแปลงรูปร่างพบว่า  
ตัวอย่างหินที่มีหนึ่งชุกรอยแตกที่ขนานกับแกนหลักจะมีสัมประสิทธิ์การเปลี่ยนแปลงรูปร่างสูงกว่า  
ตัวอย่างหินที่มีรอยแตกตั้งฉากกับแกนหลัก ตัวอย่างหินที่มีสามชุกรอยแตกมีสัมประสิทธิ์การ  
เปลี่ยนแปลงรูปร่างเหมือนกันในทุกทิศทาง เมื่อจำนวนรอยแตกเพิ่มขึ้นส่งผลให้สัมประสิทธิ์การ  
เปลี่ยนแปลงรูปร่างจะลดลง และมีแนวโน้มเพิ่มขึ้นเมื่อความดันล้อมรอบสูงขึ้น จากการศึกษาใน  
ครั้งนี้ได้เสนอสูตรเพื่อคำนวณสัมประสิทธิ์การเปลี่ยนแปลงรูปร่างที่พิจารณาจากทิศทางการวางตัว  
ของรอยแตก ซึ่งผลที่ได้สอดคล้องกับผลการทดสอบได้เป็นอย่างดี

สาขาวิชา เทคโนโลยีธรณี  
ปีการศึกษา 2557

ลายมือชื่อนักศึกษา \_\_\_\_\_  
ลายมือชื่ออาจารย์ที่ปรึกษา \_\_\_\_\_

SAISUREE THAWEEBOON : LABORATORY ASSESSMENT OF  
STRENGTHS AND DEFORMABILITY OF ROCK MASS. THESIS  
ADVISOR : PROF. KITTITEP FUENKAJORN, Ph.D., P.E., 118 PP.

TRIAXIAL COMPRESSION/ROCK MASS /DEFORMATION  
MODULUS/STRENGTH

The objective of this study is to determine rock mass strength and deformability in the laboratory by simulating joints in sandstone specimens. The predictive capability of some commonly used strength and deformability criteria is assessed. Results indicate that the larger numbers of the joint frequencies and joint sets show the lower strengths. This is true for all confining pressures. The increase of the rock mass model strength with the confining pressure tends to be non-linear, particularly for the three joint sets specimens. For single joint set specimens, the strength of the specimens with joints normal to  $\sigma_1$  axis always yields greater strength than those with joints parallel to  $\sigma_1$  axis. The lowest strengths are obtained when the joint planes make angles  $45^\circ$  with the major principal axis. The Hoek-Brown, Sheorey, Yudhbir and Ramamurthy-Arora strength criteria give equally good correlation with the test results, showing  $R^2$  greater than 0.9. The parameter  $s$  of the Hoek-Brown criterion is highly sensitive to the joint frequency while the parameter  $m$  tends to be insensitive to the joint frequency. For one joint set specimens the deformation moduli that are parallel to the joint planes show highest values compared to those that are normal to the joints. For three joint set specimens, the deformation moduli are similar for all principal directions. The deformation modulus decreases

with increasing joint frequency, and tends to increase with the confining pressure. Goodman (1970) equation is modified here to determine the deformation modulus along three principal directions. The proposed equation agrees well with the test results.



School of Geotechnology

Academic Year 2014

Student's Signature \_\_\_\_\_

Advisor's Signature \_\_\_\_\_

## **ACKNOWLEDGMENTS**

I wish to acknowledge the funding supported by Suranaree University of Technology (SUT).

I would like to express my sincere thanks to Prof. Dr. Kittitep Fuenkajorn for his valuable guidance and efficient supervision. I appreciate his strong support, encouragement, suggestions and comments during the research period. My heartiness thanks to Assoc. Prof. Ladda Wannakao, Dr. Prachya Tepnarong, Dr. Anisong Chitnarin, and Dr. Decho Phueakphum for their constructive advice, valuable suggestions and comments on my research works as thesis committee members. Grateful thanks are given to all staffs of Geomechanics Research Unit, Institute of Engineering who supported my work.

Finally, I would like to thank beloved parents for their love, support and encouragement.

Saisuree Thaweeboon

# TABLE OF CONTENTS

	<b>Page</b>
ABSTRACT (THAI) .....	I
ABSTRACT (ENGLISH).....	II
ACKNOWLEDGEMENTS.....	IV
TABLE OF CONTENTS.....	V
LIST OF TABLES.....	VIII
LIST OF FIGURES .....	X
SYMBOLS AND ABBREVIATIONS.....	XVI
<b>CHAPTER</b>	
<b>I    INTRODUCTION</b> .....	<b>1</b>
1.1 Background and rationale .....	1
1.2 Research objectives.....	2
1.3 Scope and limitations.....	2
1.4 Research methodology.....	3
1.4.1 Literature review.....	3
1.4.2 Sample preparation.....	3
1.4.3 Laboratory testing.....	5
1.4.4 Strength criteria .....	5
1.4.5 Deformation modulus .....	6
1.4.6 Discussions, conclusions and thesis writing.....	6

## TABLE OF CONTENTS (Continued)

	<b>Page</b>
1.5 Thesis contents.....	6
<b>II LITERATURE REVIEW .....</b>	<b>7</b>
2.1 Introduction.....	7
2.2 Effects of joint set on rock mass .....	7
2.3 Effects of orientation.....	9
2.4 Rock mass strength criteria.....	13
2.5 Strength comparison .....	24
2.6 Deformation modulus of rock mass .....	32
2.7 Conclusion of review .....	41
<b>III SAMPLE PREPARATION .....</b>	<b>43</b>
<b>IV TEST METHOD.....</b>	<b>46</b>
4.1 Introduction.....	46
4.2 True triaxial loading device .....	46
4.3 Test procedure.....	48
<b>V TEST RESULTS.....</b>	<b>50</b>
5.1 Introduction.....	50
5.2 Post-test observations.....	50
5.3 Stress-strain curves .....	53
5.4 Strength results.....	55
<b>VI STRENGTH CRITERIA .....</b>	<b>67</b>

## TABLE OF CONTENTS (Continued)

	<b>Page</b>
6.1 Introduction.....	67
6.2 Strength results .....	67
6.3 Strength criteria .....	68
<b>VII DEFORMATION MODULUS .....</b>	<b>73</b>
7.1 Introduction.....	73
7.2 Deformation modulus .....	73
7.3 Deformability criteria .....	76
7.4 Modified Goodman’s equation .....	79
<b>VIII DISCUSSIONS AND CONCLUSIONS .....</b>	<b>81</b>
8.1 Discussions and conclusions.....	81
8.2 Recommendations for future studies .....	84
REFERENCES .....	85
<b>APPENDICES</b>	
APPENDIX A SAMPLE DIMENSIONS .....	90
APPENDIX B STRESS-STRAIN CURVES.....	101
BIOGRAPHY .....	118

## LIST OF TABLES

Table	Page
2.1 Joint inclination factor $n$ for different joint orientation angles $\beta$ .....	9
2.2 Suggested parameter $r$ of different ranges of $\sigma_{ci}$ .....	9
2.3 Results of statistical analyses involving non-linear least squares estimation method.....	12
2.4 The range of the parameter ( $k_\beta$ ) for the rocks tested has been analytically investigated by carrying out triaxial tests, in different orientations of the foliation plane.....	18
2.5 Expressions of the uniaxial compressive strength of the rock mass for the elected estimation methods.....	26
2.6 Methods with reasonable agreement with the measured strengths.....	27
2.7 Physical properties of welded-tuff (Ohya-stone).....	33
2.8 Comparison of $E_j$ values obtained from different approaches.....	40
3.1 Specimens prepared for triaxial compression test with confining pressures of 0, 1, 3, 5, 7 and 12 MPa.....	44
5.1 Strength results of case A1.....	55
5.2 Strength results of case A2.....	56
5.3 Strength results of case B1.....	56
5.4 Strength results of case B2.....	57

## LIST OF TABLES (Continued)

<b>Table</b>	<b>Page</b>
5.5 Strength results of case C .....	57
5.6 Octahedral shear stresses at failure (Case A1) .....	61
5.7 Octahedral shear stresses at failure (Case A2) .....	62
5.8 Octahedral shear stresses at failure (Case B1) .....	63
5.9 Octahedral shear stresses at failure (Case B2) .....	64
5.10 Octahedral shear stresses at failure (Case C) .....	65
6.1 Strength criteria and their constants calibrated from the test data .....	70
7.1 Parameter N defined for modified Goodman's equation .....	79
7.2 Coefficient of correlation of each criterion .....	80
A.1 Intact rock specimens .....	91
A.2 One joint set specimens .....	91
A.3 Single rough joint specimens .....	96
A.4 Three joint sets specimens .....	98

## LIST OF FIGURES

Figure	Page
1.1 Research methodology.....	4
2.1 Two types of rock mass model: type A with two joint sets (left); and type B with three joint sets (right).....	8
2.2 Anisotropic strength of rock masses with different dip angle: (a) type A; and (b) type B.....	8
2.3 Types of joints studied.....	10
2.4 Variation of the normalized $m_i$ parameter with the orientation angle for all sedimentary rock type considered.....	12
2.5 Joint systems adopted in the test specimens by some researchers.....	14
2.6 Relationship between compressive strength of jointed specimens and joint factor.....	15
2.7 Plot of predicted uniaxial compressive strength, $\sigma_{c\beta\text{-crit}}$ , against that determined in the laboratory, $\sigma_{c\beta\text{-lab}}$ for tested specimens.....	19
2.8 Plot of proposed criterion for types of rocks.....	23
2.9 Comparison between predicted and measured strength of marble, quartzite, granite and tuff.....	23
2.10 Orientation angles of tested slate specimens.....	29

## LIST OF FIGURES (Continued)

Figure	Page
2.11	Experimental and predicted curves of uniaxial compressive strength of slates.....30
2.12	Variation of strengths versus orientation angles .....30
2.13	Comparison between predicted and experimental strength at $\sigma_3 = 3$ MPa.....31
2.14	Comparison between predicted and experimental strength at $\sigma_3 = 5$ MPa.....31
2.15	Comparison between predicted and experimental strength at $\sigma_3 = 10$ .....32
2.16	Model of a jointed rock mass subjected to three principal stresses .....34
2.17	Mechanical model for jointed rock mass with two sets of joints.....34
2.18	Loading system for jointed rock mass model, plan view.....35
2.19	Influence of joint sets on the modulus of rock masses .....36
2.20	Relationship between $E_{tj}/E_{ti}$ and joint factor for jointed specimens .....37
2.21	(a) Complete set-up of true-triaxial system (b) Schematic diagram for set-up of true-triaxial system.....39
2.22	Prediction of modulus at different confining pressures using Janbu's coefficients approach.....40
3.1	Line load applied to obtain tension-induced fracture in specimen.....45
4.1	True triaxial load frame used in this study.....46

## LIST OF FIGURES (Continued)

Figure	Page
4.2 Two main parts of true triaxial load frame .....	47
4.3 Sample preparation before installed into the load frame .....	48
5.1 Some post-test specimens of case A1. Numbers in brackets indicate $[\sigma_1, \sigma_3, \sigma_3]$ at failure in MPa .....	51
5.2 Some post-test specimens of case A2. Numbers in brackets indicate $[\sigma_1, \sigma_3, \sigma_3]$ at failure in MPa .....	52
5.3 Some post-test specimens of case B1. Numbers in brackets indicate $[\sigma_1, \sigma_3, \sigma_3]$ at failure in MPa .....	53
5.4 Some post-test specimens of case B2. Numbers in brackets indicate $[\sigma_1, \sigma_3, \sigma_3]$ at failure in MPa .....	54
5.5 Some post-test specimens of case C. Numbers in brackets indicate $[\sigma_1, \sigma_3, \sigma_3]$ at failure in MPa .....	54
5.6 Major principal stresses at failure as a function of confining pressure for various joint orientation (case A1) .....	58
5.7 Major principal stresses at failure are compared between smooth and rough surface at different orientation (case A2) .....	58
5.8 Major principal stresses at failure as a function of confining pressure for case B1(left) and B2 (right) .....	59
5.9 Major principal stresses at failure as a function of confining pressure for case C .....	59

## LIST OF FIGURES (Continued)

Figure	Page
5.10 Major principal stresses at failure as a function of confining pressure for various joint orientation (case A1).....	60
6.1 Test data (points) and curve fits of four strength criteria.....	71
6.2 Hoek-Brown parameters $m$ and $s$ as a function of joint frequency.....	71
6.3 Uniaxial compressive strengths of rock mass model ( $\sigma_{cm}$ ) with three joint sets, $\sigma_{cm}$ calculated from Sheorey and Ramamurthy-Arora criteria as a function of joint frequency.....	72
7.1 Deformation moduli parallel joint plane as a function those normal to joint plane.....	74
7.2 Deformation moduli calculated along the intermediate and minor principal axes as a function of the major principal axis.....	75
7.3 Deformation modulus as a function of confining pressure.....	75
7.4 Poisson's ratio values as a function of joint frequency for all cases.....	76
7.5 Comparisons between the test data (points) and predictions (lines).....	78
7.6 Comparisons between the test data (points) and modified Goodman equation (lines).....	80
B.1 Stress-strain curves for intact specimens. Numbers in brackets indicate $[\sigma_1, \sigma_3, \sigma_3]$ at failure in MPa.....	102
B.2 Stress-strain curves of 1 joint per set specimens for case B1. Numbers in brackets indicate $[\sigma_1, \sigma_3, \sigma_3]$ at failure in MPa.....	103

## LIST OF FIGURES (Continued)

<b>Figure</b>	<b>Page</b>
B.3	Stress-strain curves of 2 joints per set specimens for case B1. Numbers in brackets indicate $[\sigma_1, \sigma_3, \sigma_3]$ at failure in MPa.....
	104
B.4	Stress-strain curves of 3 joints per set specimens for case B1. Numbers in brackets indicate $[\sigma_1, \sigma_3, \sigma_3]$ at failure in MPa.....
	105
B.5	Stress-strain curves of 4 joints per set specimens for case B1. Numbers in brackets indicate $[\sigma_1, \sigma_3, \sigma_3]$ at failure in MPa.....
	106
B.6	Stress-strain curves of 1 joint per set specimens for case B2. Numbers in brackets indicate $[\sigma_1, \sigma_3, \sigma_3]$ at failure in MPa.....
	107
B.7	Stress-strain curves of 2 joints per set specimens for case B2. Numbers in brackets indicate $[\sigma_1, \sigma_3, \sigma_3]$ at failure in MPa.....
	108
B.8	Stress-strain curves of 3 joints per set specimens for case B2. Numbers in brackets indicate $[\sigma_1, \sigma_3, \sigma_3]$ at failure in MPa.....
	109
B.9	Stress-strain curves of 4 joints per set specimens for case B2. Numbers in brackets indicate $[\sigma_1, \sigma_3, \sigma_3]$ at failure in MPa.....
	110
B.10	Stress-strain curves of 1 joint per set specimens for case C. Numbers in brackets indicate $[\sigma_1, \sigma_3, \sigma_3]$ at failure in MPa.....
	111
B.11	Stress-strain curves of 2 joints per set specimens for case C. Numbers in brackets indicate $[\sigma_1, \sigma_3, \sigma_3]$ at failure in MPa.....
	112
B.12	Stress-strain curves of 3 joints per set specimens for case C. Numbers in brackets indicate $[\sigma_1, \sigma_3, \sigma_3]$ at failure in MPa.....
	113

## LIST OF FIGURES (Continued)

Figure	Page
B.13 Stress-strain curves of 4 joints per set specimens for case C. Numbers in brackets indicate $[\sigma_1, \sigma_3, \sigma_3]$ at failure in MPa.....	114
B.14 Stress-strain curves of 5 joints per set specimens for case C. Numbers in brackets indicate $[\sigma_1, \sigma_3, \sigma_3]$ at failure in MPa.....	115
B.15 Stress-strain curves for case A1 with joints parallel to the major principal stress. Numbers in brackets indicate $[\sigma_1, \sigma_3, \sigma_3]$ at failure in MPa.....	116
B.16 Stress-strain curves for case A2 with joints normal to the major principal stress. Numbers in brackets indicate $[\sigma_1, \sigma_3, \sigma_3]$ at failure in MPa.....	117

## SYMBOLS AND ABBREVIATIONS

$\tau_{\text{oct,f}}$	=	Octahedral shear stresses at failure
$\sigma_1$	=	Compressive strength at failure
$\sigma_2$	=	Intermediate stress
$\sigma_3$	=	Minor principal stress
$\sigma_m$	=	Mean stress
$\sigma_c$	=	Uniaxial compressive strength of intact rock
$\sigma_{\text{cm}}$	=	Uniaxial compressive strength of rock mass
$\sigma_{\text{tm}}$	=	Uniaxial tensile strength of rock mass
$\epsilon_1$	=	Major principal strains
$\epsilon_2$	=	Intermediate principal strains
$\epsilon_3$	=	Minor principal strains
$\nu$	=	Poisson's ratio
$E_1$	=	Deformation modulus along the major directions.
$E_2$	=	Deformation modulus along the intermediate directions.
$E_3$	=	Deformation modulus along the miner directions.
$m$	=	Empirical constant for equation (6.1)
$s$	=	Empirical constant for equation (6.1)
$b_m$	=	Empirical constant for equation (6.2)
$A$	=	Empirical constant for equation (6.3)
$B$	=	Empirical constant for equation (6.3)

**SYMBOLS AND ABBREVIATIONS (Continued)**

$\alpha$	=	Empirical constant for equation (6.3)
B	=	Empirical constant for equation (6.4)
$\alpha$	=	Empirical constant for equation (6.4)
$E_r$	=	Empirical constant for equation (7.4)
$k_n$	=	Empirical constant for equation (7.4)
s	=	Empirical constant for equation (7.4)
$E_n$	=	Empirical constant for equation (7.4)
$E_t$	=	Empirical constant for equation (7.5)
$E_c$	=	Empirical constant for equation (7.5)
$\theta_1$	=	Empirical constant for equation (7.5)
$\theta_2$	=	Empirical constant for equation (7.5)
$L_1$	=	Empirical constant for equation (7.5)
$L_2$	=	Empirical constant for equation (7.5)
$k_{s1}$	=	Empirical constant for equation (7.5)
$k_{s2}$	=	Empirical constant for equation (7.5)
$k_{n1}$	=	Empirical constant for equation (7.5)
$k_{n2}$	=	Empirical constant for equation (7.5)
$E_{tj}$	=	Empirical constant for equation (7.6)
$E_{ti}$	=	Empirical constant for equation (7.6)
$J_f$	=	Empirical constant for equation (7.6)
$J_n$	=	Empirical constant for equation (7.7)
n	=	Empirical constant for equation (7.7)

**SYMBOLS AND ABBREVIATIONS (Continued)**

$r$	=	Empirical constant for equation (7.7)
$E_m$	=	Empirical constant for equation (7.8)
$N$	=	Empirical constant for equation (7.8)
$k_n$	=	Empirical constant for equation (7.8)
$s$	=	Empirical constant for equation (7.8)
$E_i$	=	Empirical constant for equation (7.8)



# CHAPTER I

## INTRODUCTION

### 1.1 Background and rationale

The reliable strength estimation of a jointed rock mass is necessary to develop safe and economical designs for tunnels, open pits, dam foundations and underground chambers. Rock mass is an inhomogeneous and anisotropic material with complex behavior, which contains random planes of discontinuities. The effects of joints on the compressive strength and elastic modulus of rock mass have long been recognized. One of the most common ways of estimating the rock mass strength is by using a failure criterion. Several researchers have proposed rock mass strength criteria based on laboratory testing (Ramamurthy and Arora, 1994; Colak and Unlu, 2004; Saroglou and Tsiambaos, 2008; Rafiai, 2011; Singh and Singh, 2012), case studies (Sheorey et al., 1989) and numerical analyses (Halakatevakis and Sofianos, 2010) to determine the effects of joint frequency, joint orientation and joint set number on rock mass strengths. It has been found that compressive strength of rock mass decreases with increasing joint frequency (Ramamurthy and Arora, 1994) and joint set number (Yang et al., 1998). The effect of joint on strength depends on the orientation. The lower strengths are obtained when the joint planes make angles between  $30^\circ$ -  $40^\circ$  with the major principal stress (Ramamurthy and Arora, 1994; Colak and Unlu, 2004; Goshtasbi et al., 2006). The existing strength criteria for rock mass have been verified by comparing with the actual in-situ conditions (Edelbro,

2004). Even though several rock mass strength criteria have been proposed, verification of their accuracy and limitations under large confinements has rarely been attempted.

## **1.2 Research objectives**

The objective of this study is to determine rock mass strength and deformability in the laboratory by simulating joints in sandstone specimens with one and three joint sets under various confining pressures and joint frequencies. The results are used to assess the predictive capability of the strength criteria developed by Hoek and Brown (1980), Ramamurthy and Arora (1994), Yudhbir et al. (1983) and Sheorey et al. (1989). Empirical criteria developed by Goodman (1970), Yoshinaka and Yamabe (1986) and Ramamurthy (2001) criteria are used to predict the deformation modulus of jointed rock specimens. Triaxial compressive strength tests have been performed on cubical sandstone specimens with nominal dimensions of  $60 \times 60 \times 60 \text{ mm}^3$  and  $80 \times 80 \times 80 \text{ mm}^3$  using a true triaxial load frame. The confining pressures are varied from 0, 1, 3, 5, 7 to 12 MPa. The simulated joints are saw-cut surfaces and tension-induced fractures. The evaluation of the existing rock mass failure criteria and their parameters are useful to appropriately apply in the design and stability analysis of geologic structures.

## **1.3 Scope and limitations**

The scope and limitations of the research include as follows.

1. Laboratory testing is conducted on cubical specimens prepared from the Phra Wihan sandstone.

2. Triaxial compression tests have been performed with confining pressures of 0, 1, 3, 5, 7 and 12 MPa.
3. The specimens are prepared to have one and three joint sets with number of joint varies from 1, 2, 3, 4, 5 joints for each set.
4. Up to 80 samples are tested, with the nominal dimensions of  $60 \times 60 \times 60$  mm<sup>3</sup> for one joint set and  $80 \times 80 \times 80$  mm<sup>3</sup> for three joint sets.
5. For one joint set specimen, the joint are parallel, inclined at 45° and perpendicular to the applied major principal stress.
6. All tests are conducted under ambient temperature and dry condition.
7. The tested joint is artificially made in the laboratory by saw cut device and tension induced method.

## **1.4 Research methodology**

The research methodology shown in Figure 1.1 comprises 7 steps; including 1) literature review, 2) sample preparation, 3) laboratory testing, 4) strength criteria, 5) deformation modulus, 6) discussions and conclusions, and 7) thesis writing.

### **1.4.1 Literature review**

Literature review is carried out to study the previous researches on the effect of jointed rock and deformation. The sources of information are from text book, journals, technical reports and conference papers. A summary of the literature review is given in chapter two.

### **1.4.2 Sample preparation**

The rock samples used in this study are Phra Wihan sandstone. This rock is classified as fine-grained quartz sandstones with highly uniform texture and

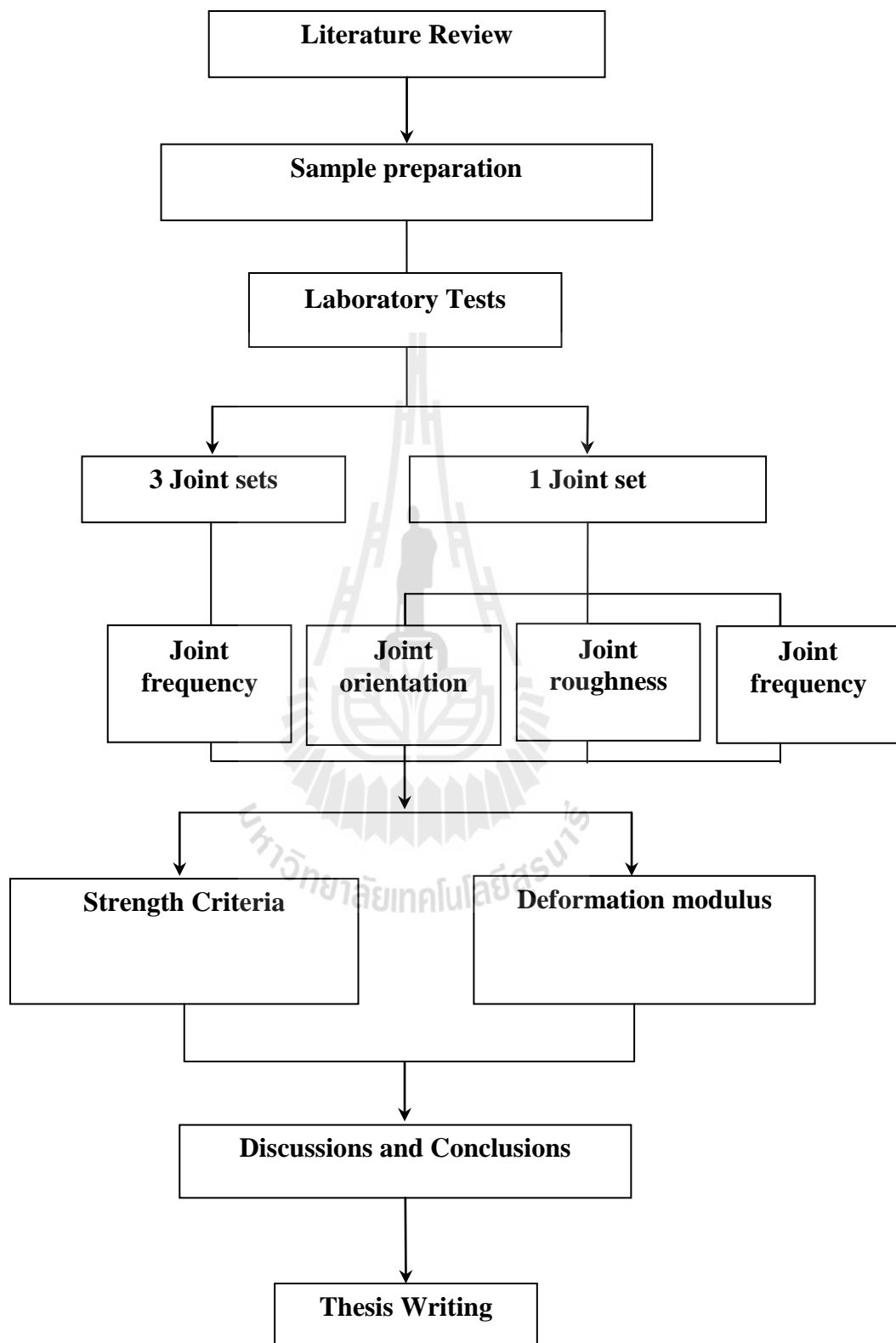


**Figure 1.1** Research methodology.

density. They are prepared to obtain cubic specimens with nominal dimensions of  $60 \times 60 \times 60 \text{ mm}^3$  and  $80 \times 80 \times 80 \text{ mm}^3$ . The simulated joints are saw-cut surfaces and tension-induced fractures. Specimens with one joint set and three mutually perpendicular joint sets are prepared. There are 1, 2, 3, 4 and 5 joints for each set (13 to 67 joints per meter). For one joint set specimens, the joint are parallel, inclined at  $45^\circ$  and perpendicular to the applied major principal stress.

#### **1.4.3 Laboratory test**

A true triaxial load frame is used to apply constant confining pressures at 0, 1, 3, 5, 7 and 12 MPa. Neoprene sheets are used to minimize the friction at all interfaces between the loading platens and the rock surface. The tests are performed by increasing the axial stress until failure occurs. The confining pressure is controlled constant by four lateral hydraulic pumps. The digital displacement gages are installed to measure the axial and lateral deformations until failure occurs. The maximum load at failure and failure modes are recorded. They are used to calculate the strength and deformation modulus of the specimen.

#### **1.4.4 Strength criteria**

Four criteria that are commonly used to determine rock mass strength are fit to the triaxial strength data. They include the Hoek and Brown (1980), Sheorey et al. (1989), Yudhbir et al. (1983) and Ramamurthy and Arora (1994) criteria. Exhaustive reviews of these criteria have been given elsewhere (Edelbro et al., 2007; Sheorey, 1997), and hence will not be repeated here. They are all formulated in the terms of  $\sigma_1$  and  $\sigma_3$ . The predictive capability of these strength criteria is determined and compared using the coefficient of correlation ( $R^2$ ) as an indicator. The higher  $R^2$  value indicates the better predictability of the criterion.

#### 1.4.5 Deformation modulus

Three empirical criteria are used to estimate rock mass deformation modulus ( $E_m$ ). They include the Goodman (1970), Yoshinaka and Yamabe (1986) and Ramamurthy criteria (2001). The deformation modulus calculated from the triaxial compression test results are compared with the rock mass deformability criteria. RMR classification is also studied. The results show that the values of RMR do not change with joint frequency because the spacing (s) of specimen is less than 60 mm.

#### 1.4.6 Discussions, conclusions and thesis writing.

All study activities, methods, and results are documented and complied in the thesis.

### 1.5 Thesis contents

This research thesis is divided into eight chapters. The first chapter includes background and rationale, research objectives, scope and limitations and research methodology. **Chapter II** presents results of the literature review to improve an understanding of the strength and deformation of rock mass, the existing strength criteria and the previous relevant testing. **Chapter III** describes sample preparation. **Chapter IV** describes the test method. **Chapter V** presents the experimental results. **Chapter VI** assesses the predictive capability of some rock mass strength criteria. **Chapter VII** determine the effects of joint frequency, orientation and set numbers on the deformation modulus of rock mass model and to assess the predictive capability of the deformability criteria. **Chapter VIII** presents discussions, conclusions and recommendation for future studies.

## **CHAPTER II**

### **LITERATURE REVIEW**

#### **2.1 Introduction**

Relevant topics and previous research results are reviewed to improve an understanding of the strength and deformation of rock mass, the existing strength criteria and the previous relevant testing. These include the effects of joint set on rock mass, effects of joint orientation, rock mass strength criterion, strength comparison and elastic modulus of rock mass. Initial review results are summarized below.

#### **2.2 Effects of joint set on rock mass**

Yang et al. (1998) perform uniaxial tests on prismatic jointed models with two joint sets (type A) and three joint sets (type B) with different surface roughness and configurations (Figure 2.1). The failure mode, failure strength and deformation behavior were investigated for each test in order to analyze the fracture mechanism of jointed rock. The model material is a mixture of plaster, sand and water in the proportions of 1:0.25:0.92 by weight. The fundamental properties of the model material are:  $\sigma_c = 7.63$  MPa,  $\sigma_t = 1.05$  MPa,  $E = 4554$  MPa,  $\nu = 0.19$ ,  $\gamma = 1.05$  g/cm<sup>3</sup>,  $\phi_b = 31^\circ$ . From the experimental results it is found that the influence of joint configuration on the strength and failure modes of jointed models is distinct. From the axial stress-stress curves of type A mass, it is observed a highly nonlinear and joint orientation dependent behavior representing jointed rocks. To design two

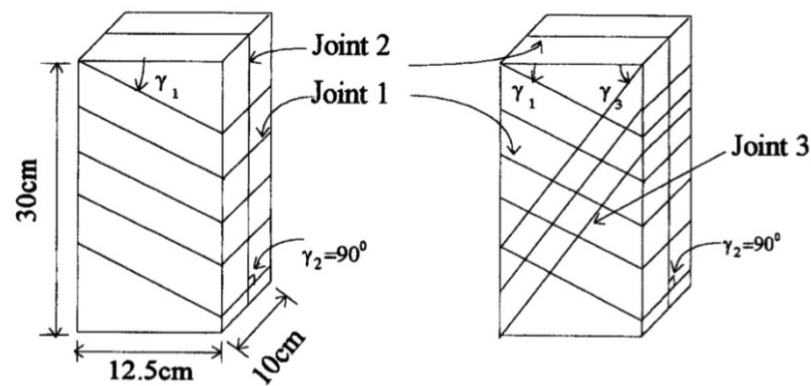


**Figure 2.1** Two types of rock mass model: type A with two joint sets (left); and type B with three joint sets (right) (Yang et al., 1998).

identical strengths of joint sets in a mass, the first and third joint sets in model B was arranged symmetrically with respect to the axial loading. In this circumstance, the shear strength of joints in each set is the same. The steeper set demonstrates a lower shear strength as shown in Figure 2.2. However, the strengths in some cases of type B are smaller than that in type A. Thus, the difference between types B and A is primarily due to the interaction of the first and third sets.

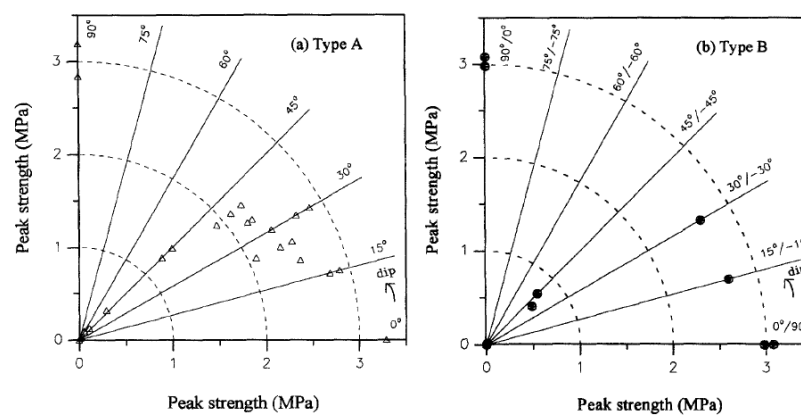


**Figure 2.2** Anisotropic strength of rock masses with different dip angle: (a) type A; and (b) type B (Yang et al., 1998).

### 2.3 Effects of joint orientation

Ramamurthy and Arora (1994) study the jointed rock mass strength to predict strength from joint factor ( $J_f$ ). The joint factors consist of joint frequency, joint orientation ( $n$ ) and shear strength along the joint ( $r$ ) (Tables 2.1 and 2.2).

**Table 2.1** Joint inclination factor  $n$  for different joint orientation angles  $\beta$  (Ramamurthy and Arora, 1994).

$\beta$ (degrees)	Values of $n$	
	Type of anisotropy	
	U-shaped	Shoulder-shaped
0	0.82	0.85
10	0.46	0.60
20	0.11	0.20
30	0.05	0.06
40	0.09	0.12
50	0.30	0.45
60	0.46	0.80
70	0.64	0.90
80	0.82	0.95
90	0.95	0.98

**Table 2.2** Suggested parameter  $r$  of different ranges of  $\sigma_{ci}$  (Ramamurthy and Arora, 1994).

Uniaxial compressive strength of intact rock, $\sigma_{ci}$ (MPa)	Joint strength parameter, $r$	Remarks
2.5	0.30	Fine-grained micaceous to coarse-grained
5.0	0.45	
15.0	0.60	
25.0	0.70	
45.0	0.80	
65.0	0.90	
100.0	1.00	

The objective was achieved by simulating joints in intact isotropic rock cores in laboratory. Anisotropy was induced into the intact specimens by developing a number of clean and rough-broken joints at  $\beta=0, 30, 40, 50, 60, 70, 80, 90^\circ$  ( $\beta$  is the angle between the joint orientation and vertical axis through the specimen). The types of joints studied are shown in Figure 2.3. The strength of a jointed rock mainly depends on the orientation of the joint with respect to the direction of axial loading. The study revealed that rocks exhibit a minimum value of strength when the joints

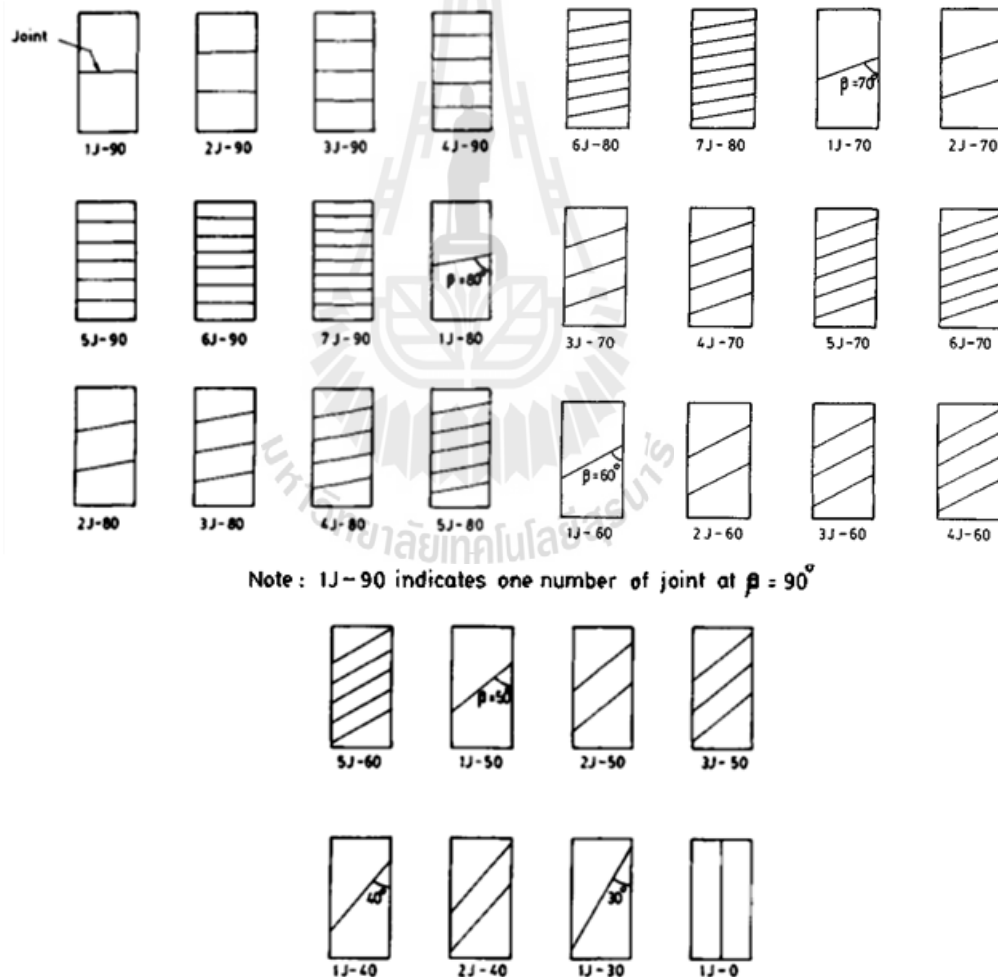


**Figure 2.3** Types of joints studied (Ramamurthy and Arora, 1994).

are oriented at  $\beta=30-40^\circ$ . Similar behavior was also observed in earlier studies. The joint which is closer to  $(45-\phi/2)^\circ$  with the major principal stress is the most probable sliding joint and should be considered in estimating the value of  $J_f$ .

Colak and Unlu (2004) study the influence of joint orientation ( $m_i$  value) for the strength anisotropy. The testing is performed in sandstone (possessing low degree of anisotropy) and siltstone, claystone (medium degree of anisotropy). The rock samples have orientations ( $\beta$ ) at 0, 30, 45, 60 and  $90^\circ$  (orientated constant named  $m_{i(\beta)}$ ). Tests were conducted according to the ISRM suggested standards. It has been noted that values of  $m_{i(\beta)}$  vary with the orientation angle, and this is considered an indication of the strength anisotropy. A suitable function that may be used to define the normalized value of  $m_{i(\beta)}$  has been derived from a similar expression given by Hoek and Brown (1980). Utilizing this equation, the following expression is obtained:

$$\frac{m_{i(\beta)}}{m_{i(90)}} = 1 - A \exp \left[ - \left( \frac{\beta - B}{C + D\beta} \right)^4 \right] \quad (2.1)$$

where  $m_{i(90)}$  is the reference value of  $m_i$ ,  $B$  is the value of  $\beta$  (in degrees) at which  $m_{i(\beta)}$  is minimum, and  $A$ ,  $C$  and  $D$  are statistical parameters given in Table 2.3. Finally, a generalized curve is obtained for all the sedimentary rocks considered (Figure 2.4). In summary, when transversely isotropic intact rock specimens exhibit strength anisotropy, the H-B strength envelope is variable, and it is influenced by the orientation angle. Using the results of basic strength tests on oriented samples, the values of the H-B strength parameter  $m_i$  are calculated for different orientation angles

**Table 2.3** Results of statistical analyses involving non-linear least squares estimation method (Colak and Unlu, 2004).

Rock type	Statistical parameters				Coefficient of determination ( $r^2$ )
	A	B	C	D	
Sandstones	0.38	17.0	14.8	0.47	0.653
Siltstones	0.77	17.4	19.8	0.31	0.840
Claystone	0.61	15.3	17.6	0.40	0.998
All sedimentary rock types considered	0.63	13.4	13.3	0.49	0.606

by conventional statistical analysis. Then, employing the expression given by Equation (2.1) as a model for non-linear statistical regression, the parameter  $m_{i(\beta)}$  can

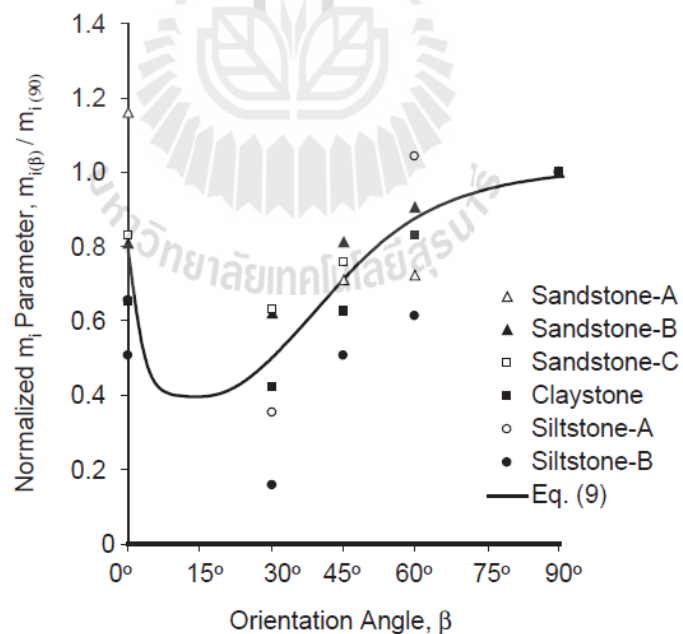


**Figure 2.4** Variation of the normalized  $m_i$  parameter with the orientation angle for all sedimentary rock type considered (Colak and Unlu, 2004).

be obtained as a function of the orientation angle ( $\beta$ ). Finally normalized H-B strength envelopes are obtained according to Equation (2.2), and they also depend on the orientation angle.

$$\sigma_{1(\beta)} / \sigma_{ci(\beta)} = \sigma_3 / \sigma_{ci(\beta)} + \left( m_{i(\beta)} \sigma_3 / \sigma_{ci(\beta)} + 1 \right)^{0.5} \quad (2.2)$$

In addition, it should be emphasized that this approach is applicable to two-dimensional transverse isotropy problems involving intact rocks. Although this approach is applicable only to plane anisotropy problems related to intact rocks, it is anticipated that it will be possible to extend it to include rock masses.

## 2.4 Rock mass strength criterion

Ramamurthy (2001) studies the shear strength response of some geological materials in triaxial compression by proposing a non-linear shear strength failure criterion. This criterion has been verified with the experimental data of 41 different soils from clay to rockfill and with the data of a number of intact rocks, jointed rocks and rock-like materials tested in the axisymmetric triaxial compression exhibiting either brittle or ductile response. Various types of joints introduced into the test specimens by the researchers are shown in Figure 2.5 and the corresponding test data are included in Figure 2.6. It is found that the compressive strength of a jointed rock can be linked to that of the intact rock through a joint factor,  $J_f$ . The strength criterion on jointed rocks is thus

$$\frac{\sigma_1' - \sigma_3'}{\sigma_3'} = B_j \left( \frac{\sigma_{cj}}{\sigma_3'} \right)^{\alpha_j} \quad (2.3)$$

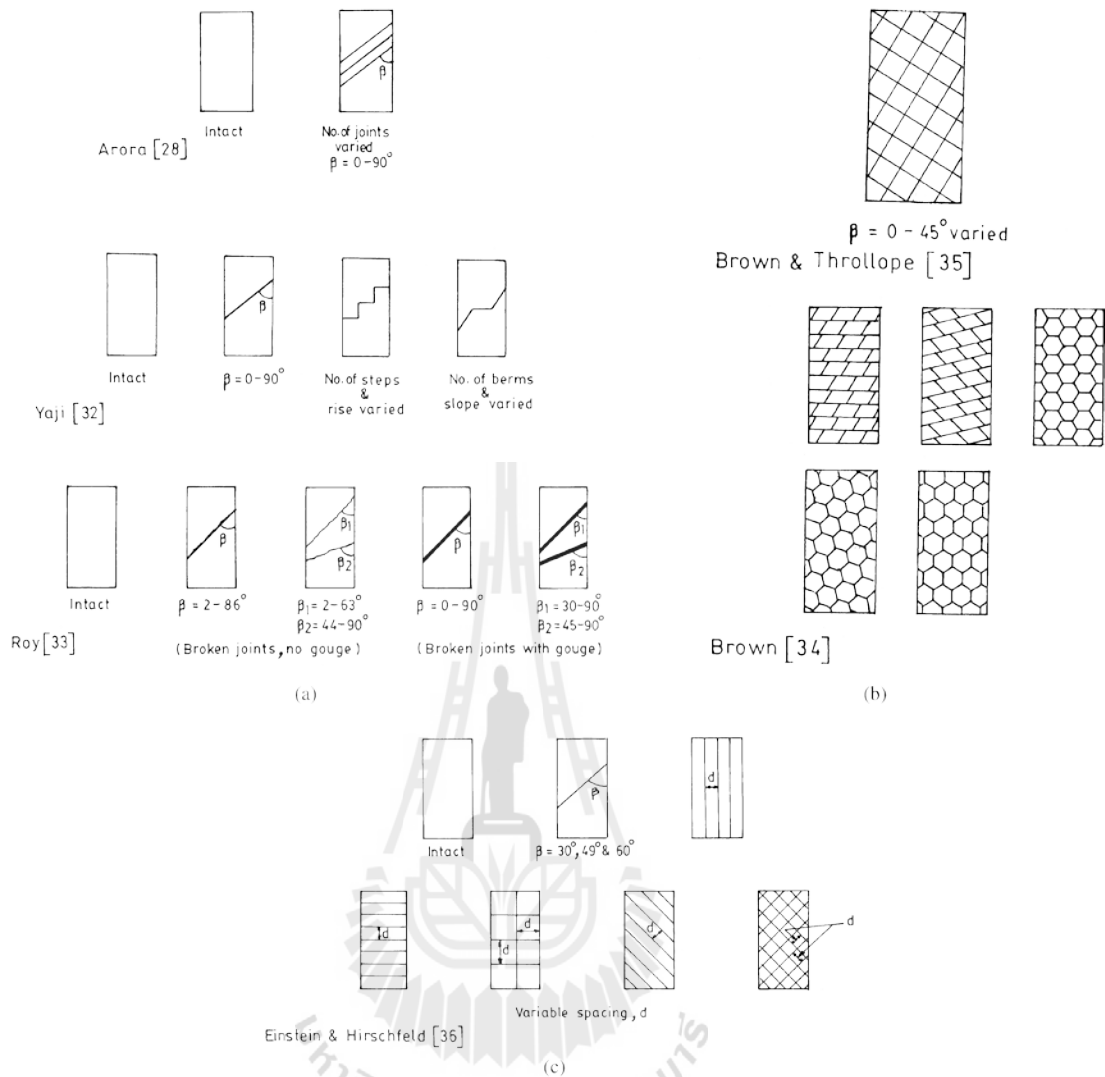


**Figure 2.5** Joint systems adopted in the test specimens by some researchers (Ramamurthy, 2001).

where  $\sigma_1'$  and  $\sigma_3'$  are major and minor effective principal stresses, respectively,  $\sigma_{cj}'$  the uniaxial compressive strength of jointed specimen obtained from,  $B_j$  and  $\alpha_j$  are strength parameters of the jointed rock. The values of  $\alpha_j$  and  $B_j$  are obtained from the following expressions:

$$\alpha_j / \alpha_i = \left( \frac{\sigma_{cj}}{\sigma_{ci}} \right)^{0.5} \quad (2.4)$$

$$B_i / B_j = 0.13 \exp[2.04 \alpha_j / \alpha_i] \quad (2.5)$$

$\alpha_i$  and  $B_i$  are the values of the strength parameters obtained from triaxial tests on intact specimens of the rock.

Since, the weakness introduced into an intact rock is essentially due to the combined effect of the joints, their inclination/orientation and the strength long these joints, represented by  $J_f$ , both compressive strength and modulus are influenced.

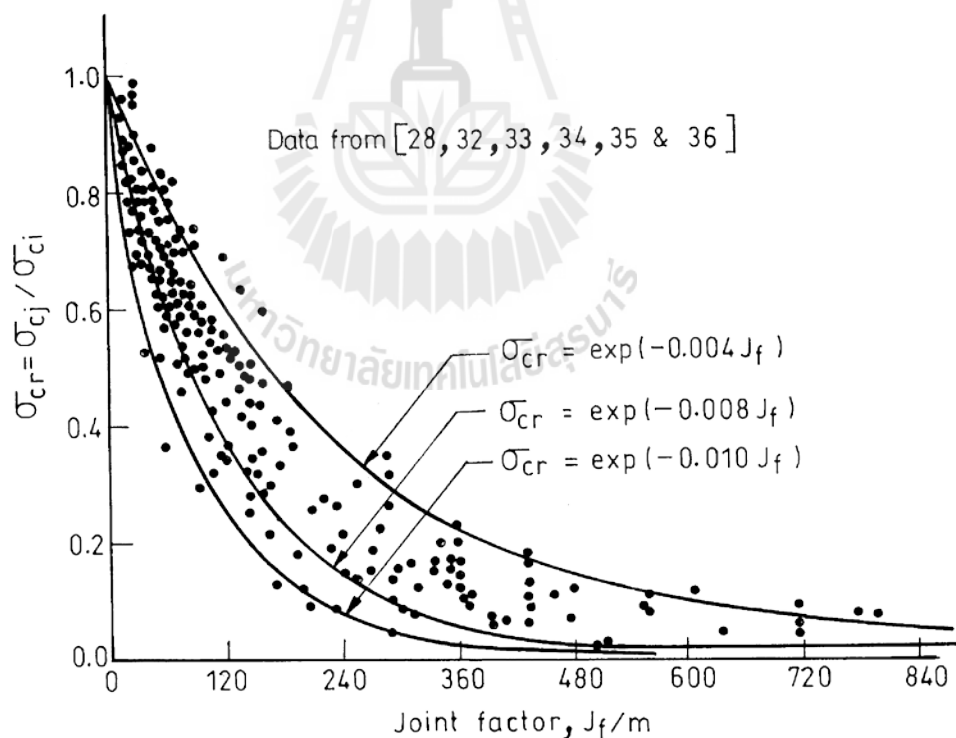


**Figure 2.6** Relationship between compressive strength of jointed specimens and joint factor (Ramamurthy, 2001).

Kulatilake et al. (2006) propose a new rock mass failure criterion for biaxial loading conditions (Equation 2.6). To simulate brittle rocks, a mixture of glastone, sand and water was used as a model material. To investigate the failure modes and strength, both the intact material blocks as well as jointed model material blocks of size 35.6×17.8×2.5 cm having different joint geometry configurations were subjected to uniaxial and biaxial compressive loadings. The results exhibited three different failure modes under different joint geometry configurations: Orientation of joint sets and the level of intermediate principal stress play major roles with respect to the mode of failure. A new intact rock failure criterion is proposed at the 3-D level. Results obtained from both the intact and jointed model material blocks are used to develop a strongly non-linear new rock mass failure criterion for biaxial loading. The criterion incorporates the fracture tensor component and covers the strengths resulting from all the three failure modes observed in the investigation. Equation (2.8) shows the fracture tensor of a jointed mass has the capability of integrating the effects of number of fracture sets (N), fracture density ( $\rho$ ), and distributions for size ( $r$ ) and orientation ( $\theta$ ) of the fracture sets. The fracture tensor component in a certain direction quantifies the directional effect of fracture geometry.

$$\frac{\sigma_{u,b}}{\sigma_{u,I}} = \exp(-\omega_0 F_{22}) \quad (2.6)$$

$$\omega = \frac{\omega_0}{a \left( \frac{\sigma_2}{\sigma_{\mu,I}} \right)^b + 1} \quad (2.7)$$

$$F_{22} = \sum_{m=1}^N (\rho r^2 \sin^2 \theta)_m \quad (2.8)$$

Saroglou and Tsiambaos (2008) propose the modified Hoek-Brown criterion by incorporating a new parameter ( $k_\beta$ ) to account for the effect of strength anisotropy, thus being able to determine the strength of intact anisotropic rock under loading in different orientations of the plane of anisotropy. The uniaxial and triaxial compression tests were performed on gneiss, schist and marble specimens in which the planes of anisotropy were oriented at angles  $\beta$  equal to  $0^\circ$ ,  $15^\circ$ ,  $30^\circ$ ,  $45^\circ$ ,  $60^\circ$ ,  $75^\circ$  and  $90^\circ$ . The specimen diameter was 54mm (NX size) with a height/diameter ratio between 2.0 and 2.5. The range of confining pressures used for the triaxial tests was  $0 < \sigma_3 < \sigma_{ci}/2$ . From the present study were fitted to the proposed failure criterion in Equation (2.9). Where  $\sigma_{c\beta}$  is the uniaxial compressive strength at an angle of loading,  $\beta$ , and  $k_\beta$  is the parameter describing the anisotropy effect (Table 2.4). In verification of proposed criterion, plotting the uniaxial compressive strength, determined by tests for different loading directions,  $\sigma_{c\beta\text{-lab}}$ , against that predicted from the failure criterion for anisotropic intact rock, can also assess the accuracy of the proposed criterion. When loading is performed perpendicular to the planes of ‘‘inherent’’ anisotropy of the intact rock, the parameter  $k_\beta$  is equal to unity ( $k_{90} = 1$ ) and the strength ( $\sigma_{c\beta}$ ) is equal to the uniaxial compressive strength  $\sigma_{ci}$ . The minimum value of this parameter,  $k_\beta = k_{30}$ , occurs when loading is performed at the angle of minimum strength which

$$\sigma_1 = \sigma_3 + \sigma_{c\beta} \left( k_\beta m_1 \frac{\sigma_3}{\sigma_{c\beta}} + 1 \right)^{0.5} \quad (2.9)$$

**Table 2.4** The range of the parameter ( $k_\beta$ ) for the rocks tested has been analytically investigated by carrying out triaxial tests, in different orientations of the foliation plane (Saroglou and Tsiambaos, 2008).

Rock type		$\beta$					
		0°	30°	45°	60°	75°	90°
Gneiss A	$k_\beta$	1.79	0.42	0.38	–	–	1
	$\sigma_{c\beta}$ (MPa)	39.4	35.5	46.7	–	–	66.5
	$r^2$	0.98	0.79	0.97	–	–	0.97
Gneiss B	$k_\beta$	0.88	0.59	0.41	–	–	1
	$\sigma_{c\beta}$ (MPa)	45.4	23.4	34.5	–	–	85.7
	$r^2$	0.97	0.96	0.96	–	–	0.96
Schist	$k_\beta$	0.96	0.75	0.76	1	–	1
	$\sigma_{c\beta}$ (MPa)	64.3	63.1	58.2	64	–	66.4
	$r^2$	0.91	0.92	0.90	0.96	–	0.99
Marble	$k_\beta$	0.99	0.91	0.93	–	1	1
	$\sigma_{c\beta}$ (MPa)	88.1	76.1	84.3	–	90.1	88.4
	$r^2$	0.98	0.96	0.96	–	0.86	0.98

usually is when the angle  $\beta$  between the major principal stress ( $\sigma_1$ ) and the foliation planes is between 30° and 45°. The prediction of uniaxial strength by the proposed criterion is quite good as the majority of the data plot on the diagonal line, shown in Figure 2.7. Although the proposed modification was studied for metamorphic rocks (gneiss, schist, marble), but could also be applied to other rock types exhibiting “inherent” anisotropy, e.g. sedimentary as well as igneous rocks. The proposed modified criterion is intended for use for prediction of strength of intact rock, but can also be extended to rock masses.

Rafiai (2011) proposes a new polyaxial criterion (Equation 2.10) and triaxial criterion (Equation 2.11) for brittle and ductile failure of intact rock and rock masses. A comprehensive database of the results of uniaxial, triaxial, and polyaxial

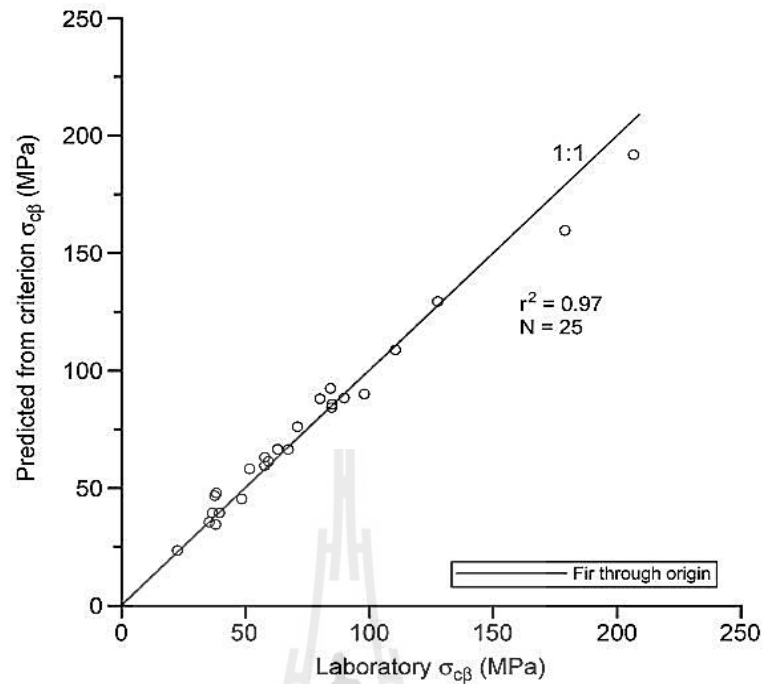


**Figure 2.7** Plot of predicted uniaxial compressive strength,  $\sigma_{c\beta\text{-crit}}$ , against that determined in the laboratory,  $\sigma_{c\beta\text{-lab}}$  for tested specimens (Saroglou and Tsiambaos, 2008).

tests on intact rock was utilized for evaluation of the new criterion and comparison of its accuracy with the most accurate and frequently used criteria.

$$\frac{\sigma_1}{\sigma_c} = \frac{\sigma_1^{\text{trx}}}{\sigma_c} + \sqrt{C \frac{\sigma_2 - \sigma_3}{\sigma_1^{\text{trx}}}} \exp\left(-\frac{\sigma_2 - D\sigma_3}{\sigma_1^{\text{trx}}}\right) \quad (2.10)$$

where C and D are constants and  $\sigma_1^{\text{trx}}$  is the rock strength in triaxial state of stresses ( $\sigma_2 = \sigma_3$ ) that can be calculated as

$$\frac{\sigma_1^{\text{trx}}}{\sigma_c} = \frac{\sigma_3}{\sigma_c} + \frac{1 + A(\sigma_3/\sigma_c)}{1 + B(\sigma_3/\sigma_c)} - r \quad (2.11)$$

where  $\sigma_c$  is the uniaxial compressive strength of intact rock, A and B are dimensionless constants that depend on the properties of rock ( $A \geq B \geq 0$ ). The parameter r is a strength reduction factor indicating the extent to which, the rock mass has been fractured. For intact rock  $r=0$  and for heavily jointed rock masses  $r=1$ .

It showed that the new criterion can maintain its accuracy over a wider range of stresses. In the absence of rock mass strength data, applicability of the new criterion for rock mass was verified by fitting it to typical Hoek–Brown failure envelopes. Regression analysis of the polyaxial strength data in the form of  $(\sigma_3, \sigma_2, \sigma_1)$  for six rock types showed that the new criterion predict the strength more accurately than the Modified Wiebols–Cook (Zhou, 1994) and You criteria (You, 2009) in all cases.

Singh and Singh (2012) state that the Mohr–Coulomb shear strength criterion is the most widely used criterion for jointed rocks. In its present form there are two major limitations of this criterion; firstly it considers the strength response to be linear, and, secondly the effect of the intermediate principal stress on the strength behavior is ignored. A modified non-linear form of Mohr–Coulomb strength criterion has been suggested in this study to overcome these limitations by following equations:

$$(\sigma_1 - \sigma_3) = \sigma_{cj} + \frac{2 \sin \phi_{jo}}{1 - \sin \phi_{jo}} \sigma_3 - \frac{1}{\sigma_{ci}} \frac{\sin \phi_{jo}}{(1 - \sin \phi_{jo})} \sigma_3^2 \quad ; \text{for } 0 \leq \sigma_3 \leq \sigma_{ci} \quad (2.12)$$

$$\sin \phi_{jo} = \frac{(1 - \text{SRF}) + \frac{\sin \phi_{i0}}{1 - \sin \phi_{i0}}}{(2 - \text{SRF}) + \frac{\sin \phi_{i0}}{1 - \sin \phi_{i0}}} \quad ; \text{SRF} = \text{Strength reduction factor} = \frac{\sigma_{cj}}{\sigma_{ci}} \quad (2.13)$$

Equations (2.12) and (2.13) were used to predict  $\sigma_1$  value for all the triaxial tests with inputting only  $\sigma_{ci}$ ,  $\sigma_{cj}$  and  $\phi_{io}$ . Where  $\sigma_{ci}$  is the UCS of the intact rock and  $\phi_{io}$  is the friction angle of the intact rock. On lines similar to intact rock criterion (Singh and Singh, 2011) the strength criterion for jointed rocks in Equation (2.12) is extended to polyaxial stress condition purely on trial basis. The criterion for polyaxial strength is expresses as:

$$(\sigma_1 - \sigma_3) = \sigma_{cj} + \frac{2 \sin \phi_{jo}}{1 - \sin \phi_{jo}} \left( \frac{\sigma_2 + \sigma_3}{2} \right) - \frac{1}{\sigma_{ci}} \frac{\sin \phi_{jo}}{(1 - \sin \phi_{jo})} \left( \frac{\sigma_2^2 + \sigma_3^2}{2} \right); \text{for } 0 \leq \sigma_3 \leq \sigma_2 \leq \sigma_{ci} \quad (2.14)$$

where  $\sigma_{cj}$  is the anisotropic strength of the rock mass under uniaxial loading condition ( $\sigma_3 = \sigma_2 = 0$ ) in the direction of  $\sigma_1$ , which will depend on the characteristics of the joints (frequency, orientation and surface roughness) and the properties of the intact rock;  $\phi_{jo}$  is the anisotropic friction angle of the rock mass at low confining stress level and may be obtained as a function of SRF and  $\phi_{jo}$  using Equation (2.13). The criterion has been found to work well for those failure patterns where assumption of equivalent continuum is valid and the equivalent properties are function of intact rock properties and joint characteristics. It is suggested that the simple polyaxial strength criterion (Equation 2.14) may be used in the non- linear stress analysis of underground openings in natural rock masses. The applicability of the proposed criterion has been verified by applying it to extensive experimental data on triaxial and polyaxial test results on jointed rocks available from literature.

Hashemnejad (2013) reviews a strength criterion must be capable to deal with different conditions of a certain type of rock having different properties. A new empirical criterion (Equation 2.15) is introduced and compared to the Hoek-Brown

(1988) criteria, Bieniawski (1974) criteria, Ramamurthy (1989) criteria and as a result.

$$\left(\frac{\sigma_1}{\sigma_3}\right) = \beta \left(\frac{3\sigma_c - 0.5\sigma_3}{\sigma_3}\right)^\alpha \quad (2.15)$$

Where  $\beta$  is rock material constant; function of rock type and quality and  $\alpha$  is slope of plot between  $(\sigma_1/\sigma_3)$  and  $((3\sigma_c - 0.5\sigma_3)/\sigma_3)$  on log-log plot. The above expression is applicable for all values of  $\sigma_3 > 0$ . For a discussion and comparison of the forms and the new form presented in this study, triaxial data of 80 samples were collected from different sources. These data are homogeneous and on specimens of almost the same size. In the new criterion defined, failure is as the failure strength and a failure criterion is not associated with the strain. Analysis of individual data sets revealed that none of the existing criteria shows perfect agreement with experimental values of stone strength. The analysis was carried out for different rock types, namely, limestone, granite, granodiorite, shale, sandstone, claystone and liparite. For each particular rock type there found to be a correlation between B in the Bieniawski criterion and m in the Hoek-Brown criterion with  $\sigma_c$ . The result show that the triaxial strength can be made by means of the Bieniawski criterion with a variable B dependent upon  $\sigma_c$  and  $\alpha$  certain constant  $\sigma$  for each particular material. The only parameter required for this criterion is the unconfined compressive strength which can be determined simply. In Figure 2.8, the results of the regression of this criterion are shown. Finally in Figure 2.9, which compares the results, obtained from the four criterions actual values obtained from triaxial tests on samples, it is better visible.

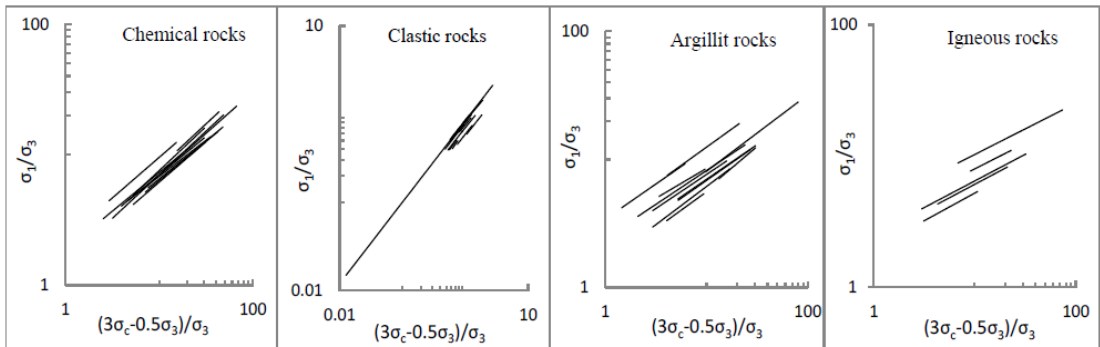


**Figure 2.8** Plot of proposed criterion for types of rocks (Hashemnejad, 2013).

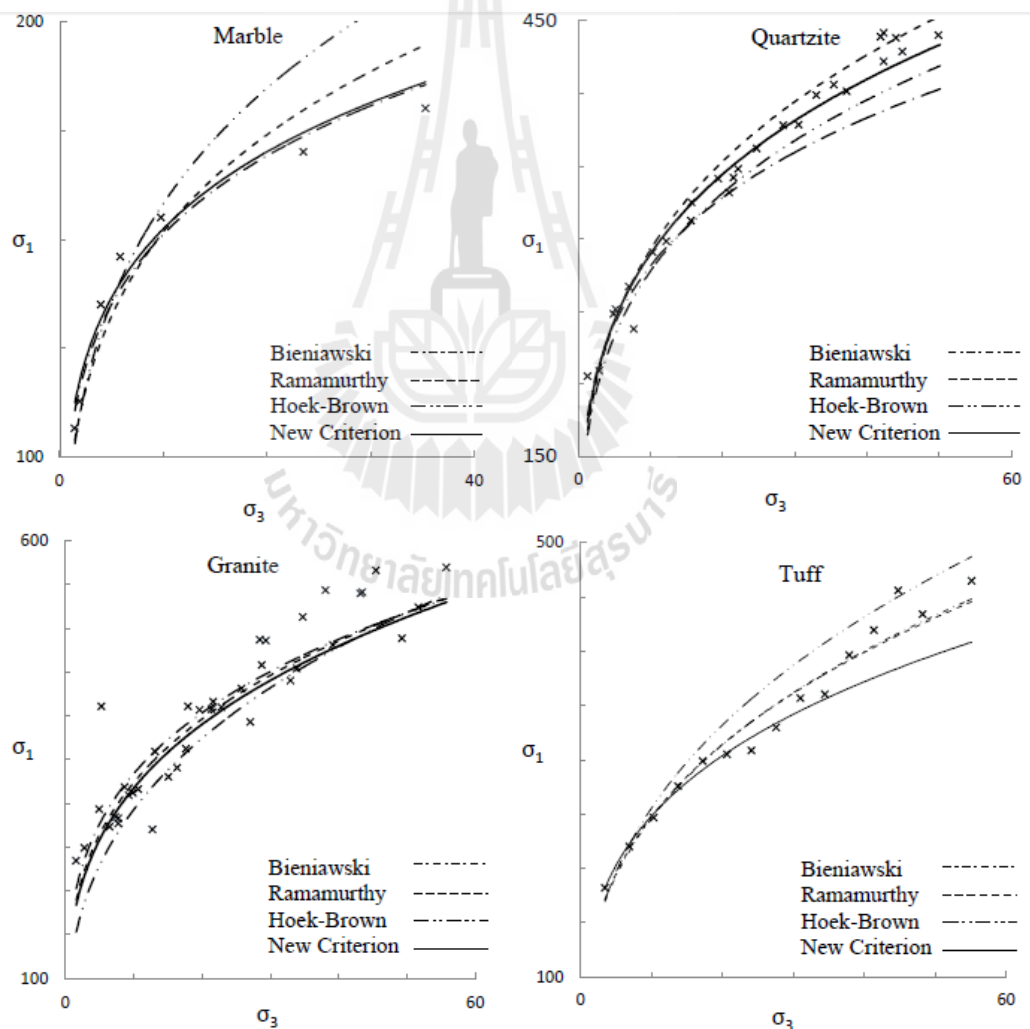


**Figure 2.9** Comparison between predicted and measured strength of marble, quartzite, granite and tuff (Hashemnejad, 2013).

## 2.5 Strength comparison

Sridevi and Sitharam (2000) study the strength and moduli of jointed rock to develop a rapid and exact technique based on equivalent continuum approach in which the properties of jointed rock masses are represented as a function of the intact rock properties and the properties of the rock joints, and comparison of empirical strength criteria of joint rock mass. In the analysis shear strength criteria proposed by Hoek and Brown (1980), Yudhbir (1983), Ramamurthy (1994) and the conventional Mohr-Coulomb criteria are used to determine the failure stress. The four empirical strength criteria are incorporated in a finite element code to determine the major principal stress at failure. The results have been presented in the form of principal stresses at failure based on the strength criteria used for different joint orientations and material properties. The results are plotted for different strength criteria and compared with the experimental results of Yaji (1984) and Brown and Trollope (1970). The results compare well within the limit of empirical relations of different strength criteria and experimental framework. From a comparison of empirical strength criteria it can be concluded that at higher confining pressures one can use any strength criteria whereas the choice of strength criteria is much more important at lower confining pressures. For jointed rocks the Mohr-Coulomb criterion gives a high estimate of failure stress for single jointed rock but gives a fair estimate of failure stress for block-jointed systems. The Hoek-Brown, Yudhbir and Ramamurthy criteria give a fair estimate of the major principal stress at failure for almost all cases although the value given by Ramamurthy's criterion is the best. This analysis, when extended to specimens with filled joints and also to an axisymmetric case, would

throw some light on the validity of these criteria in general and also help in arriving at a conclusion at which one is best for a given jointed rock mass.

Edelbro et al. (2006) presents a review of existing methods to estimate the rock mass strength using empirical failure criteria and classification/characterisation systems. To investigate the robustness and quantitatively compare the different selected estimation methods, they were used in three case studies. This paper is concerned with rocks whose failure mechanisms primarily are spalling and/or shear failure. Furthermore, the rock mass must be possible to approximate as a continuum material. For consideration, the methods had to: (i) present a numerical result that corresponds to the strength, (ii) have been used after the first publication, and (iii) be applicable to underground rock masses. All methods comprise an expression for the uniaxial rock mass compressive strength, see Table 2.5. The results from all methods and all case studies have also been summarized with respect to the span between estimated maximum and minimum values. The results from the Round Robin tests showed that the Hoek–Brown- and Sheorey-RMR76, RMS, and MRMR strength estimation methods gave results that were in poor agreement with the measured strengths. The use of the N, Yudhbir-RMR76, RMi, Q-, and Hoek–Brown-GSI methods, presented in Table 2.6, yielded reasonable agreement with the measured strengths. These methods are thus considered the best candidates for realistic strength estimation. However, the issue of “user-friendliness” must first be considered. Of these five methods, RMi seems to be least user-friendly, primarily due to the difficulties of accurately determining block size. The tables used for Hoek–Brown-GSI, are basic, but may be experienced as inaccurate by the user. In conclusion, the selected five estimation methods appear to be applicable for hard rock masses,

**Table 2.5** Expressions of the uniaxial compressive strength of the rock mass for the elected estimation methods (Edelbro et al., 2006).

Criterion	Uniaxial compressive strength of rock mass ( $\sigma_{cm}$ )						Authors
Hoek–Brown-RMR <sub>76</sub>	$\sigma_{cm} = \sigma_c \cdot \sqrt{e^{\frac{RMR_{basic}-100}{9}}}$						Hoek and Brown (1988)
Yudhbir-RMR <sub>76</sub>	$\sigma_{cm} = \sigma_c \cdot e^{[7.65(\frac{RMR_{basic}-100}{100})]}$						Yudhbir et al. (1983)
Sheorey-RMR <sub>76</sub>	$\sigma_{cm} = \sigma_c \cdot e^{(\frac{RMR_{basic}-100}{20})}$						Sheorey (1997)
MRMR	$\sigma_{cm} = \sigma_c \cdot \frac{(MRMR\text{-rating for } \sigma_c)}{100}$						Laubscher (1984)
Q	$\sigma_{cm} = 5\rho(Q \cdot \frac{\sigma_c}{100})^{1/3}$						Barton (2002)
N	$\sigma_{cm} = \frac{5.5 \cdot \rho \cdot N^{1/3}}{B^{0.1}}$						Singh and Goel (1999)
RMi	$RMi = \sigma_c \cdot JP$						Palmström (1995)
Hoek–Brown-GSI	$\sigma_{cm} = \sigma_c \cdot e^{(\frac{GSI-100}{9-3D})} (\frac{1}{2} + \frac{1}{6}(e^{-GSI/15} - e^{-20/3}))$						Hoek et al. (2002)
RMS	RMS-value <sup>a</sup>	100–81	80–61	60–41	41–20	<20	Stille et al. (1982)
	$\sigma_{cm}$ (MPa)	30	12	5	2.5	0.5	

*Notations:*  $\sigma_{cm}$  is the uniaxial compressive strength of the rock mass;  $\sigma_c$  the uniaxial compressive strength of intact rock;  $RMR_{basic}$  the rock mass rating basic value, (RMR for dry conditions and no adjustment for joint orientation); MRMR the mining rock mass rating (rock mass classification);  $\rho$  the rock density, in  $t/m^3$ ; Q the rock mass quality system (rock mass classification, NGI-index); N the rock mass number (rock mass classification); B the tunnel span or diameter (parameter in the N-system); RMi the rock mass index (rock mass classification); JP the jointing parameter (parameter in RMi); GSI the geological strength index (rock mass classification); D the disturbance factor in the Hoek–Brown criterion.

<sup>a</sup> RMS-value = RMR<sub>76</sub> adjusted for joint set reduction, see Table 4.

**Table 2.6** Methods with reasonable agreement with the measured strengths (Edelbro et al., 2006).

Methods	Parameters of interest	Remarks
Q	$J_r, J_a$	The effect on the rock mass strength due to roughness and alteration needs to be better defined
RMi	$V_b, jL, jR$ and $jA$	The block volume and joint length needs to be modified and easier to use
N	$B$	Could be interesting to study a stress free Q-system, of the newest version to determine the rock mass strength
Yudhbir-RMR <sub>76</sub>	–	$\sigma_{cm} = \frac{5.5 \cdot \rho \cdot Q^{1/3}}{B^{0.1}}$ Study the relation between RMR <sub>76</sub> and the rock mass strength
Hoek–Brown-GSI	$m, s, a$ , and GSI	–

Notations: Q the rock mass Quality system (rock mass classification, NGI-index);  $J_r$ ,  $jR$  the joint roughness number;  $J_a$ ,  $jA$  the joint alteration number; N the rock mass number (rock mass classification);  $B$  the tunnel span or diameter (parameter in the N-system); RMi the rock mass index (rock mass classification);  $V_b$  the block volume,  $jL$  the joint size factor;  $m$ ,  $s$  and  $a$  the material constants in Hoek-Brown criterion; GSI the geological strength index (rock mass classification).

provided that care is taken when choosing values for each of the included parameters in each method. However, the agreement with measured strengths is still relatively poor, implying that precise estimates cannot be expected with any method. This study has shown that the block volume was difficult to estimate; hence, a better method for block size estimation is warranted. The joint strength is included in most of the methods, where the joint alteration and joint roughness parameters (in Q, RMi and N) covers more possible geological situations and, according to this study, are better described than the joint condition parameter in RMR. The physical scale is not

included in any of the existing methods. The N method considers the tunnel span or diameter (B), but not related to the scale of the rock mass.

Goshashi et al. (2006) evaluate the most suitable criterion for predicting the anisotropic strength of rocks in uniaxial and triaxial compression. Uniaxial and triaxial tests were conducted on specimens having orientation angles ( $\beta$ ) of 0, 30, 45, 60, 75 and 90 degrees. The triaxial tests were done at confining pressures of 3, 5 and 10 MPa. Laboratory tests were carried out in accordance with ISRM standards on cylindrical samples at various orientation angles. Figure 2.10 shows the orientation angles of the tested samples. Figure 2.11 shows the variation of uniaxial compressive strength versus orientation angles. The results are based on the average experimental data obtained from three to five tests for each orientation. The results clearly show that the slate has a U-shaped anisotropy. Figure 2.12 shows the strength variations with orientation angles at various confining pressures. The plots are drawn by taking the average experimental results of three to five tests. It is clear from the results that the maximum and minimum strengths values are observed at  $\beta = 90^\circ$  and  $30^\circ$  respectively. In order to evaluate the most suitable criterion for predicting the anisotropic strength of rocks in uniaxial compression, the Liao and Huong (Liao and Hsieh, 1999) and Ramamurthy criteria (Ramamurthy, 1993) were studied. The predicted values were then plotted and compared with experimental test results. The study clearly shows that both criteria have good agreements with the test results; however, the Liao and Huong criterion predicts the strength more precisely. In order to investigate the most suitable criterion for predicting the anisotropic strength of rocks in triaxial compression, various criteria was used. The most commonly criteria utilized in this study were Donath and McLamore (McLamore and Gray, 1967;

Fahimifar and Soroush, 2003; Goodman, 1989), Hoek and Brown criterion for anisotropic rocks (Hoek and Brown, 1980), Liao & Huong (Liao and Hsieh, 1999), Tien and Kuo (Tien, and Kuo, 2001) and Ramamurthy (Ramamurthy, 1993; Nasseri et al., 2003). Figures 2.13–2.15 exhibit the comparison between the predicted strength values and the experimental data at different confining pressures. In general, the predicted strength value by Hoek and Brown and McLamore criteria agrees better with the experimental test results. However, it should be noted that in order to use these criteria, it is essential to conduct three triaxial tests at orientation angles of  $0^\circ$ ,  $30^\circ$ ,  $75^\circ$  and  $90^\circ$ . In contrast, for the Ramamurthy criterion one only needs to do three uniaxial tests at orientation angles of  $0^\circ$ ,  $30^\circ$  and  $90^\circ$  and one triaxial test in  $90^\circ$  at two confining pressures. Hence, it can be concluded that if very precise values are needed, then one should use the Hoek and Brown and McLamore criteria by conducting a large number of tests. If the number of tests is limited, then the Ramamurthy criterion can be utilized to predict the strength values reasonably.

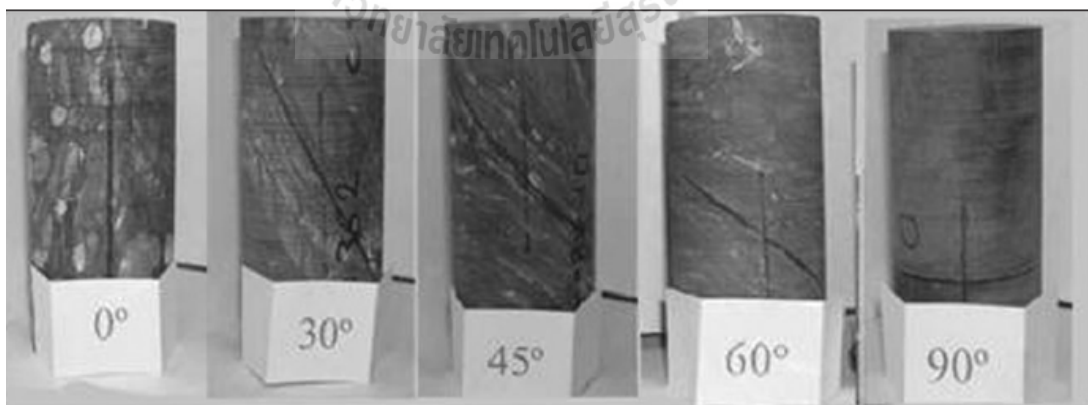


**Figure 2.10** Orientation angles of tested slate specimens (Goshashi et al., 2006).

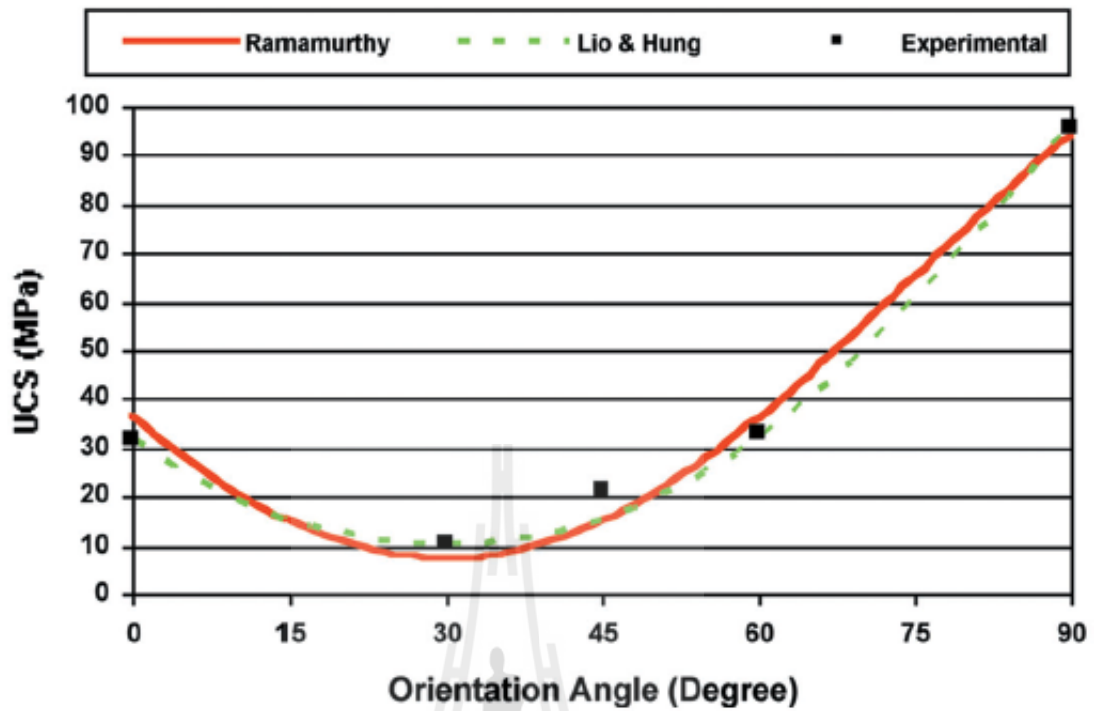


**Figure 2.11** Experimental and predicted curves of uniaxial compressive strength of slates (Goshashi et al., 2006).

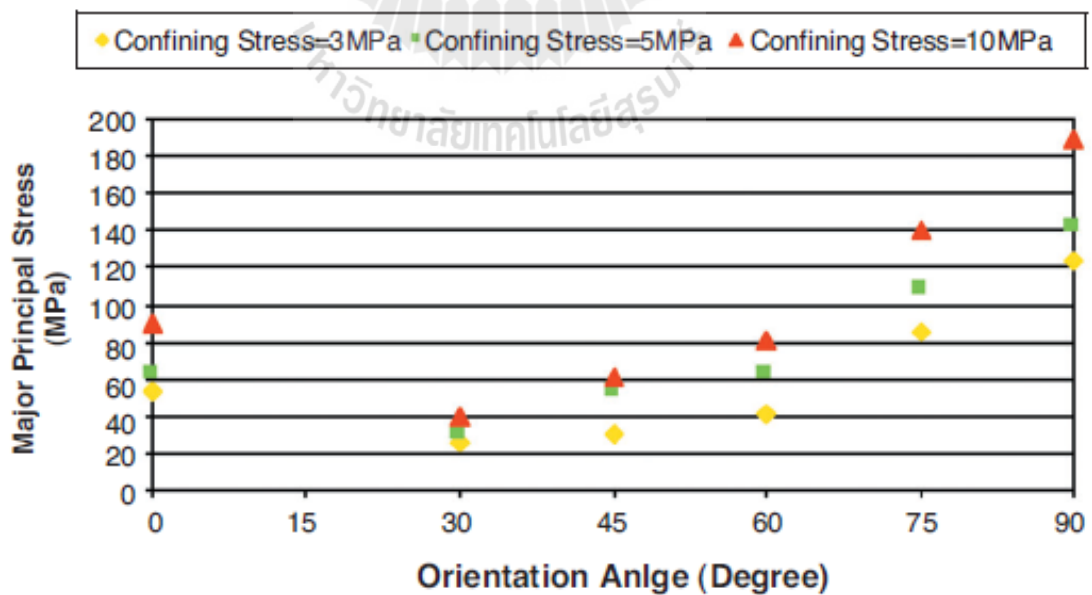


**Figure 2.12** Variation of strengths versus orientation angles (Goshashi et al., 2006).

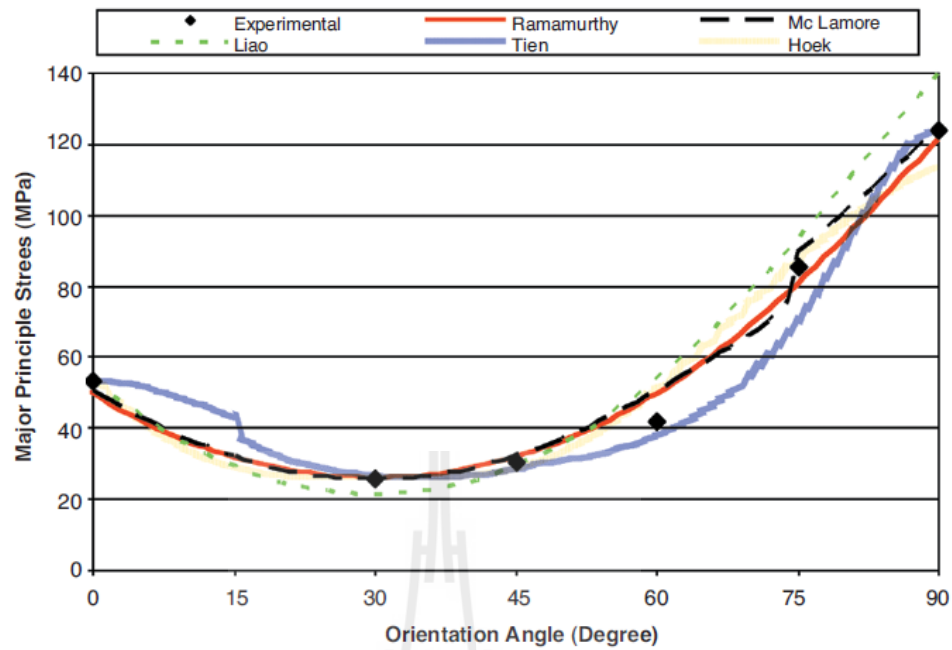


**Figure 2.13** Comparison between predicted and experimental strength at  $\sigma_3 = 3$  MPa (Goshashi et al., 2006).

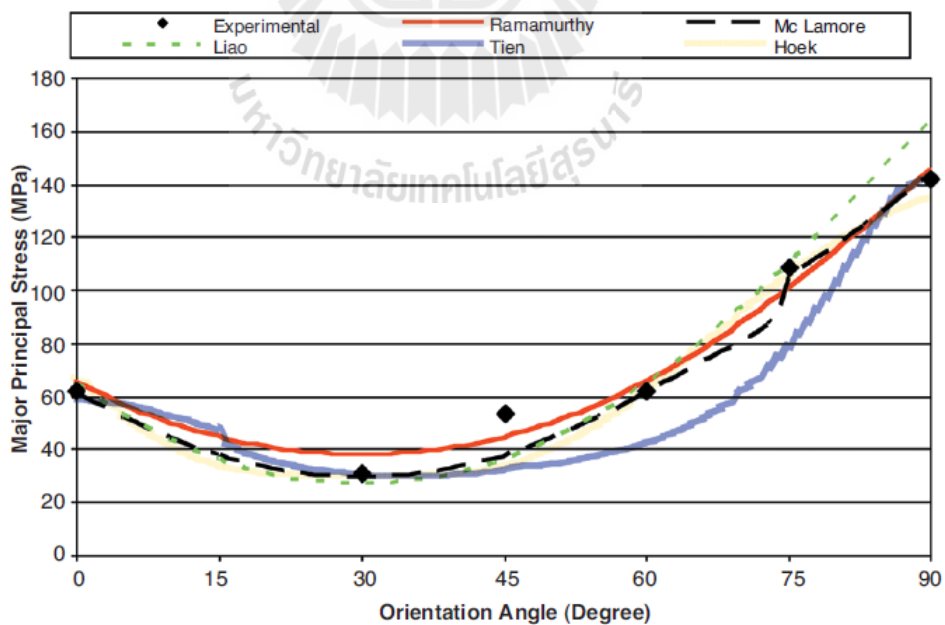


**Figure 2.14** Comparison between predicted and experimental strength at  $\sigma_3 = 5$  MPa (Goshashi et al., 2006).

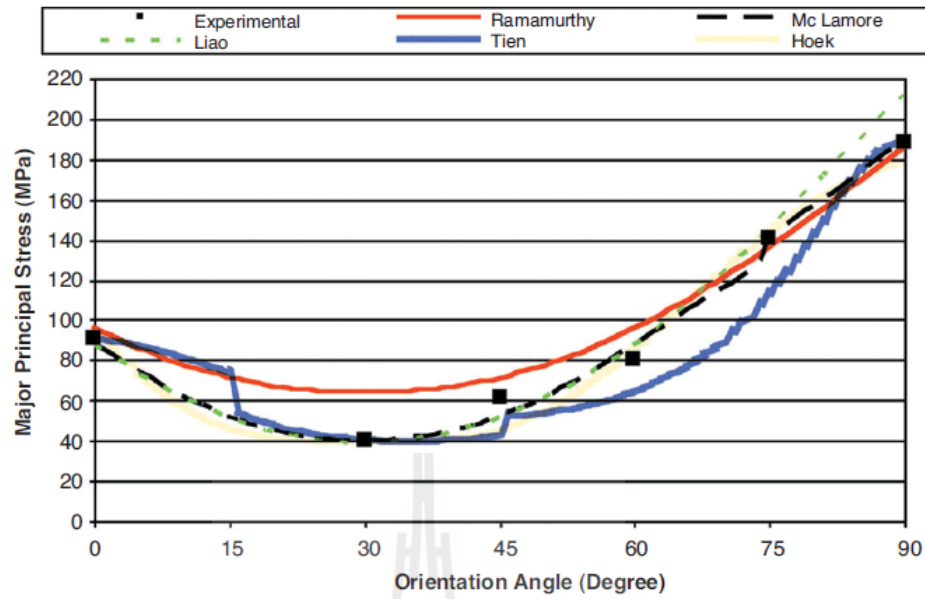


**Figure 2.15** Comparison between predicted and experimental strength at  $\sigma_3 = 10$  MPa (Goshashi et al., 2006).

## 2.6 Deformation modulus of rock mass

Yoshinaka and Yamabe (1986) present a constitutive relation for evaluating deformation behavior of regularly jointed rock. Based on the concept of joint stiffness, an equation to evaluate the deformation of jointed rock is derived as:

$$\frac{1}{E_t} = \left[ \frac{1}{E_c} + \frac{\cos^2 \theta_1}{L_1} \left( \frac{\sin^2 \theta_1}{k_{s1}} + \frac{\cos^2 \theta_1}{k_{n1}} \right) + \frac{\cos^2 \theta_2}{L_2} \left( \frac{\sin^2 \theta_2}{k_{s2}} + \frac{\cos^2 \theta_2}{k_{n2}} \right) \right]^{-1} \quad (2.16)$$

where  $E_c$  is elastic modulus of intact rock,  $\theta_1, \theta_2$  are the angles of inclination from the applied plane of major principal stress,  $L_1$  and  $L_2$  are joint spacings and  $k_s$  and  $k_n$  are joint stiffnesses. In order to confirm the constitutive relations derived here, loading tests using jointed rock mass models were carried out and the applicability of the proposed relations was confirmed from the comparison of experimental and numerical

results. To obtain the characteristics of joint deformation, joint shear and compression tests were performed in the laboratory using rock specimens with several kinds of roughness and size. The rock used in the experiments was soft welded-tuff and its physical properties are listed in Table 2.7. Now, as an example, we consider a model of the jointed rock mass shown in Figure 2.16. This model can be expressed by the mechanical model shown in Figure 2.17 with the following conditions. The state of stress is plane stress,  $\sigma_3 = 0$ . The rock mass has two sets of joints with the same dip direction parallel to the axis of minimum principal stress. Each joint has the joint stiffnesses shown in Figure 2.17, the angles of inclination at  $\theta_1$  and  $\theta_2$  from the applied plane of maximum principal stress, and joint spacings  $L_1$  and  $L_2$ , respectively. The intact rock is elastic with properties  $E_c$  and  $\nu_c$ . Loading tests have been performed in two series of rock mass models assembled as 32 element blocks with the smooth or rough surface joints. The loading system arrangement is shown in Figure 2.18 and the capacities for loading in the two perpendicular horizontal directions are 1 MN and 0.5MN respectively. The results of the loading tests are clearly shown that the stress-strain curves of jointed rock masses change remarkably according to the confining pressure and joint angle, and the curves have strong non-linearity owing to the characteristics of joint deformation.

**Table 2.7** Physical properties of welded-tuff (Ohya-stone) (Yoshinaka and Yamabe, 1986).

Specific gravity, G	Dry density, $\gamma_{dry}$ (kN/m <sup>3</sup> )	Porosity, n (%)	Uniaxial compressive strength, $\sigma_c$ (MPa)	Tensile strength, $\sigma_t$ (MPa)
2.40	14.3	41.2	11.2	1.46

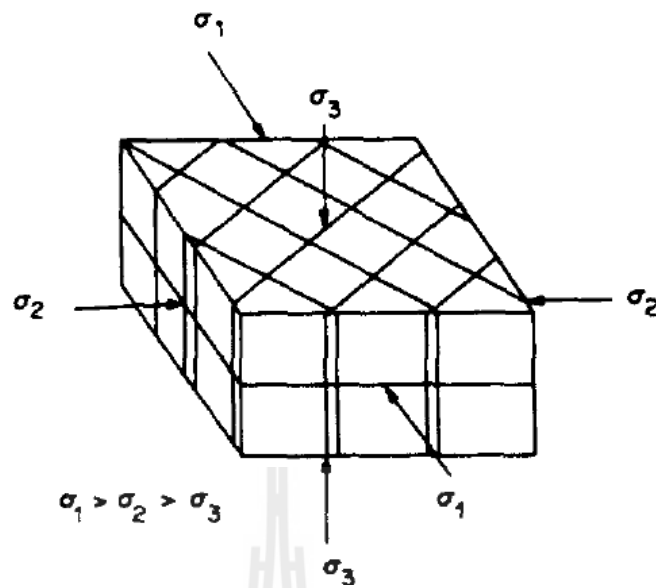


**Figure 2.16** Model of a jointed rock mass subjected to three principal stresses (Yoshinaka and Yamabe, 1986).

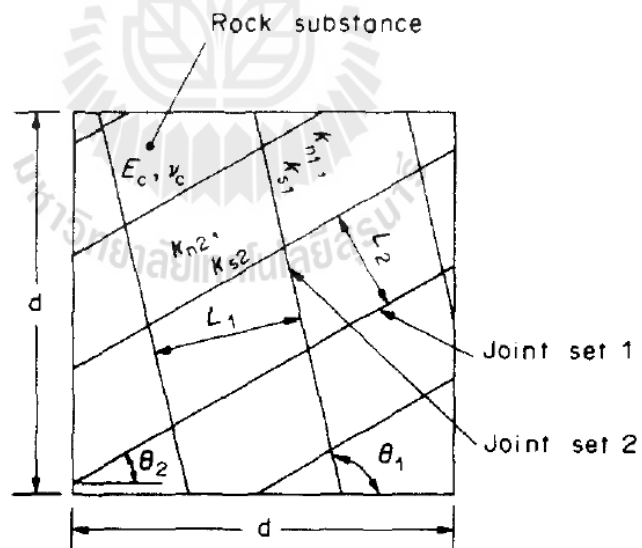


**Figure 2.17** Mechanical model for jointed rock mass with two sets of joints (Yoshinaka and Yamabe, 1986).

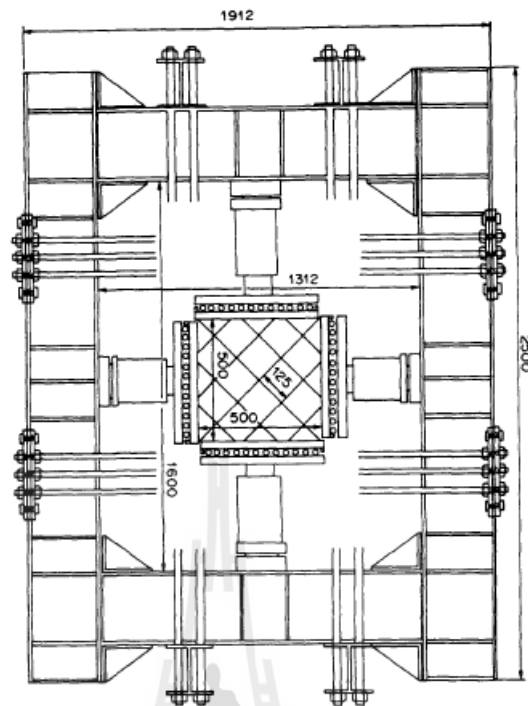


**Figure 2.18** Loading system for jointed rock mass model, plan view (figures in mm)  
(Yoshinaka and Yamabe, 1986).

Yang et al. (1998) describes a series of physical model tests for jointed rock masses with several superimposed joint sets. The objective is to study the effect of joint sets on the deformation of rock mass models. The Uniaxial tests are performed on prismatic jointed models with two joint sets and three joint sets with different surface roughness and configurations. It was observed that the axial deformation behavior of the jointed model is highly nonlinear and joint orientation dependent. The deformation moduli are less than that of the nonjointed rock. The highest value of deformation modulus in the split model only reaches 40% of the nonjointed rocks (Figure 2.19). The lowest values also occur in the range of the sliding mode. The deformation modulus reduces as the number of joint set increasing.

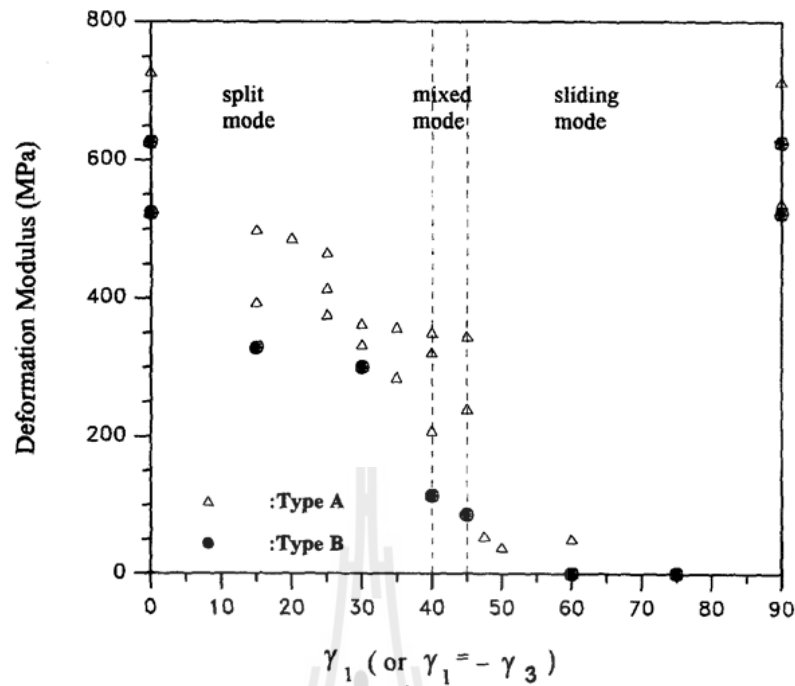


**Figure 2.19** Influence of joint sets on the modulus of rock masses (Yang et al., 1998).

Ramamurthy (2001) show the modulus ratio is also linked to the failure axial strain of jointed rocks when tested in uniaxial compression. Examination of the available experimental data of the jointed rock specimens tested in uniaxial compression and dense soil specimens also tested in uniaxial compression or under very low confining pressure suggest that when the modulus ratio ( $E_{ij}/\sigma_{cj}$  for jointed rocks and  $E_t/\sigma_c$  for soils, where  $E_t$  is the tangent modulus) is less than 50, the material may be considered to behave as a soil; most dense/stiff soils will have this ratio in the range of 50. All the available data on the ratios of moduli,  $E_{ij}/E_{ti}$ , obtained from tests in uniaxial compression with  $J_f$  for the jointed specimens are presented in Figure 2.20. An average relation may be represented by Equation (2.17):

$$E_{ij}/E_{ti} = \exp(-1.15 \times 10^{-2} J_f) \quad (2.17)$$

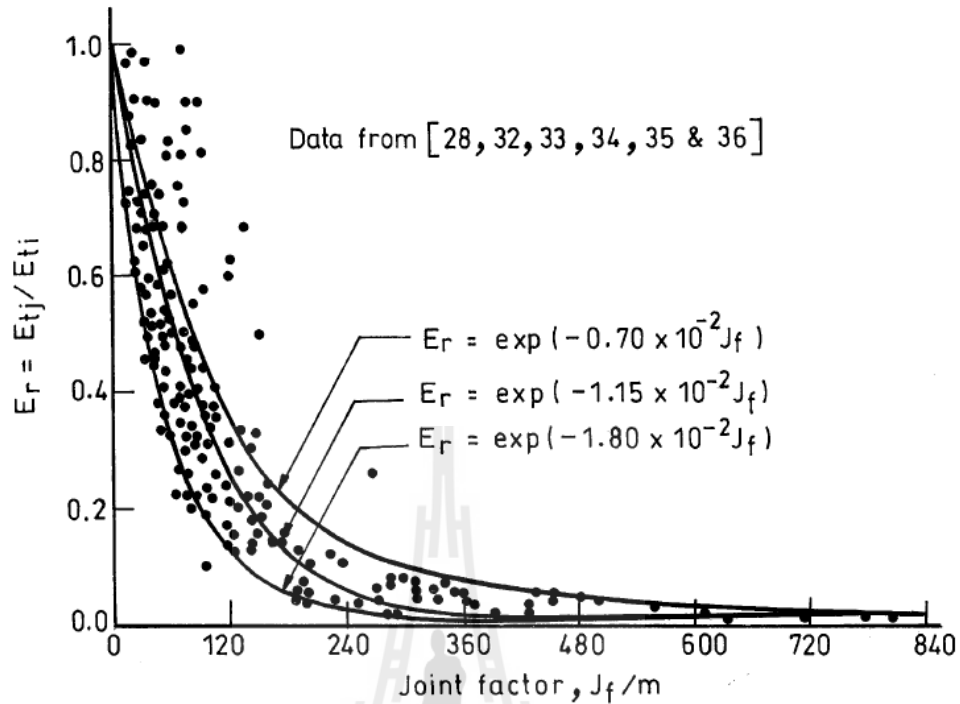


**Figure 2.20** Relationship between  $E_{tj}/E_{ti}$  and joint factor for jointed specimens (Ramamurthy, 2001).

where  $E_{tj}$  is the jointed rock deformation modulus,  $E_{ti}$  is the intact deformation modulus, and  $J_f$  is the joint factor. Figure 2.20 infer that when a rock mass assumes a value of  $J_f$  greater than 200/m, it may be treated to respond as a soil.

Tiwari and Rao (2006) study an experimental on rock mass model with three joint sets under triaxial and true-triaxial stress states to assess the influence of joint geometry and stress ratios on deformational behavior of rock mass. The true-triaxial system (TTS) developed by Rao and Tiwari (2002) was used in the present study (Figure 2.21a and b). The results from experimental study are used to develop expressions for predicting modulus values of rock mass. As expected, the modulus values are increasing at all dipping with increasing confining stress,  $\sigma_3$  (see Figure

2.22). The modulus values predicted using the Janbu (1963) and  $J_f$  (Ramamurthy, 1993) approaches are presented along with the experimental data for comparison as shown in Table 2.8. The modulus values are minimum at  $\theta=60^\circ$  and maximum at  $\theta=90^\circ$  obtained by both approaches and show anisotropy at all confining stresses. It can be seen that joint factor approach may not be applicable in describing the deformation behavior of rock mass under confining stress state because  $J_f$  assumes U shaped anisotropy behavior of jointed rock mass, which is possible in UCS conditions only. In the field a method should be selected based on input parameters available. It can be seen that both approaches require entirely separate type of input parameters for their applicability. Hence, the use of any approach in field solely depends upon availability of parameters at the site suiting with the requirement of that method. Further Janbu coefficient approach is recommended over joint factor approach. The modulus value  $E_j$  ( $=E_{ij} = E_{tm50}$ ) value in triaxial stress state is once known using Janbu's coefficients and joint factor approaches as discussed above. Then, based on the extensive data of true-triaxial test results, the expression of  $E_j$  in true-triaxial stress states ( $\sigma_2 > \sigma_3$ ) is suggested as in Equation (2.18).

$$\frac{E_j(\sigma_2 > \sigma_3)}{E_j(\sigma_2 = \sigma_3)} = 1 + T \left( \frac{\sigma_2}{\sigma_3 - 1} \right)^r \quad (2.18)$$

where  $T$ ,  $r$  joint inclination parameters and vary with inclination of joint set-I. Once the  $E_j$  value in triaxial stress state is known by any of the approach discussed above, the Equation (2.18) can be conveniently used for prediction of modulus at any joint dip  $\theta$  of rock mass under true-triaxial stress conditions at any  $\sigma_2/\sigma_3$  level.

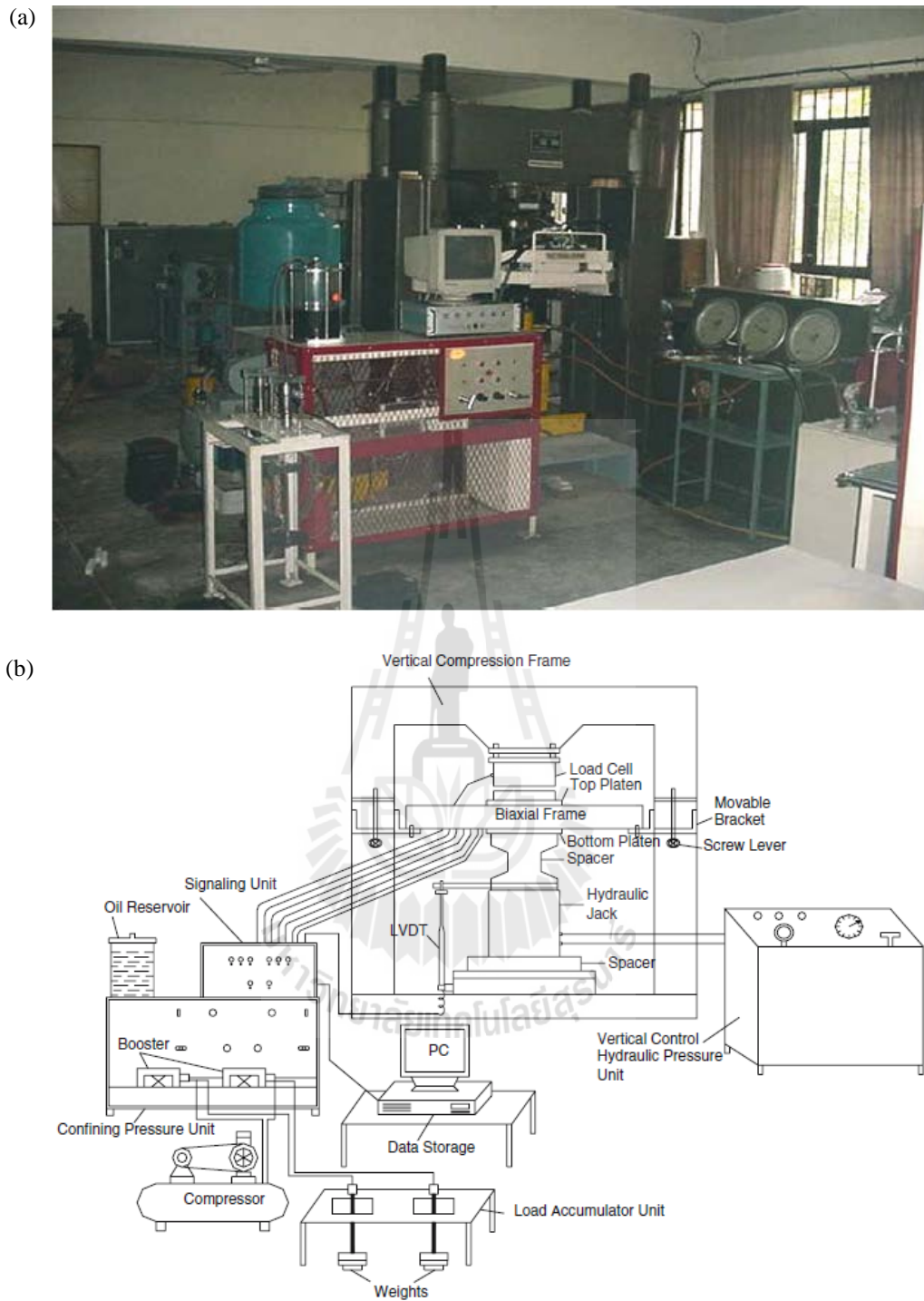


**Figure 2.21** (a) Complete set-up of true-triaxial system (after Rao and Tiwari, 2002).

(b) Schematic diagram for set-up of true-triaxial system (Tiwari and Rao, 2006).

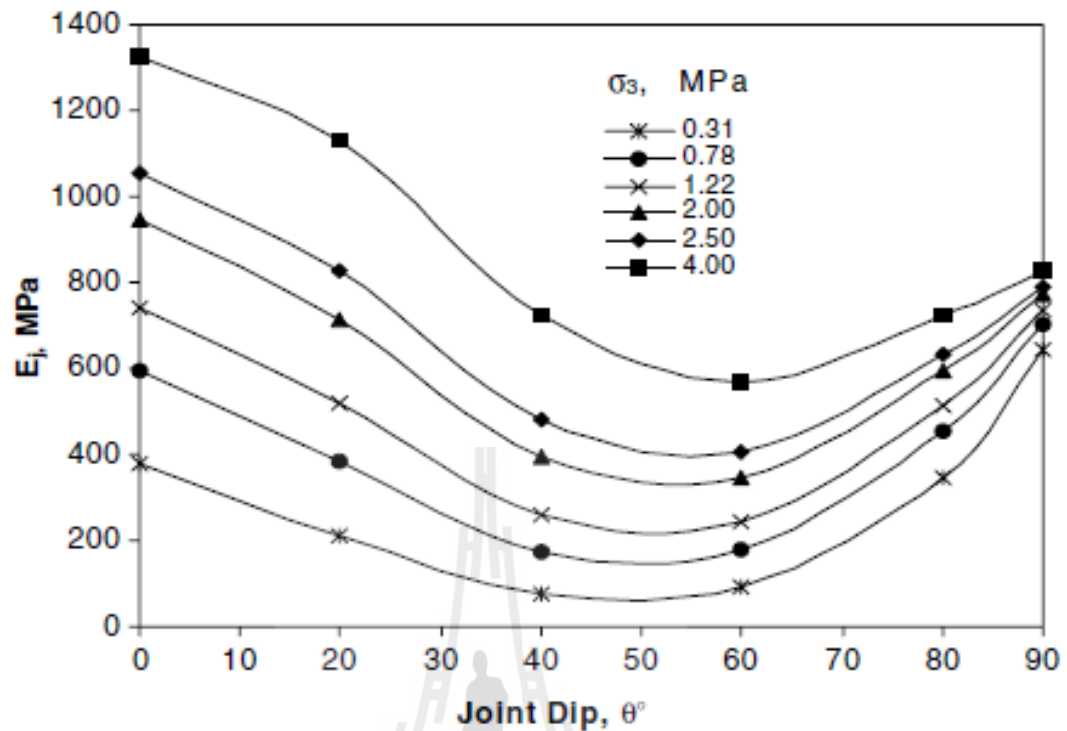


**Figure 2.22** Prediction of modulus at different confining pressures using Janbu's coefficients approach (Tiwari and Rao, 2006).

**Table 2.8** Comparison of  $E_j$  values obtained from different approaches (Tiwari and Rao, 2006).

$\theta$ (°)	$E_j$ (MPa)								
	$\sigma_3 = 0.31$ MPa			$\sigma_3 = 0.78$ MPa			$\sigma_3 = 1.22$ MPa		
	Experimental	Janbu approach	$J_f$ approach	Experimental	Janbu approach	$J_f$ approach	Experimental	Janbu approach	$J_f$ approach
0	380.5	378.9	2276.1	711.5	595.5	3325.1	718.0	741.4	4342.2
20	200	209.2	317.8	456.4	384.6	578.2	464.1	516.6	746.1
40	84.5	78.3	49.1	142.2	174.7	61.6	298.8	257.8	65.6
60	32.9	92.5	$1.3 \times 10^{-13}$	124.3	178.1	$1.3 \times 10^{-13}$	189.6	244.7	$1.3 \times 10^{-13}$
80	357.9	345.6	117.4	503.2	451.6	182.5	517.7	514.1	211.7
90	631.5	640.9	1916.9	671.4	702.9	2900.6	723.8	735.0	3822.3

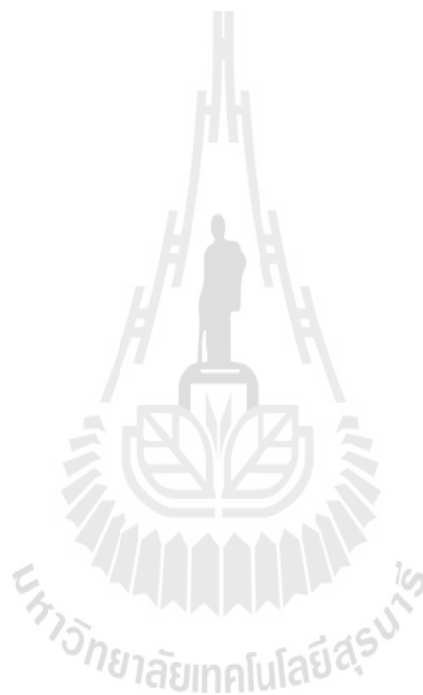
Maji and Sitharam (2008) use two artificial neural network models for the efficient prediction of the elastic moduli of jointed rocks from the elastic modulus of intact rocks and different joint parameters for various different confining pressure

conditions. The important joint parameters which are taken into consideration independently are joint frequency ( $J_n$ ), joint inclination parameter ( $n$ ) and joint roughness parameter ( $r$ ). The results of this analysis are compared with the experimental results of Arora (1987), Roy (1993) and Yaji (1984). First all the 896 experimental data sets are systematically analyzed to check the correlation among elastic modulus ratio (EMR, ratio of elastic modulus of jointed rock to the intact rock) and joint factor ( $J_f$ ) which takes care for the joint frequency, joint inclination and joint roughness. Finally, artificial neural network models provide significant advantage for handling problems involving practical discontinuous system. The present work supports the use of neural networks for the successful prediction of elastic properties jointed rocks and opens up the possibility of embedding neural networks into numerical modeling codes for modeling the structures in jointed rocks.

## **2.7 Conclusion of review**

The anisotropy can reduce the strength of rock mass. The rock mass compressive strengths decrease significantly as the number of joints increases. The increasing of joint set also reduces the strength of jointed rock mass. Joint orientations are one parameter that describes rock mass properties. The results indicate that the strength exhibit a U-shaped anisotropic behavior. The minimum strength was observed at the angle between the joint orientation and vertical axis through the specimen ranging from 30 to 40°. At the higher confining pressures the strengths are unaffected by joint orientation. Confining pressure is adequately effective to compressive strength. In term of deformability, the joint is also reflected as a reduction of elastic modulus, which indicates that the jointed rocks are less than

that of the nonjointed rock. The axial deformation behavior of the jointed model is highly nonlinear and joint orientation dependent. The existing methods to estimate the rock mass strength using empirical failure criteria and classification/characterisation systems are reviewed and evaluated the most suitable criterion for predicting the anisotropic strength of rocks.



## **CHAPTER III**

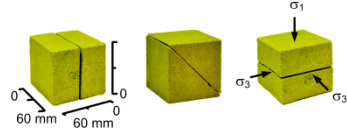
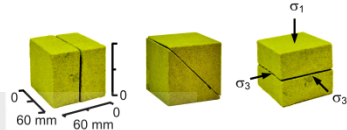
### **SAMPLE PREPARATION**

The rock samples used in this study are Phra Wihan sandstone. This rock is classified as fine-grained quartz sandstones with highly uniform texture and density (Boonsener and Sonpiron, 1997). They are prepared to obtain cubic specimens with nominal dimensions of  $60 \times 60 \times 60 \text{ mm}^3$  and  $80 \times 80 \times 80 \text{ mm}^3$ . Appendix A (Tables A.1 through A.4) gives dimensions and density of the rock samples. Artificial joints are induced into the intact specimens by developing a number of smooth and rough joints at different orientations. The specimens are prepared with three different characteristics for triaxial compression tests. Each case is shown in Table 3.1 and is described below.

**Case A:** The single joint specimens are prepared with joint making angles of 0, 45 and 90° to the major principal stress. The simulated joints are saw-cut surfaces (case A1) and tension-induced fractures (case A2). These specimens are prepared to study the effect of joint orientation and roughness. Case A1 shows single joint plane with smooth surface obtain by saw-cut device. Case A2 shows single joint plane simulated by a line load applied to obtain a tension-induced fracture diagonally across the sandstone block to study the effect of joint roughness. The normal to the fracture plane makes angles of 0, 45 and 90° with the major axis of the specimen (Figure 3.1). The joint roughness coefficient is averaged as 6.

**Case B:** One joint set specimens with four joint frequencies are prepared to study the effect of joint frequency. The numbers of joints are 1, 2, 3 and 4 joints

**Table 3.1** Specimens prepared for triaxial compression test with confining pressures of 0, 1, 3, 5, 7 and 12 MPa.

CASES		SPECIMENS
A: Effect of joint orientation and roughness	A1: Single joint specimen using saw-cut surface	
	A2: Single joint specimen using tension-induced fracture	
B: Effect of joint frequencies	B1: One joint set with joints parallel to the major principal stress direction	
	B2: One joint set with joints normal to the major principal stress direction	
C: Effect of number of joint sets	C: Three mutually perpendicular joint sets with different joint frequencies	

for each set (equivalent to 17 to 67 joints per meter). Joints are prepared by saw-cut method. This case is separated into 2 cases; cases B1 and B2. For case B1 the specimens are simulated by joints parallel to the major principal stress direction ( $\beta=90^\circ$ ) ( $\beta$  is the angle between the normal to the jointed plane and vertical axis through the specimen). For case B2 the specimens are simulated with joints normal to the major principal stress direction ( $\beta=0^\circ$ ).

**Case C:** Specimens with three mutually perpendicular joint sets are prepared. There are 1, 2, 3, 4 and 5 joints for each set (equivalent to 13 to 63 joints per meter). Joints are prepared by saw-cut method. This case is simulated to study the effect of joint set number under various confining pressures and joint frequencies.

All tests are conducted under ambient temperature and dry condition.

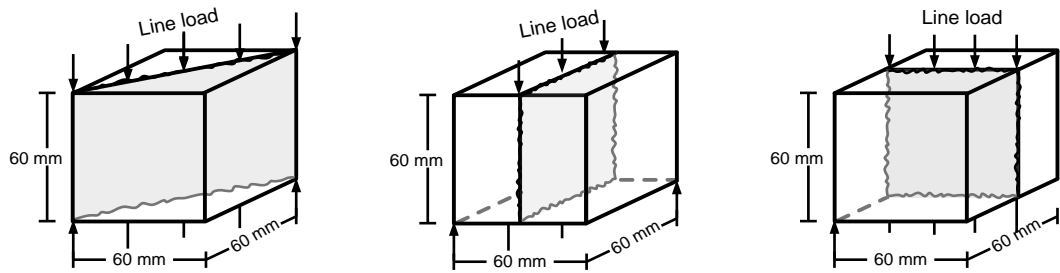


**Figure 3.1** Line load applied to obtain tension-induced fracture in specimen.



## CHAPTER IV

### TEST METHOD

#### 4.1 Introduction

The objective of this section is to describe the components of the true triaxial load frame and the test procedure for the triaxial compression tests.

#### 4.2 True triaxial loading device

The true triaxial loading device is developed in order to test rock specimens under biaxial, triaxial and polyaxial stress states (Komenthammasopon and Fuenkajorn, 2014). Figure 4.1 shows the true triaxial load frame. This device is divided into two parts; lateral and vertical load frame (Figure 4.2). Lateral load frame comprises two steel cross load frames, four

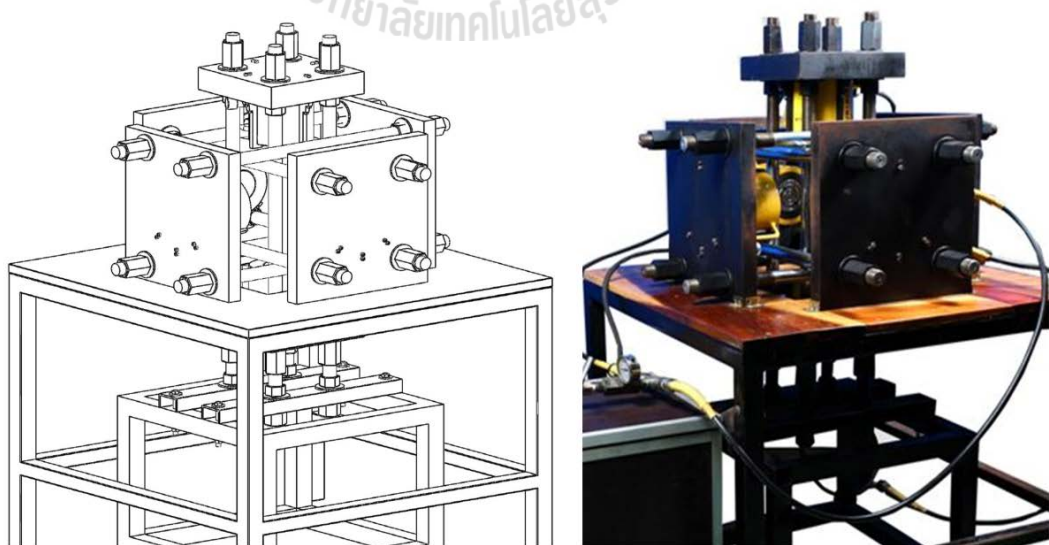


**Figure 4.1** True triaxial load frame used in this study.

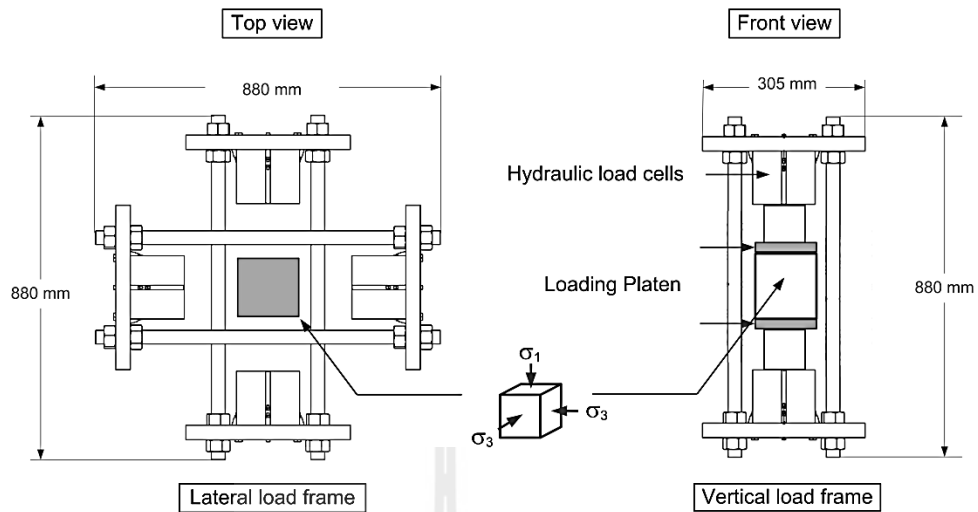


**Figure 4.2** Two main parts of true triaxial load frame.

hydraulic load cells and two hand pumps. And vertical load frame is the set of load frame which is inserted vertically into the crossed load frame consists of one steel cross load frame, two hydraulic load cells and one hand pump. Each load frame has two thick supporting steel plates ( $430 \times 430 \times 38 \text{ mm}^3$ ), connected by four steel rods with 36 millimeters in diameter. They support the structures of the two load cells. The load cells, installed at the supporting plates, are connected to the hand pumps which have the capacity of applying load up to 1000 kN. Besides the three main parts, other accessories designed to measure and monitor the rock stresses and deformations during testing include three 4-inch pressure gauges and three displacement dial gauges. The three pressure gauges are installed at three hand pumps to measure the applied load, while the three dial gauges measure the deformations along the principal axes for further strain calculation. During the test each set of the frame will apply the independent loads to provide different principal stresses ( $\sigma_1 \neq \sigma_2 \neq \sigma_3$ ) onto the rock specimens. This loading device can accommodate

the cubic or rectangular specimens of different sizes by adjusting the distances between the opposite steel loading platens.

### 4.3 Test procedure

A true triaxial load frame is used to apply axial stress ( $\sigma_1$ ) and constant lateral stresses ( $\sigma_3$ ) to the intact and jointed rock specimens. Before testing these specimens are wrapped with plastic film. Neoprene sheets are placed in all interfaces between the loading platens and specimen surfaces to minimize the friction (Figure 4.3). The testing system is always calibrated before

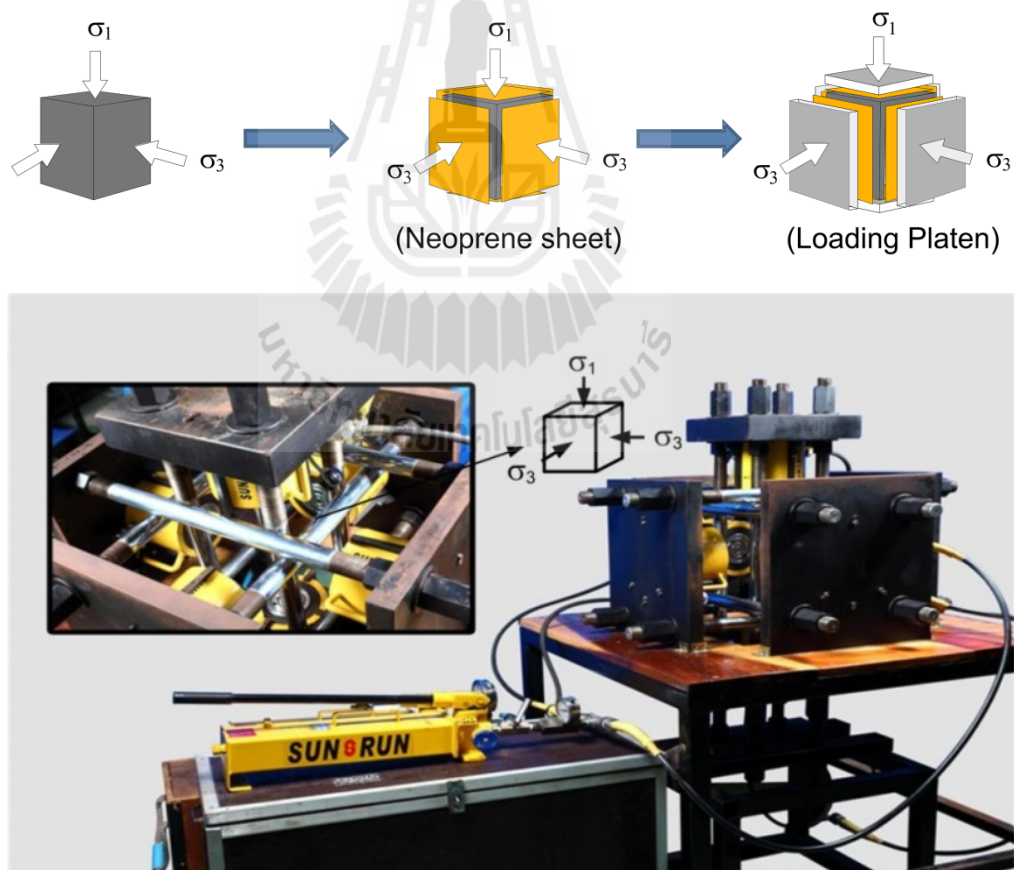


**Figure 4.3** Sample preparation before installed into the load frame.

testing using an electronic load cell. The axial stress is applied along the axial direction of the specimen. The constant lateral confining pressures ( $\sigma_2=\sigma_3$ ) on the specimens range from 0, 1, 3, 5, 7 to 12 MPa. After installing the jointed rock specimen into the load frame, four lateral hydraulic pumps apply loads to obtain the pre-defined magnitude of the uniform lateral stress ( $\sigma_3$ ) on the specimen. Simultaneously the axial stress is increased to the pre-defined  $\sigma_3$  value. The test is started by that the axial stress (major principal stress) is increased at a constant rate ( $\partial\sigma_1/\partial t$ ) of 0.1 MPa/s using the hydraulic pump. The specimen deformations are monitored in the three loading directions and are used to calculate the principal strains during loading. The readings are recorded every 8.4 kN (equivalent to the 100 psi on the pump pressure gauges) of load increment until the applied axial stress is dropped, which indicates the failure of the specimen. Photograph is taken of the post-test specimens and the modes of failure are identified. All tests are conducted under ambient temperature.

# **CHAPTER V**

## **TEST RESULTS**

### **5.1 Introduction**

The objective of this section is to present the experimental results for each case, which comprise post-test failure mode, stress-strain curves and strengths.

### **5.2 Post-test observations**

Figures 5.1 through 5.5 show some post-test specimens. Throughout these tests, the specimens showed different failure patterns, depending upon joint configurations, stress ratios, and stress orientations. The failure mode can be divided into 3 types:

(1) Extensile splitting mode: This mode of failure involves tensile fractures which almost are parallel to the major principal stress direction. The main mechanism of failure is the extensile failure through the intact pieces and pre-existing joints of the specimen.

(2) Sliding mode: This mode of failure is characterized by movement of the intact pieces of the jointed specimens parallel to the joint planes.

(3) Crushing mode: This mode of failure shows combination of large number of minute cracks, tensile fractures, crushed pieces and rock powder. There was always a combination of more than one mechanism.

The failure modes in each case are described below.

**Cases A1 and A2:** The single joint specimens are subjected to the applied load at various constant confining pressures. The results show that extensile splitting mode is observed with specimens of joint parallel to the major principal stress direction by tensile fractures parallel to the jointed planes. The extensile splitting mode is also observed with specimens of joint normal to the major principal stress direction by fracturing through the pre-existing joint planes. For case A1, the specimens with joint making angle of  $45^\circ$  show sliding mode under low confining pressures and combinations of extensile splitting fracture and sliding under high confining pressures. For case A2, single rough joint specimens show combinations of extensile splitting mode and sliding mode under all confining pressures.



**Figure 5.1** Some post-test specimens of case A1. Numbers in brackets indicate  $[\sigma_1, \sigma_3, \sigma_3]$  at failure in MPa.

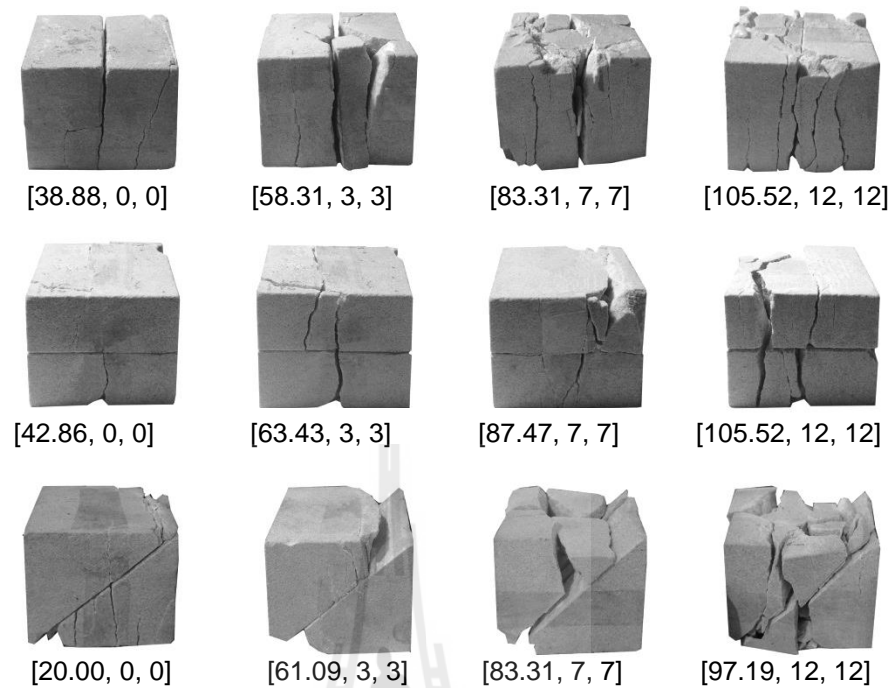


**Figure 5.2** Some post-test specimens of case A2. Numbers in brackets indicate  $[\sigma_1, \sigma_3, \sigma_3]$  at failure in MPa.

**Case B1:** Specimens with one joint set with four joint frequencies are tested under various confining pressures. The specimens show the failure of extensile splitting mode. The specimens at high confining pressures show large number of minute cracks.

**Case B2:** The one joint set specimens are tested with joints frequencies ranging from 1 to 4 joints per set. Under confining pressures and increasing axial stress the specimens show extensile splitting mode.

**Case C:** The three joint sets specimens show the failure of extensile splitting mode with large number of minute cracks. When increasing of joint frequency, the failures tend to show crushing mode.

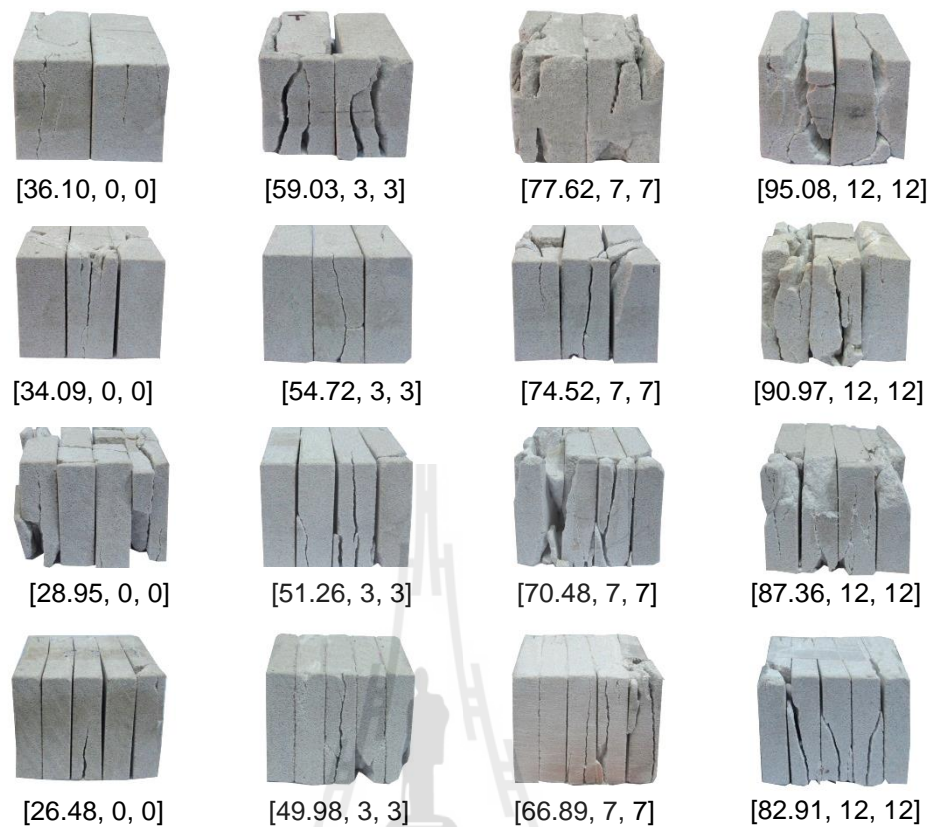


**Figure 5.3** Some post-test specimens of case B1. Numbers in brackets indicate  $[\sigma_1, \sigma_3, \sigma_3]$  at failure in MPa.

### 5.3 Stress-strain curves

Figures B.1 through B.16 (Appendix B) show stress-strain curves at different numbers of joint per meter and confining pressures for one joint set and three joint sets conditions. The stress-strain curves tend to show nonlinear behavior, particularly under high confining pressures and high joint frequencies. Under the same joint frequency, the stress and strain increase with confining pressure. The effect of the joint fracture on the rock is reflected as the reduction of stresses and increment of strains. Results for the compressive strength, elastic modulus and Poisson's ratio are calculated from these curves.

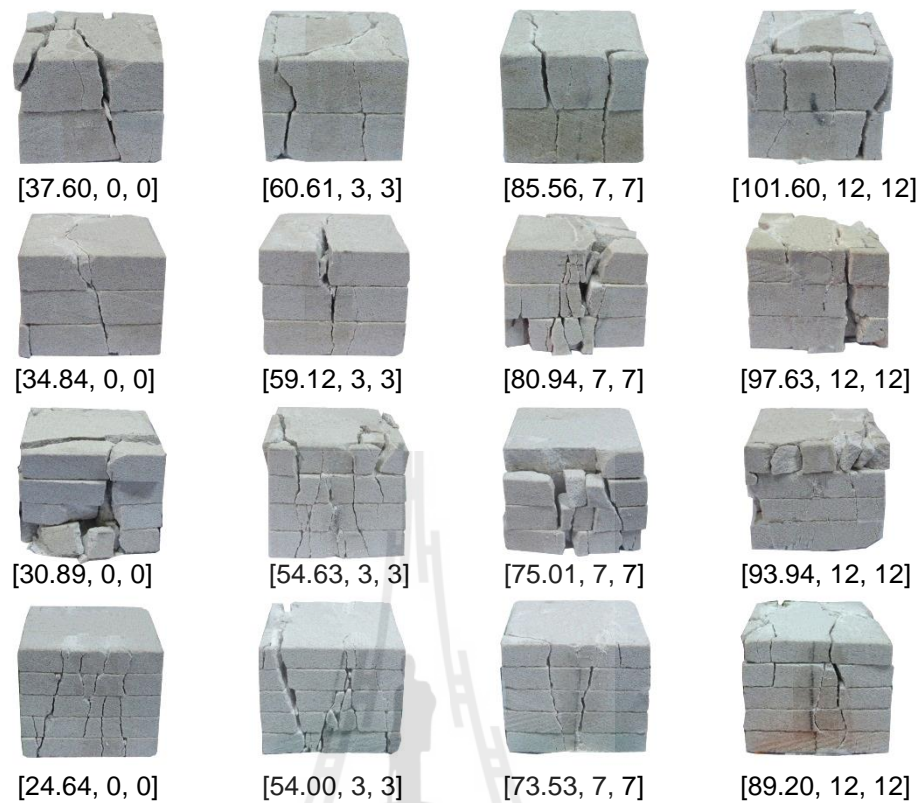


**Figure 5.4** Some post-test specimens of case B2. Numbers in brackets indicate  $[\sigma_1, \sigma_3, \sigma_3]$  at failure in MPa.



**Figure 5.5** Some post-test specimens of case C. Numbers in brackets indicate  $[\sigma_1, \sigma_3, \sigma_3]$  at failure in MPa.

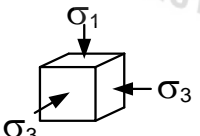
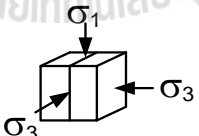
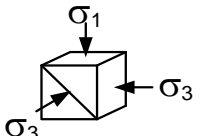
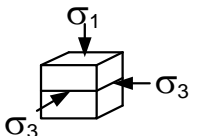
## 5.4 Strength results

The compressive strength results obtained from the laboratory testing are shown in Tables 5.1 through 5.5. Confining pressures vary from 0 to 12 MPa. Figures 5.6 through 5.9 show the major principal stresses for each case plotted as a function of confining pressure. The test results can be presented in terms of the octahedral shear stress at failure ( $\tau_{\text{oct},f}$ ) as a function of mean stress ( $\sigma_m$ ), as shown in Tables 5.6 through 5.10 and Figure 5.10, where (Jaeger et al., 2007):

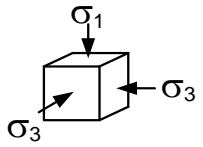
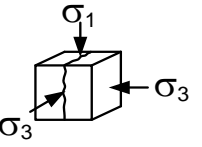
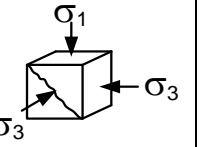
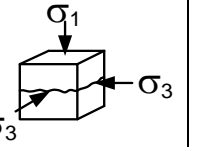
$$\tau_{\text{oct},f} = \left\{ \frac{1}{3} \left[ (\sigma_1 - \sigma_2)^2 + (\sigma_2 - \sigma_3)^2 + (\sigma_3 - \sigma_1)^2 \right] \right\}^{0.5} \quad (5.1)$$

$$\sigma_m = \frac{1}{3}(\sigma_1 + \sigma_2 + \sigma_3) \quad (5.2)$$

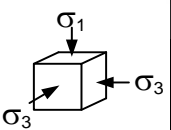
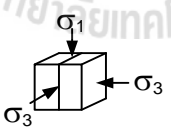
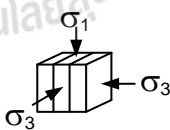
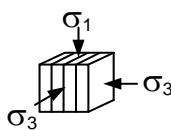
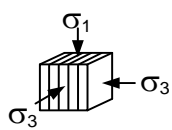
**Table 5.1** Strength results of case A1.

Confining pressures, $\sigma_3$ (MPa)	Major principal stresses at failure, $\sigma_1$ (MPa)			
	 -	 $\beta = 90^\circ$	 $\beta = 45^\circ$	 $\beta = 0^\circ$
0	43.34	36.10	0.00	37.64
1	47.80	43.08	13.88	44.65
3	63.40	59.03	36.10	60.61
5	74.10	68.80	44.43	71.35
7	88.90	77.62	49.98	85.56
12	106.87	95.08	81.92	101.60

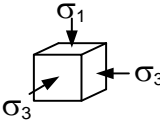
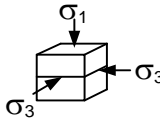
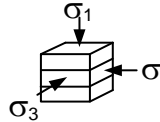
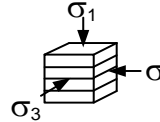
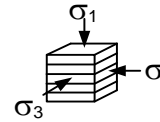
**Table 5.2** Strength results of case A2.

Confining pressures, $\sigma_3$ (MPa)	Major principal stresses at failure, $\sigma_1$ (MPa)			
	 -	 $\beta = 90^\circ$	 $\beta = 45^\circ$	 $\beta = 0^\circ$
0	43.34	38.88	21.49	42.86
1	47.80	42.00	30.55	44.57
3	63.40	58.31	55.54	63.43
5	74.10	72.20	69.42	72.20
7	88.90	83.31	83.31	87.47
12	106.87	105.52	97.19	105.52

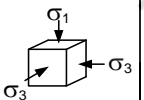
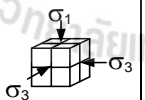
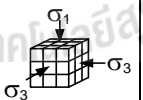
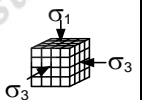
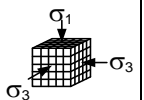
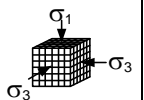
**Table 5.3** Strength results of case B1.

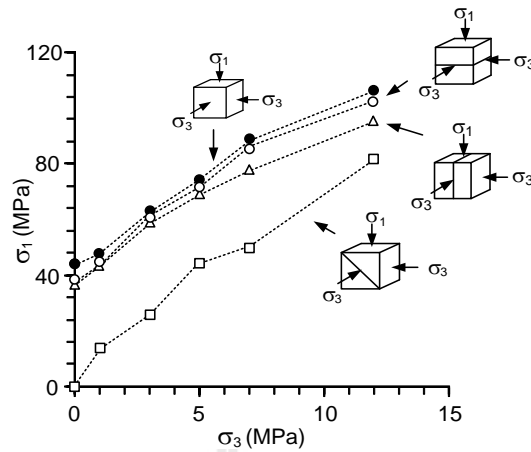
Confining pressures, $\sigma_3$ (MPa)	Major principal stresses at failure, $\sigma_1$ (MPa)				
	 Intact	 1 Joint/set	 2 Joints/set	 3 Joints/set	 4 Joints/set
0	43.34	36.10	34.09	28.95	26.48
1	47.80	43.08	41.11	36.57	34.76
3	63.40	59.03	54.72	51.26	48.98
5	74.10	68.80	65.98	64.65	59.40
7	88.90	77.62	74.50	70.48	66.89
12	106.87	95.08	90.97	87.36	82.91

**Table 5.4** Strength results of case B2.

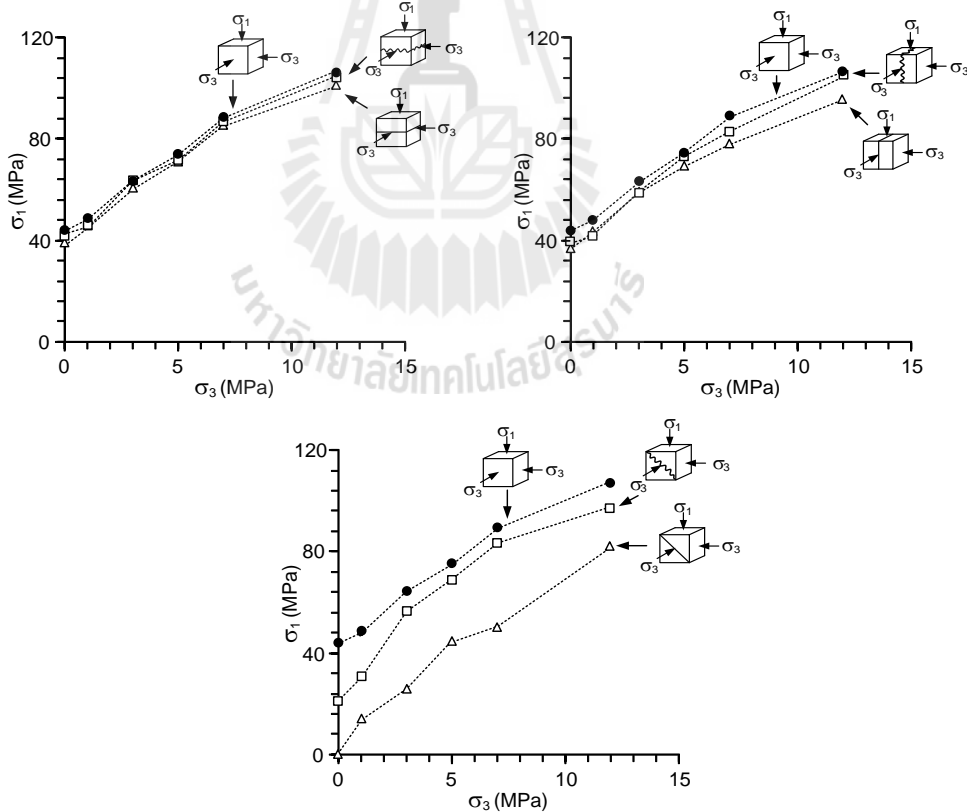
Confining pressures, $\sigma_3$ (MPa)	Major principal stresses at failure, $\sigma_1$ (MPa)				
	 Intact	 1 Joint/set	 2 Joints/set	 3 Joints/set	 4 Joints/set
0	43.34	37.64	34.84	30.89	28.64
1	47.80	44.65	42.16	39.25	37.60
3	63.40	60.61	59.12	54.63	54.00
5	74.10	71.35	70.04	67.67	63.73
7	88.90	85.56	80.94	75.01	73.53
12	106.87	101.60	97.63	30.89	89.20

**Table 5.5** Strength results of case C.

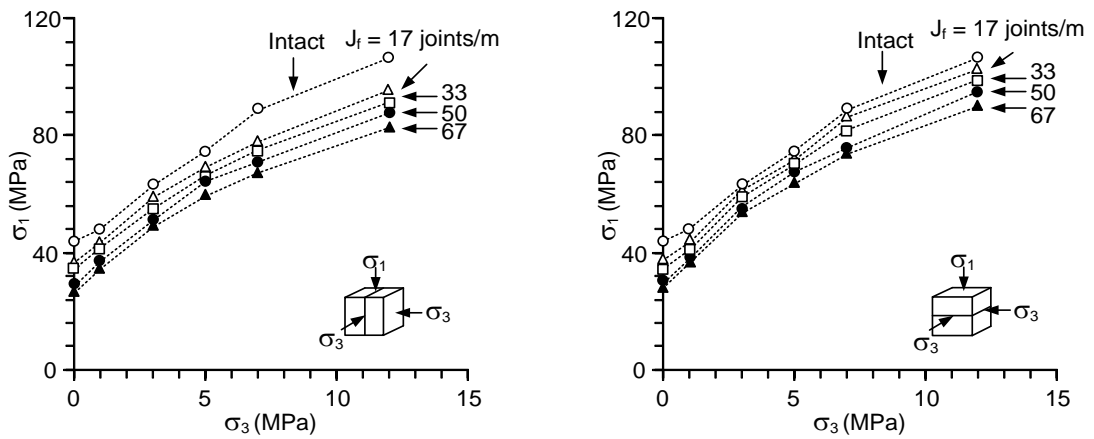
Confining pressures, $\sigma_3$ (MPa)	Major principal stresses at failure, $\sigma_1$ (MPa)					
	 Intact	 1 Joint/set	 2 Joints/set	 3 Joints/set	 4 Joints/set	 5 Joints/set
0	43.34	37.64	34.84	30.89	28.64	28.64
1	47.80	44.65	42.16	39.25	37.60	37.60
3	63.40	60.61	59.12	54.63	54.00	54.00
5	74.10	71.35	70.04	67.67	63.73	63.73
7	88.90	85.56	80.94	75.01	73.53	73.53
12	106.87	101.60	97.63	93.94	89.20	89.20



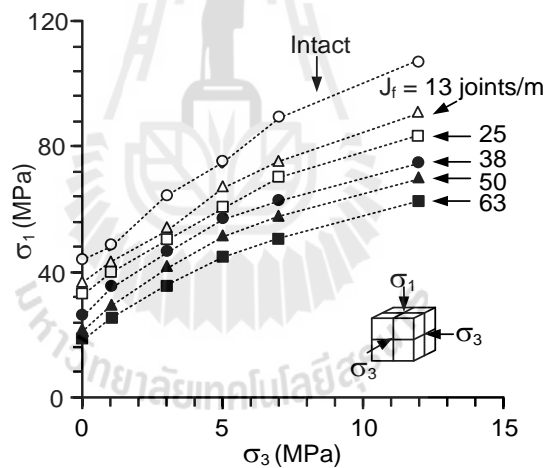
**Figure 5.6** Major principal stresses at failure as a function of confining pressure for various joint orientation (case A1).



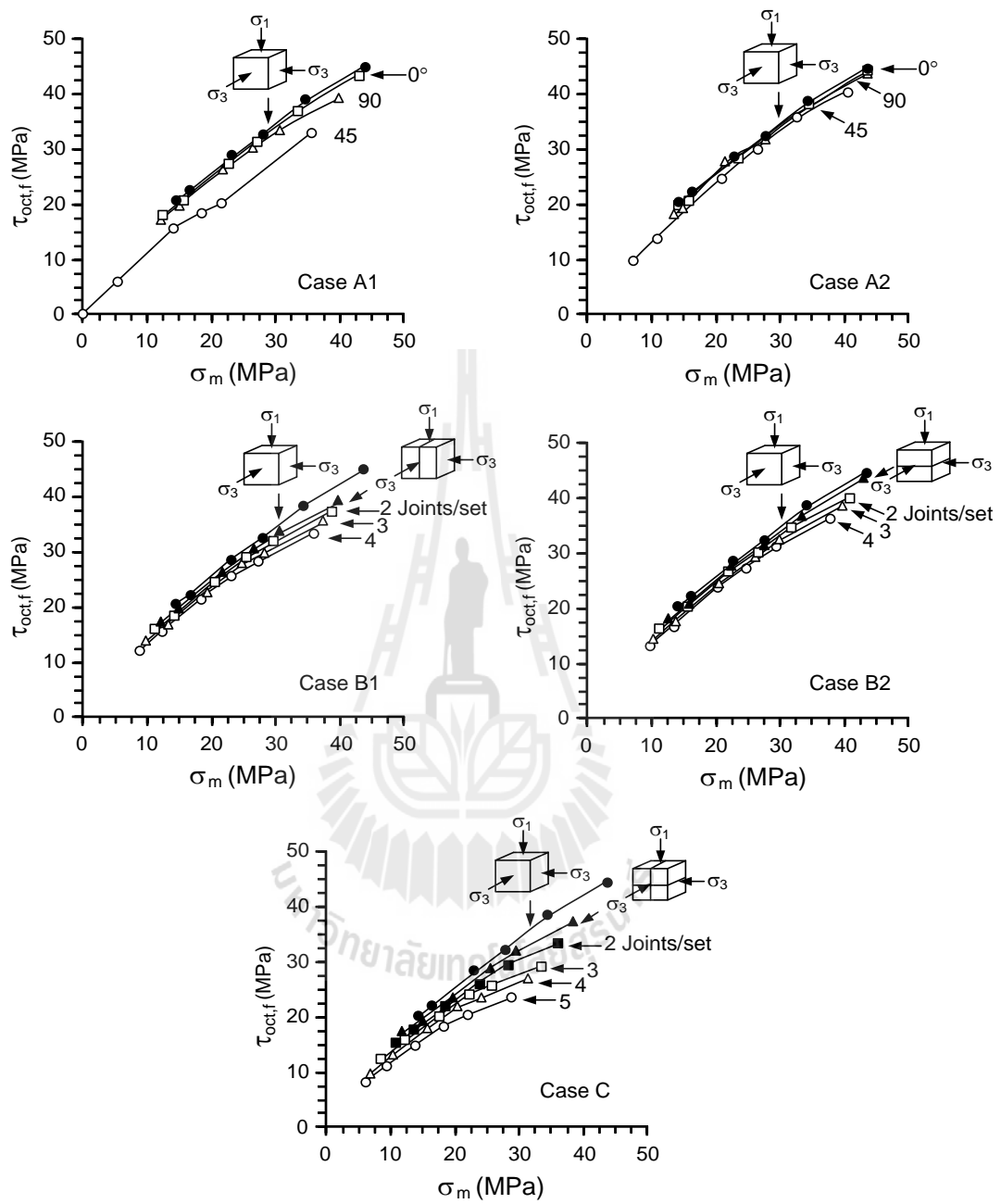
**Figure 5.7** Major principal stresses at failure are compared between smooth and rough surface at different orientation (case A2).



**Figure 5.8** Major principal stresses at failure as a function of confining pressure for case B1(left) and B2 (right).

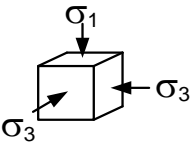
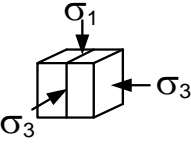
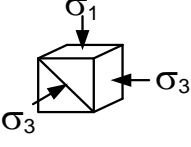
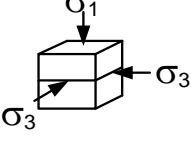


**Figure 5.9** Major principal stresses at failure as a function of confining pressure for case C.

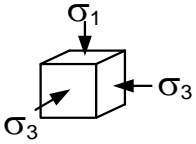
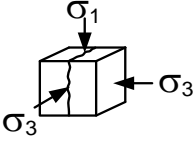
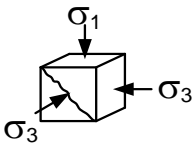
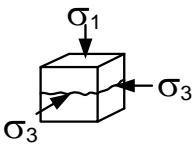


**Figure 5.10** Octahedral shear stresses at failure ( $\tau_{oct,f}$ ) as a function of mean stress ( $\sigma_m$ ).

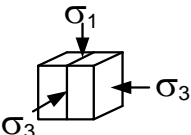
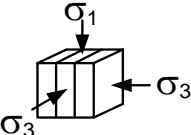
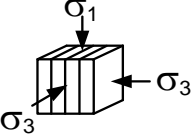
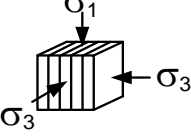
**Table 5.6** Octahedral shear stresses at failure (Case A1).

specimens	$\sigma_3$ (MPa)	$\sigma_1$ (MPa)	$\sigma_m$ (MPa)	$\tau_{oct,f}$ (MPa)
 Intact	0	43.34	14.45	20.43
	1	47.80	16.60	22.07
	3	63.40	23.14	28.48
	5	74.10	28.03	32.57
	7	88.90	34.33	38.64
	12	106.87	43.62	44.72
 $\beta = 90^\circ$	0	36.10	12.03	17.02
	1	43.08	15.03	19.84
	3	59.03	21.68	26.41
	5	68.80	26.27	30.08
	7	77.62	30.54	33.29
	12	95.08	39.69	39.16
 $\beta = 45^\circ$	0	0.00	0	0
	1	13.88	5.29	6.07
	3	36.10	14.03	15.60
	5	44.43	18.14	18.59
	7	49.98	21.33	20.26
	12	81.92	35.31	32.96
 $\beta = 0^\circ$	0	0	12.5	17.7
	1	1	15.5	20.6
	3	3	22.2	27.2
	5	5	27.1	31.3
	7	7	33.2	37.0
	12	12	42.9	43.7

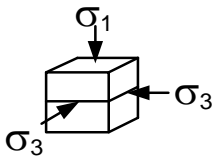
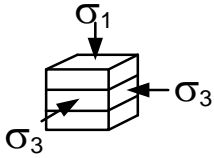
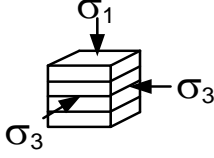
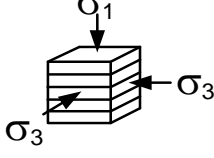
**Table 5.7** Octahedral shear stresses at failure (Case A2).

specimens	$\sigma_3$ (MPa)	$\sigma_1$ (MPa)	$\sigma_m$ (MPa)	$\tau_{oct,f}$ (MPa)
 Intact	0	43.34	14.45	20.43
	1	47.80	16.60	22.07
	3	63.40	23.14	28.48
	5	74.10	28.03	32.57
	7	88.90	34.33	38.64
	12	106.87	43.62	44.72
 $\beta = 90^\circ$	0	38.88	12.96	18.33
	1	42.00	14.67	19.16
	3	58.31	21.44	28.06
	5	72.20	27.4	31.68
	7	83.31	32.44	35.97
	12	105.52	43.17	44.09
 $\beta = 45^\circ$	0	21.49	7.16	10.13
	1	30.55	10.85	13.93
	3	55.54	20.51	24.77
	5	69.42	26.47	30.37
	7	83.31	32.44	35.97
	12	97.19	40.40	40.16
 $\beta = 0^\circ$	0	42.86	14.29	20.20
	1	44.57	15.52	20.54
	3	63.43	23.14	28.49
	5	72.20	27.4	31.68
	7	87.47	33.82	37.93
	12	105.52	43.17	44.09

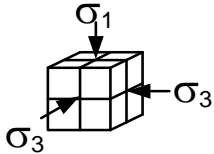
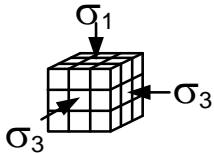
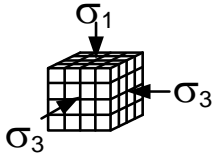
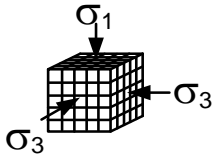
**Table 5.8** Octahedral shear stresses at failure (Case B1).

specimens	$\sigma_3$ (MPa)	$\sigma_1$ (MPa)	$\sigma_m$ (MPa)	$\tau_{oct,f}$ (MPa)
 1 Joint/set	0	36.10	12.03	17.02
	1	43.08	15.03	19.84
	3	59.03	21.68	26.41
	5	68.80	26.27	30.08
	7	77.62	30.54	33.29
	12	95.08	39.69	39.16
 2 Joints/set	0	34.09	11.36	16.07
	1	41.11	14.37	18.91
	3	54.72	20.24	24.38
	5	65.98	25.33	28.75
	7	74.50	29.50	31.82
	12	90.97	38.32	37.22
 3 Joints/set	0	28.95	9.65	13.65
	1	36.57	12.86	16.77
	3	51.26	19.09	22.75
	5	64.65	24.88	28.12
	7	70.48	28.16	29.92
	12	87.36	37.12	35.53
 4 Joints/set	0	26.48	8.83	12.48
	1	34.76	12.25	15.91
	3	48.98	18.33	21.68
	5	59.40	23.13	25.64
	7	66.89	26.96	28.23
	12	82.91	35.64	33.43

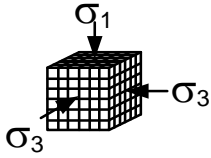
**Table 5.9** Octahedral shear stresses at failure (Case B2).

specimens	$\sigma_3$ (MPa)	$\sigma_1$ (MPa)	$\sigma_m$ (MPa)	$\tau_{oct,f}$ (MPa)
 1 Joint/set	0	37.64	12.5	17.7
	1	44.65	15.5	20.6
	3	60.61	22.2	27.2
	5	71.35	27.1	31.3
	7	85.56	33.2	37.0
	12	101.60	42.9	43.7
 2 Joints/set	0	34.84	11.61	16.42
	1	42.16	14.72	19.40
	3	59.12	21.71	26.46
	5	70.04	26.68	30.66
	7	80.94	31.65	34.86
	12	97.63	40.54	40.36
 3 Joints/set	0	30.89	10.3	14.6
	1	39.25	13.8	18.0
	3	54.63	20.2	24.3
	5	67.67	25.9	29.5
	7	75.01	29.7	32.1
	12	30.89	39.3	38.6
 4 Joints/set	0	28.64	9.5	13.5
	1	37.60	13.2	17.3
	3	54.00	20.0	24.0
	5	63.73	24.6	27.7
	7	73.53	29.2	31.4
	12	89.20	37.7	36.4

**Table 5.10** Octahedral shear stresses at failure (Case C).

specimens	$\sigma_3$ (MPa)	$\sigma_1$ (MPa)	$\sigma_m$ (MPa)	$\tau_{oct,f}$ (MPa)
 1 Joint/set	0	37.64	11.81	16.71
	1	44.65	14.63	19.28
	3	60.61	19.71	23.63
	5	71.35	25.43	28.90
	7	85.56	29.57	31.92
	12	101.60	38.23	37.09
 2 Joints/set	0	34.84	10.95	15.49
	1	42.16	13.75	18.03
	3	59.12	18.68	22.17
	5	70.04	23.32	25.90
	7	80.94	27.98	29.67
	12	97.63	35.77	33.61
 3 Joints/set	0	30.89	8.51	12.04
	1	39.25	12.23	15.88
	3	54.63	17.39	20.35
	5	67.67	22.24	24.39
	7	75.01	25.48	26.13
	12	93.94	32.81	29.42
 4 Joints/set	0	28.64	6.80	9.61
	1	37.60	10.07	12.83
	3	54.00	15.70	17.95
	5	63.73	20.41	21.79
	7	73.53	23.68	23.59
	12	89.20	31.14	27.07

**Table 5.10** Octahedral shear stresses at failure (Continue).

specimens	$\sigma_3$ (MPa)	$\sigma_1$ (MPa)	$\sigma_m$ (MPa)	$\tau_{oct,f}$ (MPa)
 5 Joints/set	0	28.64	6.04	8.55
	1	37.60	9.11	11.47
	3	54.00	13.74	15.18
	5	63.73	18.13	18.56
	7	73.53	21.54	20.57
	12	89.20	28.75	23.68



# CHAPTER VI

## STRENGTH CRITERIA

### 6.1 Introduction

The objective of this section is to assess the predictive capability of some rock mass strength criteria developed by Hoek-Brown, Sheorey, Yudhbir and Ramamurthy-Arora by comparing with the test results.

### 6.2 Strength results

The triaxial compressive strength of the test models decreases with increasing joint frequency for all cases. For single joint set specimens, the strength of the specimens with joints normal to  $\sigma_1$  axis always yields greater strength than those with joints parallel to  $\sigma_1$  axis. The lowest strengths are obtained when the joint planes make angles  $45^\circ$  with the major principal stress. It can be postulated that the rock mass model strengths would be lower if the applied stress makes oblique angles with the joint planes. The single joints studied here are simulated from smooth saw-cut surfaces and tension-induced fractures. The strengths of the rock mass model for saw-cut surfaces are lower than those of the tension-induced fractures. The drop of strengths for the three joint set specimens tends to be more rapid than those of the single joint set specimens. One important finding from the study is that the decrease of rock mass strength as the joint frequency increases tends to be equally act throughout the ranges of confining pressures used here (1-12 MPa).

### 6.3 Strength criteria

Four strength criteria that are commonly used to determine rock mass strength are compared against the triaxial strength data obtained from three mutually perpendicular joint set specimens. These include the Hoek and Brown (1980), Sheorey (1989), Yudhbir (1983) and Ramamurthy and Arora (1994) criteria. Exhaustive reviews of these criteria have been given elsewhere (Edelbro et al., 2007; Sheorey, 1997), and hence will not be repeated here. They are all formulated in the terms of  $\sigma_1$  and  $\sigma_3$ . The predictive capability of these strength criteria is determined and compared using the coefficient of correlation ( $R^2$ ) as an indicator. The higher  $R^2$  value indicates the better predictability of the criterion. Governing equations of these strength criteria used in the regression are described briefly below.

The Hoek and Brown criterion defines the relationship between the major and minor stresses at failure by

$$\sigma_1 = \sigma_3 + \sqrt{m\sigma_c\sigma_3 + s\sigma_c^2} \quad (6.1)$$

where  $m$  and  $s$  are constants which depend on the properties of the rock.

The sheorey criterion defines the relationship between the major and minor principal stresses at failure by:

$$\sigma_1 = \sigma_{cm} \left( 1 + \frac{\sigma_3}{\sigma_{tm}} \right)^{b_m} \quad (6.2)$$

where  $b_m$  is a constant,  $\sigma_{cm}$  is the uniaxial compressive strength of rock mass, and  $\sigma_{tm}$  is the uniaxial tensile strength of rock mass.

Yudhbir et al. (1983) modify the original Bieniawski criterion (1974). The new criterion can be written in a more general form as:

$$\frac{\sigma_1}{\sigma_c} = A + B \left( \frac{\sigma_3}{\sigma_c} \right)^\alpha \quad (6.3)$$

where A is a dimensionless parameter whose value depends on rock mass quality, and B is material constant depending on rock type

Ramamurthy and Arora (1994) present a nonlinear shear strength response of intact rocks in the form of a modified Mohr-Coulomb theory. For a jointed rock mass the criterion can be written as:

$$\frac{\sigma_1 - \sigma_3}{\sigma_3} = B \left( \frac{\sigma_c}{\sigma_3} \right)^\alpha \quad (6.4)$$

where  $\alpha$  and B are the material constants for the rock mass, and  $\sigma_{cm}$  is the uniaxial compressive strength of rock mass. The results show that  $\sigma_{cm}$  is the most effective parameter to dictate the strength of rock mass. However, this criterion can not be used to predict rock mass strength under unconfined condition. Ramamurthy suggests an alternative formula in terms of joint factor  $J_f$  which can be written by:

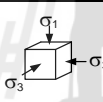
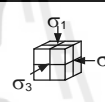
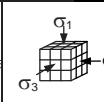
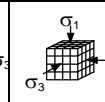
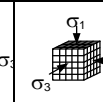
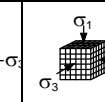
$$\sigma_{cm} = \sigma_c \exp(-0.008J_f) \quad (6.5)$$

$$B = B_i / 0.13 \exp \left[ 2.037 \left( \frac{\sigma_{cm}}{\sigma_c} \right)^{0.5} \right] \quad (6.6)$$

$$\alpha = \alpha_i \left( \sigma_{cm} / \sigma_c \right)^{0.5} \quad (6.7)$$

The constants calculated from SPSS program for strength criteria are shown in Table 6.1. All criteria can provide good correlation with the test data, with  $R^2$  greater than 0.9. Figure 6.1 compares the test data with curve fits of the strength criteria in the terms of  $\sigma_1$  as a function of  $\sigma_3$  at failure. Figure 6.2 shows the decrease of parameters  $m$  and  $s$  of Hoek-Brown criterion as the joint frequency increases. The parameters  $m$  and  $s$  of one joint set specimen are greater than those of the three joint set specimens. The uniaxial compressive strengths of rock mass models predicted by sheorey and Ramamurthy-Arora strength criteria are shown in Figure 6.3.

**Table 6.1** Strength criteria and their constants calibrated from the test data.

Specimens	Parameters						
Hoek-Brown (1980) $\sigma_1 = \sigma_3 + (m\sigma_c \sigma_3 + s\sigma_c^2)^a$	$m$	14.10	11.30	9.22	7.89	6.03	4.83
	$s$	1.0	0.7	0.5	0.4	0.3	0.2
	$a$	0.5	0.5	0.5	0.5	0.5	0.5
	$R^2$	0.992	0.969	0.984	0.971	0.979	0.986
Sheorey et al. (1989) $\sigma_1 = \sigma_{cm}(1 + \sigma_3/\sigma_{tm})^{b_m}$	$\sigma_{cm}$	41.8	35.8	31.0	26.5	22.9	19.6
	$\sigma_{tm}$	2.6	2.1	1.8	1.4	1.2	1.0
	$b_m$	0.54	0.51	0.48	0.47	0.46	0.45
	$R^2$	0.991	0.986	0.988	0.991	0.992	0.997
Yudhbir et al. (1983) $\sigma_1/\sigma_c = A + B(\sigma_3/\sigma_c)^\alpha$	$A$	0.97	0.82	0.70	0.59	0.50	0.43
	$B$	4.04	3.64	3.31	2.98	2.71	2.44
	$\alpha$	0.79	0.76	0.72	0.70	0.68	0.65
	$R^2$	0.986	0.984	0.986	0.987	0.989	0.993
Ramamurthy-Arora (1994) $(\sigma_1 - \sigma_3)/\sigma_3 = B(\sigma_{cm}/\sigma_3)^\alpha$	$\sigma_{cm}$	43.3	37.4	32.3	27.5	24.0	20.7
	$B$	3.19	3.15	3.13	3.08	3.00	2.90
	$\alpha$	0.69	0.69	0.69	0.69	0.69	0.69
	$R^2$	0.989	0.973	0.979	0.980	0.997	0.995

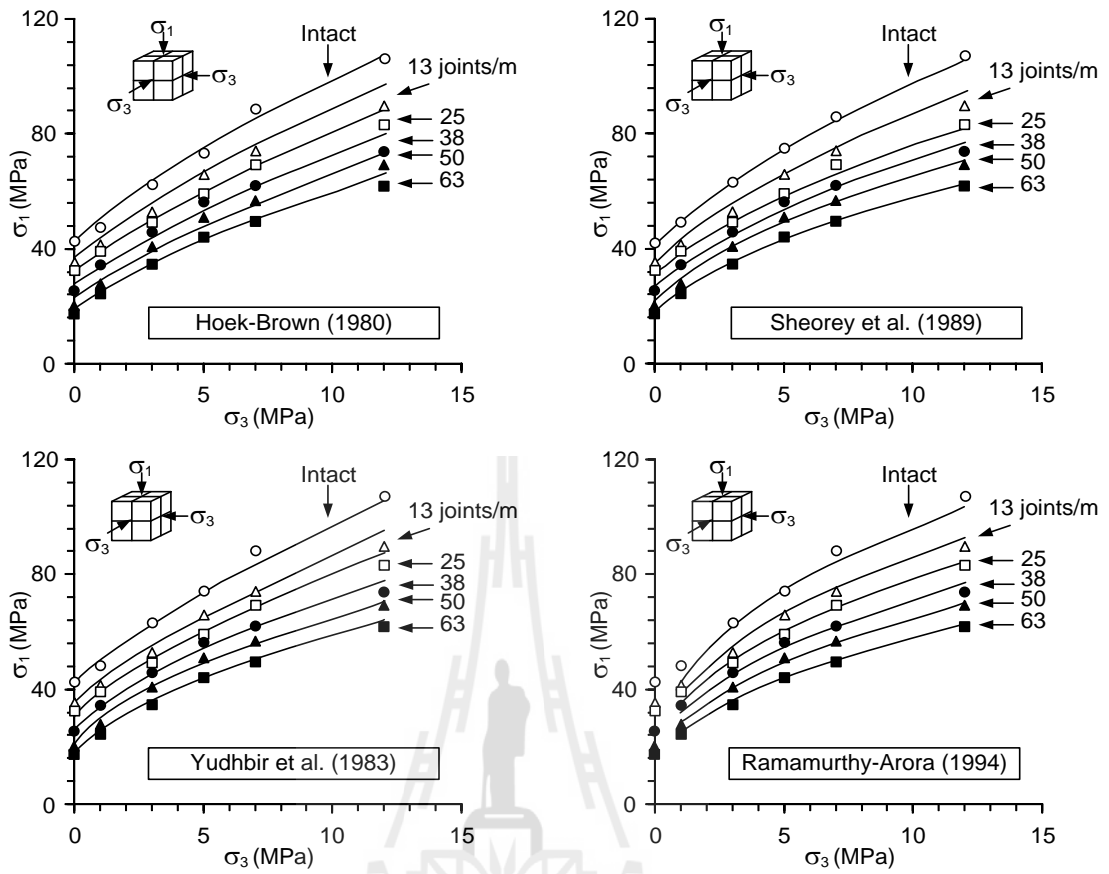


Figure 6.1 Test data (points) and curve fits of four strength criteria.

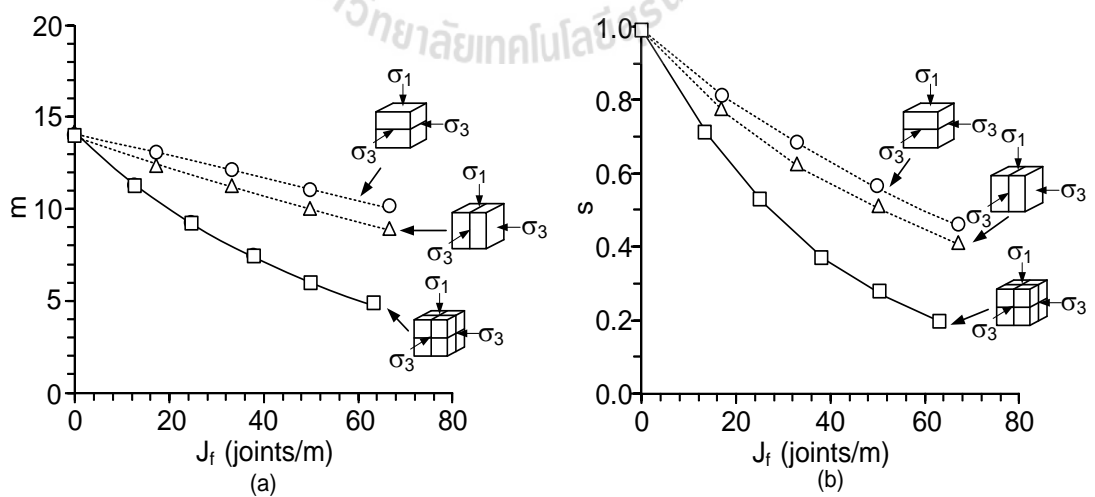
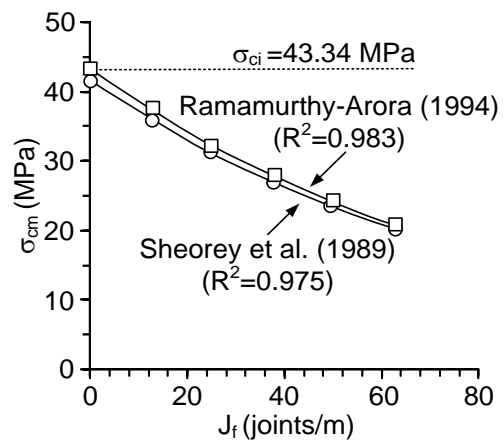
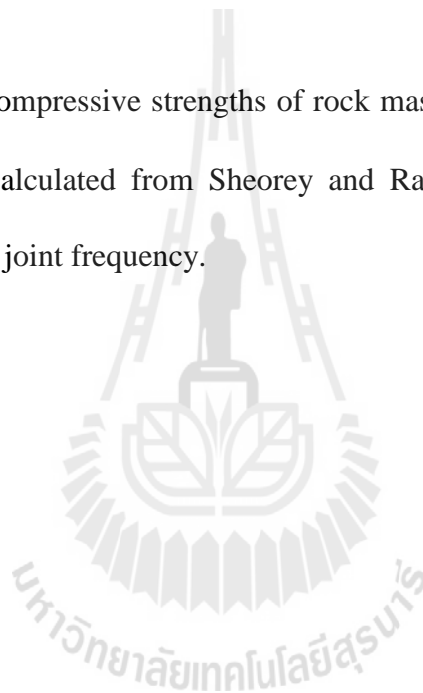


Figure 6.2 Hoek-Brown parameters  $m$  and  $s$  as a function of joint frequency.



**Figure 6.3** Uniaxial compressive strengths of rock mass model ( $\sigma_{cm}$ ) with three joint sets,  $\sigma_{cm}$  calculated from Sheorey and Ramamurthy-Arora criteria as a function of joint frequency.



# CHAPTER VII

## DEFORMATION MODULUS

### 7.1 Introduction

The objective of this section is to determine the effects of joint frequency, orientation and set numbers on the deformation modulus of rock mass model and to assess the predictive capability of the empirical criteria developed by Goodman (1970), Yoshinaka and Yamabe (1986) and Ramamurthy (2001) by comparing with the test results.

### 7.2 Deformation modulus

The deformation parameters are determined from the tangent of the stress-strain curves at about 50% of the failure stress. An attempt is made to calculate the deformation moduli along the three loading directions. It is initially assumed that the Poisson's ratio ( $\nu$ ) of the specimens is the same for all principal planes. The deformation moduli along the major, intermediate and minor principal directions can then be calculated by (Jaeger et al., 2007):

$$\varepsilon_1 = \sigma_1/E_1 - \nu (\sigma_2/E_2 + \sigma_3/E_3) \quad (7.1)$$

$$\varepsilon_2 = \sigma_2/E_2 - \nu (\sigma_1/E_1 + \sigma_3/E_3) \quad (7.2)$$

$$\varepsilon_3 = \sigma_3/E_3 - \nu (\sigma_1/E_1 + \sigma_2/E_2) \quad (7.3)$$

where  $\varepsilon_1$ ,  $\varepsilon_2$  and  $\varepsilon_3$  are the major intermediate and minor principal strains, and  $E_1$ ,  $E_2$  and  $E_3$  are the deformation moduli along the major, intermediate and minor principal directions. The results show that for one joint set specimens the deformation moduli that are parallel to the joint planes show highest values compared to those that are normal to the joints. This is true for all joint frequencies as shown in Figure 7.1. For three joint set specimens, the deformation moduli are similar for all principal directions (Figure 7.2). The deformation modulus decreases with increasing joint frequency, and tends to increase with confining pressure (Figure 7.3). The Poisson's ratio of the specimens with different joint frequencies ranges from 0.23 to 0.29 (Figure 7.4). The effect of the confining pressure on the Poisson's ratio cannot be clearly observed from the test results. This may be due to the intrinsic variability among the test models.

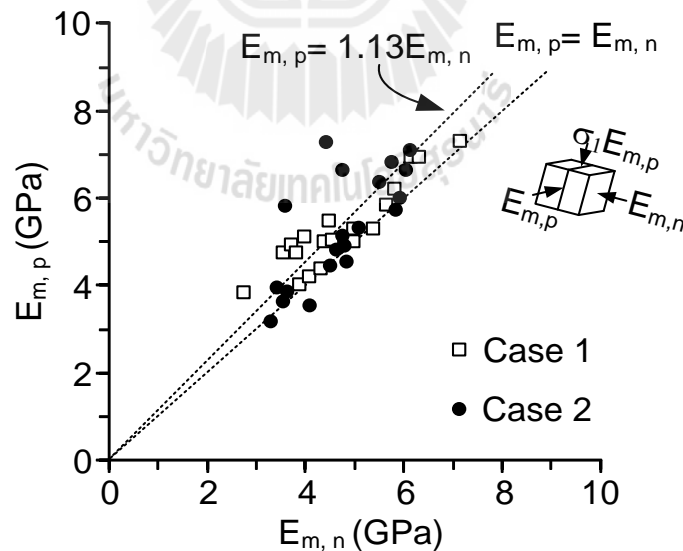


**Figure 7.1** Deformation moduli parallel joint plane as a function those normal to joint plane.

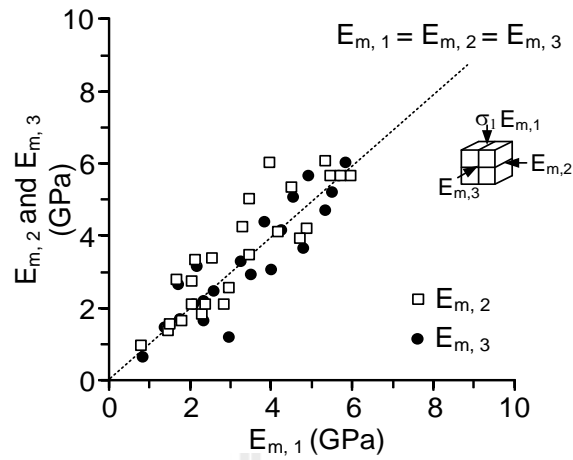


**Figure 7.2** Deformation moduli calculated along the intermediate and minor principal axes as a function of the major principal axis.

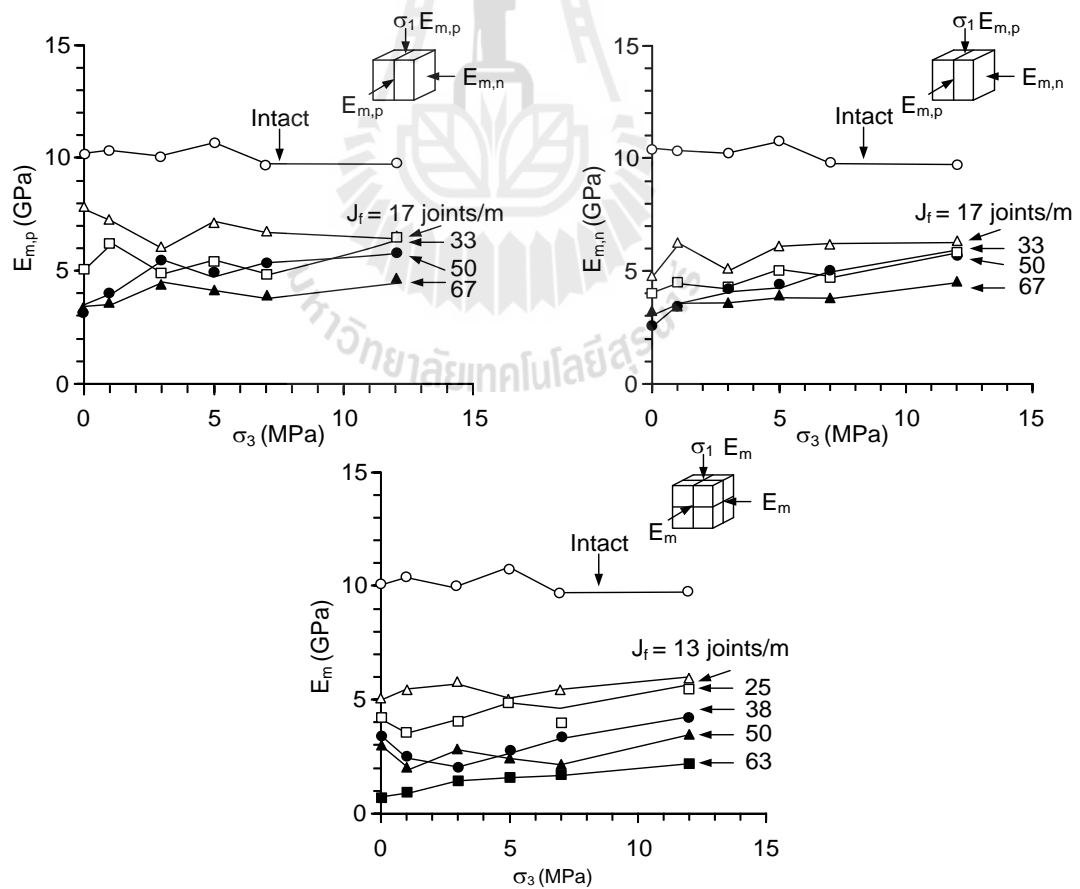


**Figure 7.3** Deformation modulus as a function of confining pressure.

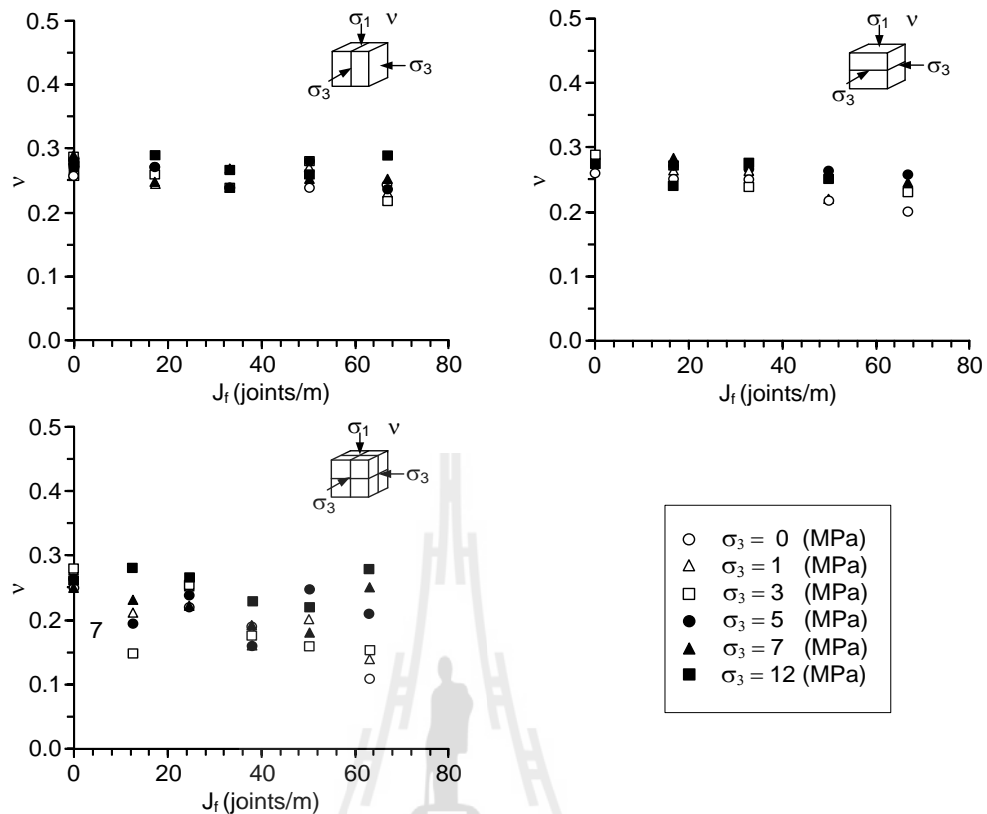


**Figure 7.4** Poisson's ratio values as a function of joint frequency for all cases.

### 7.3 Deformability criteria

Three empirical criteria are used to estimate rock mass deformation modulus ( $E_m$ ). They include the Goodman (1970), Yoshinaka and Yamabe (1986) and Ramamurthy criteria (2001). The deformation modulus calculated from the triaxial compression test results for each case are compared with the rock mass deformability criteria. A brief description of each criterion is described below.

Goodman (1970) has presented a method to evaluate the elastic constants for an equivalent continuous material representative of a rock mass regularly crossed by a single set of joints using the concept of joint stiffness. The criterion can be written as:

$$\frac{1}{E_r} = \frac{1}{k_n s} + \frac{1}{E_n} \quad (7.4)$$

where  $E_r$  is the rock deformation modulus,  $k_n$  is the joint normal stiffness,  $s$  is the average joint spacing and  $E_n$  is the equivalent deformation modulus.

Yoshinaka and Yamabe (1986) study the stress-strain behavior of a discontinuous rock mass. Based on the concept of joint stiffness, an equation to evaluate the deformation of jointed rock is derived as:

$$\frac{1}{E_t} = \left[ \frac{1}{E_c} + \frac{\cos^2 \theta_1}{L_1} \left( \frac{\sin^2 \theta_1}{k_{s1}} + \frac{\cos^2 \theta_1}{k_{n1}} \right) + \frac{\cos^2 \theta_2}{L_2} \left( \frac{\sin^2 \theta_2}{k_{s2}} + \frac{\cos^2 \theta_2}{k_{n2}} \right) \right]^{-1} \quad (7.5)$$

where  $E_c$  is elastic modulus of intact rock,  $\theta_1$ ,  $\theta_2$  are the angles of inclination from the applied plane of major principal stress,  $L_1$  and  $L_2$  are joint spacings and  $k_s$  and  $k_n$  are joint stiffnesses.

Ramamurthy (2001) defines the relationship between the ratios of moduli,  $E_{tj}/E_{ti}$  and  $J_f$ , which can be represented by:

$$\frac{E_{tj}}{E_{ti}} = \exp(-1.15 \times 10^{-2} J_f) \quad (7.6)$$

where  $E_{tj}$  is the jointed rock deformation modulus,  $E_{ti}$  is the intact deformation modulus, and  $J_f$  is the joint factor which has been defined by the following relation:

$$J_f = \frac{J_n}{n \cdot r} \quad (7.7)$$

where  $J_n$  is joint frequency, i.e. number of joints per meter,  $n$  is inclination parameter depending upon the orientation of the joint  $\beta$  (Table 2.1),  $r$  is joint strength parameter dependent upon the joint condition (Table 2.2).

The comparisons between the test data and predictions are shown in Figure 7.5. Results indicated that the Goodman (1970) and Yoshinaka and Yamabe (1986) equations give good prediction for the deformation modulus normal to joint planes,  $E_{m,n}$  ( $R^2=0.954$ ). Yoshinaka and Yamabe (1986) equation also predicts the deformation modulus of rock mass model with three joint sets given  $R^2=0.839$ . Ramamurthy (2001) equation gives a fair estimation for the deformation modulus normal to the joint planes,  $E_{m,n}$  ( $R^2=0.869$ ). It gives a slightly better prediction ( $R^2=0.968$ ) for the deformation modulus that is parallel to the joint planes ( $E_{m,p}$ ).

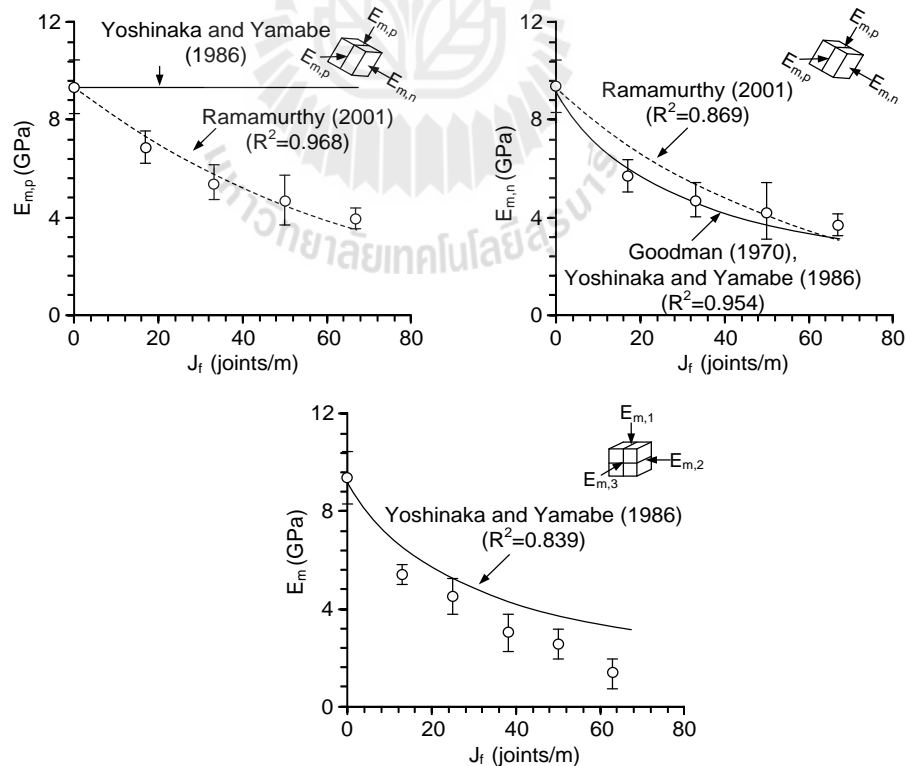


**Figure 7.5** Comparisons between the test data (points) and predictions (lines).

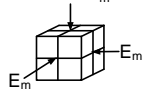
## 7.4 Modified Goodman's equation

The Goodman (1970) equation is modified to determine deformation modulus in different directions. It is proposed as:

$$\frac{1}{E_m} = \frac{N}{k_n s} + \frac{1}{E_i} \quad (7.8)$$

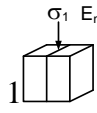
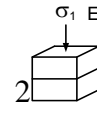
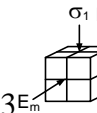
where  $E_m$  is the jointed rock deformation modulus,  $E_i$  is the intact deformation modulus,  $s$  is the joint spacing,  $k_n$  is the joint normal stiffness and  $N$  is a parameter which value depends on joint set direction (Table 7.1). The equation shows well prediction for all cases as shown in Table 7.2 and Figure 7.6. The proposed equation however can only predict the deformation modulus in the directions normal and parallel to the joint planes.

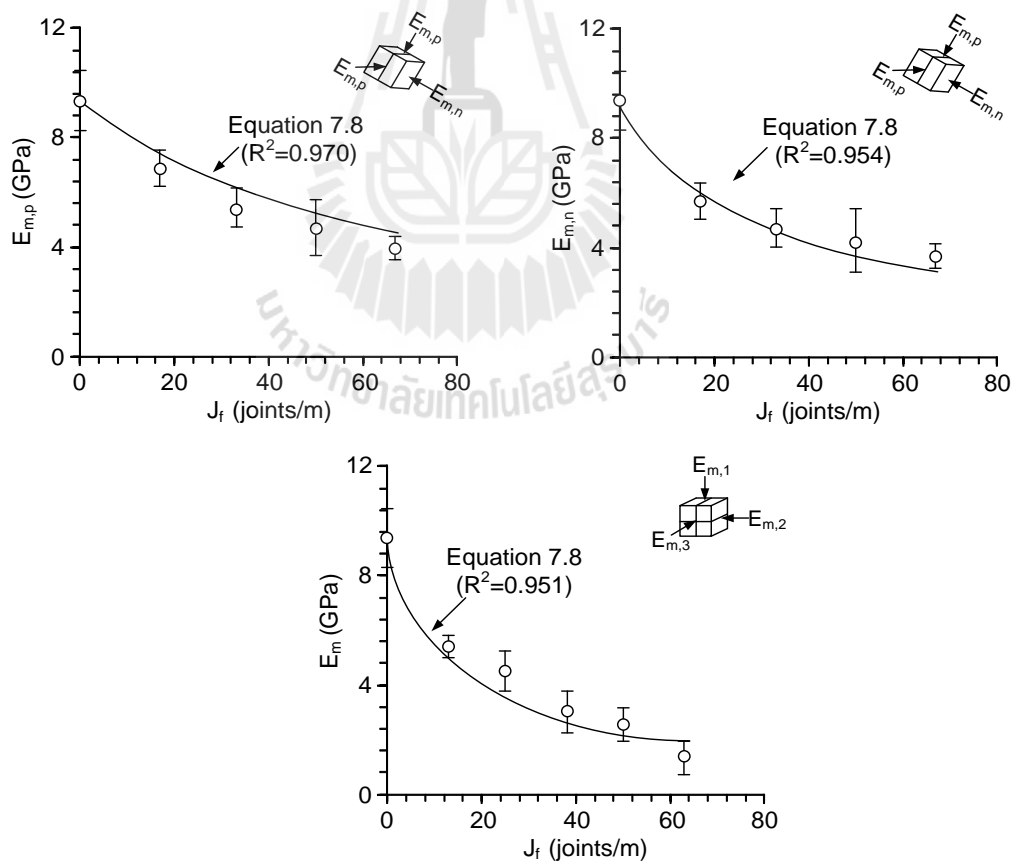
**Table 7.1** Parameter  $N$  defined for modified Goodman's equation.

Number of joint sets	Orientation of joint set to $\sigma_1$	Case	$N$
1	1 parallel	$\sigma_1 E_{m,p}$ 	0.5*
1	1 normal	$\sigma_1 E_{m,n}$ 	1.0* (original Goodman)
2	1 parallel, 1 normal	$\sigma_1 E_{m,p} E_{m,n}$ 	1.5
3	2 parallels, 1 normal	$\sigma_1 E_m$ 	2.0*

\* Verified by the test results

**Table 7.2** Coefficient of correlation of each criterion.

Criteria	$R^2$		
	Case 1 $\sigma_1 E_{m,p}$ 	Case 2 $\sigma_1 E_{m,n}$ 	Case 3 $\sigma_1 E_m$ 
Goodman (1970)	-	0.954	-
Yoshinaka and Yamabe (1986)	-	0.954	0.839
Ramamurthy (2001)	0.968	0.869	-
Modified Goodman	0.970	0.954	0.951

**Figure 7.6** Comparisons between the test data (points) and modified Goodman equation (lines).

## CHAPTER VIII

### DISCUSSIONS AND CONCLUSIONS

#### 8.1 Discussions and conclusions

Triaxial compressive strength tests have been performed to determine strength and deformability of rock mass model with multiple joint sets and joint frequencies under confining pressures up to 12 MPa. The results indicate that the triaxial compressive strength of the test models decreases with increasing joint frequency for all cases. These generally agree with the experimental observations by Ramamurthy and Arora (1994) on jointed specimens of plaster of Paris. For single joint set specimens, the strength of the specimens with joints normal to  $\sigma_1$  axis always yields greater strength than those with joints parallel to  $\sigma_1$  axis. The lowest strengths are obtained when the joint planes make angles  $45^\circ$  with the major principal stress. These agree reasonably well with experimental observations by Nasser et al. (2002), Colak and Unlu (2004), Goshtasbi et al. (2006) and Saroglou and Tsiambaos (2008). It can be postulated that the rock mass model strengths would be lower if the applied stress makes oblique angles with the joint planes. The single joints are simulated from both smooth saw-cut surfaces and tension-induced fracture. The strengths of saw-cut surface specimens are lower than those of the tension-induced fractures. The strengths of the rock mass model with smooth joint surfaces obtained here, therefore, represent the lower bound of the strengths of actual rock mass where most fractures are rough. The decrease of the strengths for the three joint set specimens tends to be more rapid

than those of the single joint set specimens. One important finding from the study is that the decrease of rock mass strength as the joint frequency increases tends to be equally act throughout the ranges of confining pressures used here (1-12 MPa).

Four strength criteria that are commonly used to determine rock mass strength are compared against the triaxial strength data obtained from three mutually perpendicular joint set specimens. These include the Hoek and Brown (1980), Sheorey (1989), Yudhbir (1983) and Ramamurthy and Arora (1994) criteria. All strength criteria used here give a good estimation of the specimen compressive strengths. The Hoek-Brown criterion can effectively describe the effect of joint frequency on the strength results. The parameter  $s$  decreases rapidly with increasing joint frequency while parameters  $m$  tend to be insensitive with the joint frequency, ranging between 4.83 and 14.10. The parameters  $m$  and  $s$  of the one joint set specimens are higher than those of the three joint set specimens. This suggests that decreasing of joint set numbers will increase the rock mass strength. The uniaxial compressive strength of rock mass model ( $\sigma_{cm}$ ) decreases with increasing joint frequency, which agrees reasonably well with the  $\sigma_{cm}$  calculated from Sheorey and Ramamurthy-Arora criteria.

The deformation parameters are determined from the tangent of the stress-strain curves at about 50% of the failure stress. An attempt is made to calculate the deformation moduli along the three loading principal directions. The results show that for one joint set specimens the deformation moduli that are parallel to the joint planes show highest values compared to those that are normal to the joints. This is true for all joint frequencies. For three joint set specimens, the deformation moduli are similar for all principal directions. The deformation modulus decreases with

increasing joint frequency, and tends to increase with the confining pressure. These agree with the experimental observations by Tiwari and Rao (2006). The Poisson's ratio of the specimens with different joint frequencies ranges from 0.23 to 0.29. The effect of the confining pressure on the Poisson's ratio cannot be clearly observed from the test results. This may be due to the intrinsic variability among the test models.

Three empirical criteria are used to estimate rock mass deformation modulus ( $E_m$ ). They include the Goodman (1970), Yoshinaka and Yamabe (1986) and Ramamurthy criteria (2001). The deformation modulus calculated from the triaxial compression test results for each case are compared with the rock mass deformability criteria. The results show that Goodman (1970) criterion gives the good prediction of the deformation moduli for one joint set specimens with joint normal to the major principal axis (Case 2) but cannot determine the deformation modulus for specimens with more than one joint set. Yoshinaka and Yamabe (1986) equation can determine the specimen with more than one joint set and orientation but this equation does not consider the deformation modulus that have joint planes parallel to  $\sigma_1$ . This is opposite to the results from testing where the deformation moduli decrease with increasing joint frequency. Ramamurthy criterion can predict the deformation moduli along the joint plane (Case 1) and perpendicular to the joint plane (Case 2). The deformation moduli of specimens with three joint set cannot be predicted with this criterion. Goodman (1970) equation is modified here to determine the deformation modulus along three principal directions. The parameter N is proposed whose value depends on joint set direction. The proposed equation can only predict the deformation modulus in the directions normal and parallel to the joint planes.

## 8.2 Recommendations for future studies

The uncertainties of the investigation and results discussed above lead to the recommendations for further studies. More testing is required on a variety of rocks with different joint roughness and orientations. More investigation is also desirable to confirm or verify that the effect of joint frequency by using the rock mass classification system. The test results under higher confining pressure should be obtained.



## REFERENCES

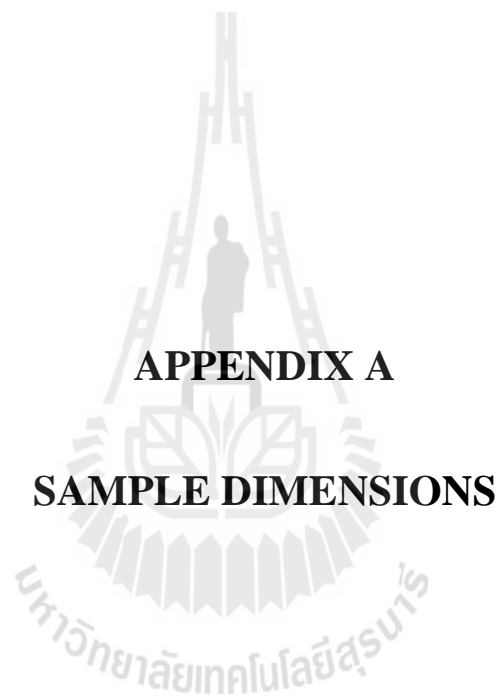
- Arora, V.K. (1987). Strength and deformational behaviour of jointed rocks. **Ph.D. thesis, Indian Institute of Technology, Delhi, India.**
- Bieniawski, Z.T. (1974). Estimating the strength of rock materials. **Journal of the South African Institute of Mining and Metallurgy.** 74: 312-320.
- Boonsener, M. and Sonpiron, K. (1997). Correlation of tertiary rocks in northeast, Thailand. **International Conference on Stratigraphy and Tectonic Evolution of Southeast Asia and the South Pacific** (pp. 656-661). Bangkok.
- Brown, E.T. and Trollope, D.H. (1970). Strength of model of jointed rock. **Journal of Soil Mechanics and Foundation Division, ASCE** 96. SM2, 685–704.
- Colak, K. and Unlu, T. (2004). Effect of transverse anisotropy on the Hoek–Brown strength parameter ‘ $m_i$ ’ for intact rocks. **International Journal of Rock Mechanics and Mining Sciences.** 41(6): 1045-1052.
- Edelbro, C. (2004). Evaluation of rock mass strength criteria. **PhD. Thesis, Lulea University of Technology, Sweden.**
- Edelbro, C., Sjöberg, J., and Nordlund, E. (2007). A quantitative comparison of strength criteria for hard rock masses. **Tunnelling and Underground Space Technology.** 22(1): 57-68.
- Fahimifar, A. and Soroush, H. (2003). Geotechnical parameters characteristics for a kind of schist in Iran. **ISRM 2003-Technology roadmap for rock mechanics, South Africa Institute of Mining and Metallurgy.**

- Goodman, R.E. (1970). The deformability of joints, determination of the in situ modulus of deformation of rock. ASTM STP 447, **American Society for Testing and Materials**, pp. 174-196.
- Goodman, R.E. (1989). **Introduction to rock mechanics**, 2nd ed. John Wiley & Sons, New York.
- Goshtasbi, K., Ahmadi, M., and Seyedi, J. (2006). Anisotropic strength behavior of slates in the Sirjan-Sanandaj zone. **Journal of the South African Institute of Mining and Metallurgy**. 106: 71-76.
- Halakatevakis, N. and Sofianos, A.I. (2010). Strength of a blocky rock mass based on an extended plane of weakness theory. **International Journal of Rock Mechanics and Mining Sciences**. 47: 568-582.
- Hashemnejad, A., Aghamolaei, I., Ghafoori, M., and Lashkaripour, G. (2013). Providing a new empirical failure criterion for intact rock and comparing it with three criteria Bieniawski, Ramamurthy and Hook-Brown. **International Journal of Emerging Technology and Advanced Engineering**. 3(5): 43-49.
- Hoek, E. and Brown, E.T. (1980). Empirical strength criterion for rock masses. **Journal of Geotechnical Engineering ASCE**. 160(GT9): 1013-1035.
- Hoek, E. and Brown, T. (1988). The Hoek-Brown failure criteria- a 1988 update. In **Proc. 15th Canadian Rock Mech. Symp.** pp. 3-31.
- Jaeger, J.C., Cook, N.G.W., and Zimmerman, R.W. (2007). **Fundamentals of rock mechanics**, 4th ed. Blackweel: Oxford.
- Komenthammasopon, S. and Fuenkajorn, K. (2014). Effect of stress path on biaxial strengths of three Thai sandstones. **International Conferences on Advance in Civil Engineering for Sustainable Development** (pp. 249-254). Thailand.

- Kulatilake, P.H.S, Park, J., and Malama, B. (2006). A new rock mass failure criterion for biaxial loading conditions. **Geotechnical and Geological Engineering**, 24: 871-888.
- Liao, J.J. and Hsieh, H.Y. (1999). **Triaxial residual strength of an anisotropic rock**. Rock mechanics for industry, Amadei et al, Balkema, Rotterdam.
- Maji, V.B. and Sitharam, T.G. (2008). Prediction of elastic modulus of jointed rock mass using artificial neural networks. **Geotechnical and Geological Engineering**. 26: 443-452.
- Mclamore, R. and Gray, K.E. (1967). The mechanical behaviour of anisotropic sedimentary rocks. **Transactions of the American Society of Mechanical Engineers**. 89 (1): 62–79.
- Nasseri, M.H.B., Rao, K.S., and Ramamurthy, T. (2002) Anisotropic strength and deformational behavior of Himalayan schists. **International Journal of Rock Mechanics and Mining Sciences**. 40(1): 3-23.
- Rafiai, H. (2011). New empirical polyaxial criterion for rock strength. **International Journal of Rock Mechanics and Mining Sciences**. 48(6): 922-931.
- Ramamurthy, T. (1989). Stability of Rock Mass. **8 IGS Annual Lecture delivered on the occasion of its 27th Annual eral Session half at roorkee, india.**
- Ramamurthy, T. (1993). **Strength, modulus responses of anisotropic rocks**. In: Hudson JA, editor. Comprehensive rock engineering (vol. 1, pp. 313–29). Oxford: Pergamon Press.

- Ramamurthy, T. (2001). Shear strength response of some geo-logical materials in triaxial compression. **International Journal of Rock Mechanics and Mining Sciences.** 38(5): 683-697.
- Ramamurthy, T. and Arora, V.K. (1994). Strength predictions for jointed rocks in confined and unconfined states. **International Journal of Rock Mechanics and Mining Sciences.** 31(1): 9-22.
- Roy, N. (1993). Engineering behaviour of rock masses through study of jointed models. **Ph.D. Thesis, Indian Institute of Technology, Delhi.**
- Saroglou, H. and Tsiambaos, G. (2008). A modified Hoek–Brown failure criterion for anisotropic intact rock. **International Journal of Rock Mechanics and Mining Sciences.** 45(2): 223-234.
- Sheorey, P.R. (1997). **Empirical rock failure criterion**, Balkema, Rotterdam.
- Sheorey, P.R., Biswas, A.K., and Choubey, V.D. (1989). An empirical failure criterion. **Journal of the Soil Mechanics and Foundations Division.** 99 (3): 229–248.
- Singh, M. and Singh, B. (2012). Modified Mohr-Coulomb criterion for non-linear triaxial and polyaxial strength of jointed rocks. **International Journal of Rock Mechanics and Mining Sciences.** 51: 43-52.
- Sridevi, J. and Sitharam, T. G. (2000). Analysis of strength and moduli of jointed rocks. **Geotechnical and Geological Engineering.** 18: 3-21.
- Tien, Y.M. and Kuo, M.C. (2001). A failure criterion for transversely isotropic rocks. **International Journal of Rock Mechanics and Mining Sciences.** 38: 399-412.

- Tiwari, R. and Rao, K.S. (2006). Deformability characteristics of a rock mass under true-triaxial stress compression. **Geotechnical and Geological Engineering**. 24: 1039-1063.
- Yaji, R.K. (1984). Shear strength and deformation response of jointed rock. **Ph.D. Thesis, Indian Institute of Technology, Delhi.**
- Yang, Z.Y., Chen, J. M., and Huang, T.H. (1998). Effect of joint sets on the strength and deformation of rock mass models. **International Journal of Rock Mechanics and Mining Sciences**. 35(1): 75-84.
- Yoshinaka, R. and Yamabe, T. (1986). Joint stiffness and the deformation behaviour of discontinuous rock. **International Journal of Rock Mechanics and Mining Sciences**. 23(1): 19-28.
- You, M.Q. (2009). True-triaxial strength criteria for rock. **International Journal of Rock Mechanics and Mining Sciences**. 46: 115-127.
- Yudhbir, Lemanza, W., and Prinzl, F. (1983). An empirical failure criterion for rock masses, In **Proceedings of the 5th International Congress Society of Rock Mechanics Melbourne**. 1: 1-8.
- Zhou, S. (1994). A program to model the initial shape and extent of borehole breakout. **Computers and Geosciences**. 20(7/8):1143–1160.



**APPENDIX A**

**SAMPLE DIMENSIONS**

**Table A.1** Intact rock specimens.

Specimen No.	Dimension (mm <sup>3</sup> )	Density (g/cc)
PWSS-01-I	61.50×61.00×60.80	2.24
PWSS-02-I	60.40×60.50×60.70	2.25
PWSS-03-I	60.20×61.40×62.30	2.31
PWSS-04-I	60.70×62.00×62.00	2.30
PWSS-05-I	59.40×61.40×62.60	2.24
PWSS-06-I	59.50×60.40×60.00	2.29
PWSS-07-I	60.80×61.40×51.60	2.26
PWSS-08-I	60.50×61.00×60.70	2.25
PWSS-09-I	61.10×61.70×60.15	2.24
PWSS-10-I	61.00×61.75×60.00	2.22

**Table A.2** One joint set specimens.

Specimen No.	Cases	Number of joints per set	Dimension (mm <sup>3</sup> )	Density (g/cc)
PWSS-1S-1J -01	A1	1	62.00×62.00×62.26	2.22
PWSS-1S-1J -02	A1	1	62.00×62.36×62.00	2.25
PWSS-1S-1J -03	A1	1	62.56×62.78×62.36	2.28
PWSS-1S-1J -04	A1	1	62.48×61.70×62.30	2.17
PWSS-1S-1J -05	A1	1	62.30×62.88×62.80	2.30
PWSS-1S-1J -06	A1	1	62.40×63.50×62.30	2.26
PWSS-1S-1J -07	A1	1	62.30×62.90×63.20	2.28
PWSS-1S-1J -08	A1	1	62.90×62.10×63.00	2.33
PWSS-1S-1J -09	A1	1	62.20×62.42×63.54	2.24
PWSS-1S-1J -10	A1	1	61.40×61.38×63.26	2.12
PWSS-1S-1J -11	A1	1	62.76×62.36×63.82	2.27
PWSS-1S-1J -12	A1, B1	1	62.00×62.00×62.26	2.22
PWSS-1S-1J -13	A1, B1	1	60.00×61.00×60.00	2.28

**Table A.2** One joint set specimens (continue).

<b>Specimen No.</b>	<b>Cases</b>	<b>Number of joints per set</b>	<b>Dimension (mm<sup>3</sup>)</b>	<b>Density (g/cc)</b>
PWSS-1S-1J -14	A1, B1	1	61.50×61.00×60.32	2.26
PWSS-1S-1J -15	A1, B1	1	60.00×60.30×59.78	2.30
PWSS-1S-1J -16	A1, B1	1	60.00×60.30×60.30	2.27
PWSS-1S-1J -17	A1, B1	1	60.70×60.00×60.00	2.29
PWSS-1S-1J -18	A1, B1	1	59.90×60.40×60.30	2.30
PWSS-1S-1J -19	A1, B1	1	60.60×60.80×60.30	2.30
PWSS-1S-1J -20	A1, B1	1	60.40×60.60×60.70	2.24
PWSS-1S-1J -21	A1, B1	1	60.50×60.60×60.60	2.21
PWSS-1S-1J -22	A1, B1	1	60.60×60.30×60.10	2.25
PWSS-1S-1J -23	A1, B1	1	59.00×60.70×58.70	2.35
PWSS-1S-1J -24	A1, B2	1	60.50×60.50×60.70	2.19
PWSS-1S -1J-25	A1, B2	1	60.90×60.80×60.90	2.22
PWSS-1S -1J-26	A1, B2	1	60.60×60.80×60.90	2.19
PWSS-1S -1J-27	A1, B2	1	60.10×60.80×60.50	2.22
PWSS-1S -1J-28	A1, B2	1	60.20×60.30×60.30	2.29
PWSS-1S -1J-29	A1, B2	1	60.40×60.30×60.50	2.21
PWSS-1S -1J-30	A1, B2	1	60.00×60.50×58.40	2.27
PWSS-1S -1J-31	A1, B2	1	60.70×60.30×60.30	2.24
PWSS-1S -1J-32	A1, B2	1	60.40×60.70×60.60	2.20
PWSS-1S -1J-33	A1, B2	1	58.60×60.70×60.20	2.24
PWSS-1S -1J-34	A1, B2	1	60.60×60.60×60.50	2.23
PWSS-1S -1J-35	A1, B2	1	60.50×60.50×60.30	2.24
PWSS-1S -1J-36	A1, B2	1	60.40×60.60×60.40	2.25
PWSS-1S-2J -01	B1	2	60.70×60.60×60.50	2.22
PWSS-1S-2J -02	B1	2	60.70×60.20×60.70	2.23
PWSS-1S-2J -03	B1	2	60.10×60.80×60.50	2.22

**Table A.2** One joint set specimens (continue).

<b>Specimen No.</b>	<b>Cases</b>	<b>Number of joints per set</b>	<b>Dimension (mm<sup>3</sup>)</b>	<b>Density (g/cc)</b>
PWSS-1S-2J -04	B1	2	60.50×60.50×60.50	2.20
PWSS-1S-2J -05	B1	2	52.56×52.70×53.52	2.25
PWSS-1S-2J -06	B1	2	52.50×52.00×52.56	2.26
PWSS-1S-2J -07	B1	2	52.50×51.50×51.60	2.24
PWSS-1S-2J -08	B1	2	50.30×53.40×51.20	2.25
PWSS-1S-2J -09	B1	2	49.84×53.20×51.80	2.23
PWSS-1S-2J -10	B1	2	48.56×52.76×51.60	2.28
PWSS-1S-2J -11	B1	2	52.10×51.40×50.50	2.29
PWSS-1S-2J -12	B1	2	52.16×50.50×51.46	2.24
PWSS-1S-2J -13	B2	2	62.10×63.00×63.30	2.21
PWSS-1S-2J -14	B2	2	51.80×50.00×50.00	2.22
PWSS-1S-2J -15	B2	2	61.50×61.50×62.36	2.21
PWSS-1S-2J -16	B2	2	53.00×51.48×52.00	2.23
PWSS-1S-2J -17	B2	2	60.70×58.00×59.20	2.22
PWSS-1S-2J -18	B2	2	60.20×61.10×60.80	2.26
PWSS-1S-2J -19	B2	2	60.70×60.70×61.00	2.25
PWSS-1S-2J -20	B2	2	58.44×61.00×60.00	2.27
PWSS-1S-2J -21	B2	2	61.00×61.00×61.00	2.21
PWSS-1S-2J -22	B2	2	58.00×60.50×59.90	2.23
PWSS-1S-2J -23	B2	2	59.80×60.00×58.24	2.24
PWSS-1S-2J -24	B2	2	61.80×61.25×61.15	2.25
PWSS-1S-3J -01	B1	3	60.00×59.20×57.90	2.24
PWSS-1S-3J -02	B1	3	61.15×60.80×60.50	2.23
PWSS-1S-3J -03	B1	3	59.50×59.30×61.60	2.24
PWSS-1S-3J -04	B1	3	58.60×60.20×59.40	2.25
PWSS-1S-3J -05	B1	3	60.80×59.65×60.50	2.27

**Table A.2** One joint set specimens (continue).

<b>Specimen No.</b>	<b>Cases</b>	<b>Number of joints per set</b>	<b>Dimension (mm<sup>3</sup>)</b>	<b>Density (g/cc)</b>
PWSS-1S-3J -06	B1	3	60.75×60.50×60.70	2.22
PWSS-1S-3J -07	B1	3	61.10×59.00×61.40	2.24
PWSS-1S-3J -08	B1	3	61.45×59.20×62.30	2.26
PWSS-1S-3J -09	B1	3	60.50×59.10×59.50	2.27
PWSS-1S-3J -10	B1	3	61.30×59.60×62.80	2.25
PWSS-1S-3J -11	B1	3	61.50×59.70×62.70	2.24
PWSS-1S-3J -12	B1	3	61.45×59.20×62.30	2.27
PWSS-1S-3J -13	B2	3	60.40×61.10×61.10	2.28
PWSS-1S-3J -14	B2	3	60.75×61.30×60.10	2.32
PWSS-1S-3J -15	B2	3	61.80×59.80×59.90	2.24
PWSS-1S-3J -16	B2	3	60.80×60.30×58.50	2.25
PWSS-1S-3J -17	B2	3	58.45×59.70×61.20	2.25
PWSS-1S-3J -18	B2	3	58.00×62.50×60.85	2.23
PWSS-1S-3J -19	B2	3	61.65×61.20×61.70	2.30
PWSS-1S-3J -20	B2	3	58.10×60.85×61.35	2.29
PWSS-1S-3J -21	B2	3	59.60×61.10×62.00	2.22
PWSS-1S-3J -22	B2	3	59.10×60.00×61.80	2.27
PWSS-1S-3J -23	B2	3	61.00×62.50×61.50	2.23
PWSS-1S-3J -24	B2	3	61.15×62.10×59.80	2.25
PWSS-1S-4J -01	B1	4	60.20×60.20×59.40	2.23
PWSS-1S-4J -02	B1	4	60.45×61.20×60.40	2.25
PWSS-1S-4J -03	B1	4	59.20×60.10×60.00	2.24
PWSS-1S-4J -04	B1	4	59.60×60.00×61.40	2.25
PWSS-1S-4J -05	B1	4	60.10×60.15×60.40	2.26
PWSS-1S-4J -06	B1	4	59.95×60.40×60.60	2.23
PWSS-1S-4J -07	B1	4	60.10×59.90×61.10	2.27

**Table A.2** One joint set specimens (continue).

<b>Specimen No.</b>	<b>Cases</b>	<b>Number of joints per set</b>	<b>Dimension (mm<sup>3</sup>)</b>	<b>Density (g/cc)</b>
PWSS-1S-4J -08	B1	4	60.15×59.90×61.20	2.26
PWSS-1S-4J -09	B1	4	60.00×59.90×59.90	2.24
PWSS-1S-4J -10	B1	4	60.30×59.85×60.80	2.28
PWSS-1S-4J -11	B1	4	60.20×59.90×61.70	2.23
PWSS-1S-4J -12	B1	4	60.30×60.40×61.30	2.23
PWSS-1S-4J -13	B2	4	60.70×61.70×61.30	2.25
PWSS-1S-4J -14	B2	4	60.15×60.30×60.80	2.24
PWSS-1S-4J -15	B2	4	60.20×59.70×61.10	2.26
PWSS-1S-4J -16	B2	4	60.10×60.50×59.80	2.23
PWSS-1S-4J -17	B2	4	59.75×59.80×60.25	2.27
PWSS-1S-4J -18	B2	4	59.90×61.50×60.00	2.22
PWSS-1S-4J -19	B2	4	60.75×61.00×60.70	2.25
PWSS-1S-4J -20	B2	4	59.10×60.55×61.15	2.26
PWSS-1S-4J -21	B2	4	60.60×60.10×60.00	2.27
PWSS-1S-4J -22	B2	4	60.30×60.50×61.25	2.24
PWSS-1S-4J -23	B2	4	61.50×62.00×61.00	2.24
PWSS-1S-4J -24	B2	4	60.45×60.10×60.20	2.23

**Table A.3** Single rough joint specimens.

<b>Specimen No.</b>	<b>Cases</b>	<b>Number of joints per set</b>	<b>Dimension (mm<sup>3</sup>)</b>	<b>Density (g/cc)</b>
PWSS-R-1J-01	A2	1	61.50×62.12×62.16	2.21
PWSS-R-1J-02	A2	1	61.78×62.04×62.22	2.25
PWSS-R-1J-03	A2	1	63.14×62.38×62.82	2.32
PWSS-R-1J-04	A2	1	62.16×62.70×61.38	2.17
PWSS-R-1J-05	A2	1	62.40×62.36×61.92	2.18
PWSS-R-1J-06	A2	1	62.16×63.44×62.94	2.25
PWSS-R-1J-07	A2	1	62.28×62.26×62.32	2.21
PWSS-R-1J-08	A2	1	61.30×61.96×61.18	2.20
PWSS-R-1J-09	A2	1	62.06×61.98×62.16	2.22
PWSS-R-1J-10	A2	1	63.38×62.20×62.36	2.26
PWSS-R-1J-11	A2	1	62.06×62.26×62.30	2.21
PWSS-R-1J-12	A2	1	61.38×62.16×61.98	2.25
PWSS-R-1J-13	A2	1	63.32×62.86×62.56	2.26
PWSS-R-1J-14	A2	1	62.30×62.06×62.06	2.22
PWSS-R-1J-15	A2	1	62.38×61.98×62.26	2.20
PWSS-R-1J-16	A2	1	62.16×61.40×62.34	2.24
PWSS-R-1J-17	A2	1	62.38×62.06×62.54	2.19
PWSS-R-1J-18	A2	1	61.98×61.98×62.22	2.23
PWSS-R-1J-19	A2	1	62.00×62.00×62.26	2.39
PWSS-R-1J-20	A2	1	62.78×63.30×62.20	2.28
PWSS-R-1J-21	A2	1	62.06×62.60×63.30	2.28
PWSS-R-1J-22	A2	1	62.10×63.00×63.30	2.25
PWSS-R-1J-23	A2	1	61.50×61.50×62.36	2.27
PWSS-R-1J-24	A2	1	61.20×61.70×62.00	2.24
PWSS-R-1J-25	A2	1	62.60×62.70×62.40	2.29
PWSS-R-1J-26	A2	1	62.00×62.00×62.00	2.22

**Table A.3** Single rough joint specimens (continue).

<b>Specimen No.</b>	<b>Cases</b>	<b>Number of joints per set</b>	<b>Dimension (mm<sup>3</sup>)</b>	<b>Density (g/cc)</b>
PWSS-R-1J-27	A2	1	62.00×62.00×61.62	2.23
PWSS-R-1J-28	A2	1	61.70×61.60×61.50	2.20
PWSS-R-1J-29	A2	1	62.10×61.60×61.80	2.21
PWSS-R-1J-30	A2	1	62.90×62.20×62.70	2.30
PWSS-R-1J-31	A2	1	62.40×63.50×62.20	2.34
PWSS-R-1J-32	A2	1	63.00×63.00×62.00	2.30
PWSS-R-1J-33	A2	1	61.70×61.90×61.50	2.24
PWSS-R-1J-34	A2	1	62.60×63.54×62.00	2.28
PWSS-R-1J-35	A2	1	61.90×62.70×62.50	2.38
PWSS-R-1J-36	A2	1	63.10×62.90×62.30	2.32
PWSS-R-1J-37	A2	1	61.70×61.50×61.50	2.31
PWSS-R-1J-38	A2	1	61.70×61.80×61.40	2.27
PWSS-R-1J-39	A2	1	63.40×62.16×62.60	2.29
PWSS-R-1J-40	A2	1	62.50×63.00×62.30	2.35
PWSS-R-1J-41	A2	1	62.50×62.60×62.30	2.30
PWSS-R-1J-42	A2	1	62.26×62.36×63.54	2.29
PWSS-R-1J-43	A2	1	63.00×62.66×62.26	2.33
PWSS-R-1J-44	A2	1	62.76×62.56×62.60	2.27
PWSS-R-1J-45	A2	1	62.40×62.36×63.74	2.24
PWSS-R-1J-46	A2	1	62.30×62.00×62.00	2.24
PWSS-R-1J-47	A2	1	62.00×62.70×63.30	2.26
PWSS-R-1J-48	A2	1	63.56×62.00×63.00	2.27

**Table A.4** Three joint sets specimens.

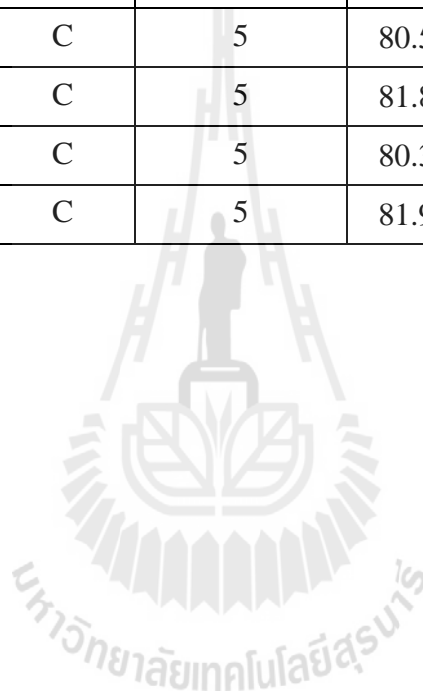
Specimen No.	Cases	Number of joints per set	Dimension (mm <sup>3</sup> )	Density (g/cc)
PWSS-3S-1J -01	C	1	80.50×80.90×80.80	2.28
PWSS-3S-1J -02	C	1	81.00×80.20×80.90	2.26
PWSS-3S-1J -03	C	1	80.80×80.43×80.12	2.29
PWSS-3S-1J -04	C	1	80.73×81.00×82.00	2.23
PWSS-3S-1J -05	C	1	80.53×80.73×81.33	2.25
PWSS-3S-1J -06	C	1	80.63×80.90×80.90	2.26
PWSS-3S-1J -07	C	1	80.00×80.76×80.00	2.26
PWSS-3S-1J -08	C	1	80.56×81.54×80.48	2.25
PWSS-3S-1J -09	C	1	80.36×80.56×80.68	2.27
PWSS-3S-1J -10	C	1	80.00×80.36×79.88	2.28
PWSS-3S-1J -11	C	1	80.46×80.00×80.56	2.23
PWSS-3S-1J -12	C	1	81.00×81.00×79.80	2.29
PWSS-3S -2J -01	C	2	80.00×79.60×81.60	2.29
PWSS-3S -2J -02	C	2	81.00×81.00×79.00	2.29
PWSS-3S -2J -03	C	2	82.00×79.60×78.30	2.30
PWSS-3S -2J -04	C	2	81.70×81.50×79.60	2.21
PWSS-3S -2J -05	C	2	80.00×83.00×79.36	2.24
PWSS-3S -2J -06	C	2	79.50×78.00×81.00	2.33
PWSS-3S -2J -07	C	2	78.70×79.00×80.50	2.30
PWSS-3S -2J -08	C	2	79.20×80.80×80.40	2.27
PWSS-3S -2J -09	C	2	79.70×80.80×81.40	2.23
PWSS-3S -2J -10	C	2	80.00×80.40×81.70	2.26
PWSS-3S -2J -11	C	2	79.60×80.00×81.00	2.29
PWSS-3S -2J -12	C	2	79.86×79.70×81.00	2.25
PWSS-3S-3J -01	C	3	80.00×80.00×80.40	2.26
PWSS-3S-3J -02	C	3	80.70×81.50×79.40	2.23

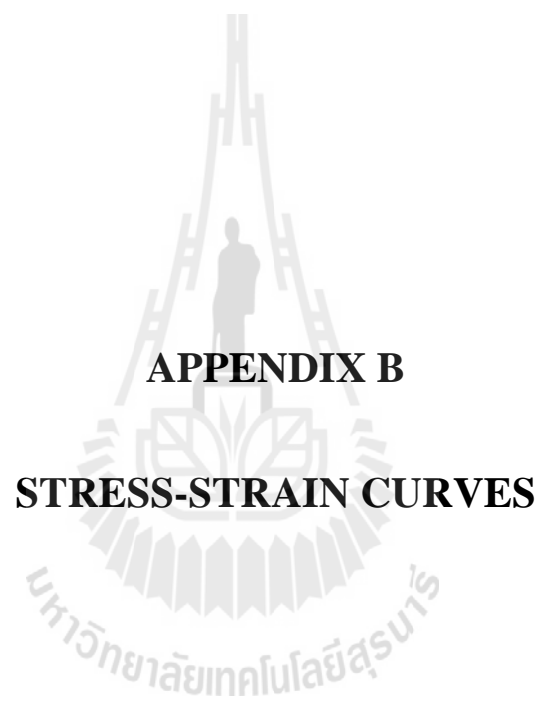
**Table A.4** Three joint sets specimens (continue).

<b>Specimen No.</b>	<b>Case</b>	<b>Number of joints per set</b>	<b>Dimension (mm<sup>3</sup>)</b>	<b>Density (g/cc)</b>
PWSS-3S-3J -03	C	3	81.40×80.90×83.00	2.23
PWSS-3S-3J -04	C	3	81.70×80.40×81.30	2.25
PWSS-3S-3J -05	C	3	80.50×82.00×78.50	2.33
PWSS-3S-3J -06	C	3	80.30×81.30×9.00	2.23
PWSS-3S-3J -07	C	3	81.30×80.90×79.00	2.20
PWSS-3S-3J -08	C	3	80.20×83.00×79.30	2.18
PWSS-3S-3J -09	C	3	82.30×81.48×80.00	2.20
PWSS-3S-3J -10	C	3	82.00×80.00×79.00	2.20
PWSS-3S-3J -11	C	3	81.40×81.00×80.50	2.24
PWSS-3S-3J -12	C	3	81.80×80.50×79.80	2.27
PWSS-3S-4J -01	C	4	81.70×82.50×78.73	2.19
PWSS-3S-4J -02	C	4	82.00×81.50×79.00	2.22
PWSS-3S-4J -03	C	4	80.00×80.00×81.60	2.24
PWSS-3S-4J -04	C	4	81.00×88.00×81.50	2.06
PWSS-3S-4J -05	C	4	80.00×79.50×79.00	2.35
PWSS-3S-4J -06	C	4	80.00×80.00×80.20	2.29
PWSS-3S-4J -07	C	4	80.00×80.00×80.46	2.30
PWSS-3S-4J -08	C	4	80.36×80.50×79.50	2.24
PWSS-3S-4J -09	C	4	80.00×80.30×80.00	2.29
PWSS-3S-4J -10	C	4	80.20×80.00×80.36	2.28
PWSS-3S-4J -11	C	4	78.50×80.56×80.00	2.35
PWSS-3S-4J -12	C	4	79.90×81.64×80.44	2.19
PWSS-3S-5J -01	C	5	81.60×81.80×79.60	2.25
PWSS-3S-5J -02	C	5	81.30×80.20×78.40	2.29
PWSS-3S-5J -03	C	5	80.30×82.50×81.20	2.23

**Table A.4** Three joint sets specimens (continue).

<b>Specimen No.</b>	<b>Cases</b>	<b>Number of joints per set</b>	<b>Dimension (mm<sup>3</sup>)</b>	<b>Density (g/cc)</b>
PWSS-3S-5J -04	C	5	82.40×81.30×82.30	2.28
PWSS-3S-5J -05	C	5	82.00×80.70×81.50	2.20
PWSS-3S-5J -06	C	5	81.00×80.60×80.20	2.25
PWSS-3S-5J -07	C	5	80.00×80.20×82.00	2.22
PWSS-3S-5J -08	C	5	79.60×80.00×80.70	2.26
PWSS-3S-5J -09	C	5	80.50×81.70×80.00	2.17
PWSS-3S-5J -10	C	5	81.80×82.80×79.70	2.20
PWSS-3S-5J -11	C	5	80.36×81.32×79.20	2.26
PWSS-3S-5J -12	C	5	81.90×80.00×78.50	2.23





**APPENDIX B**

**STRESS-STRAIN CURVES**

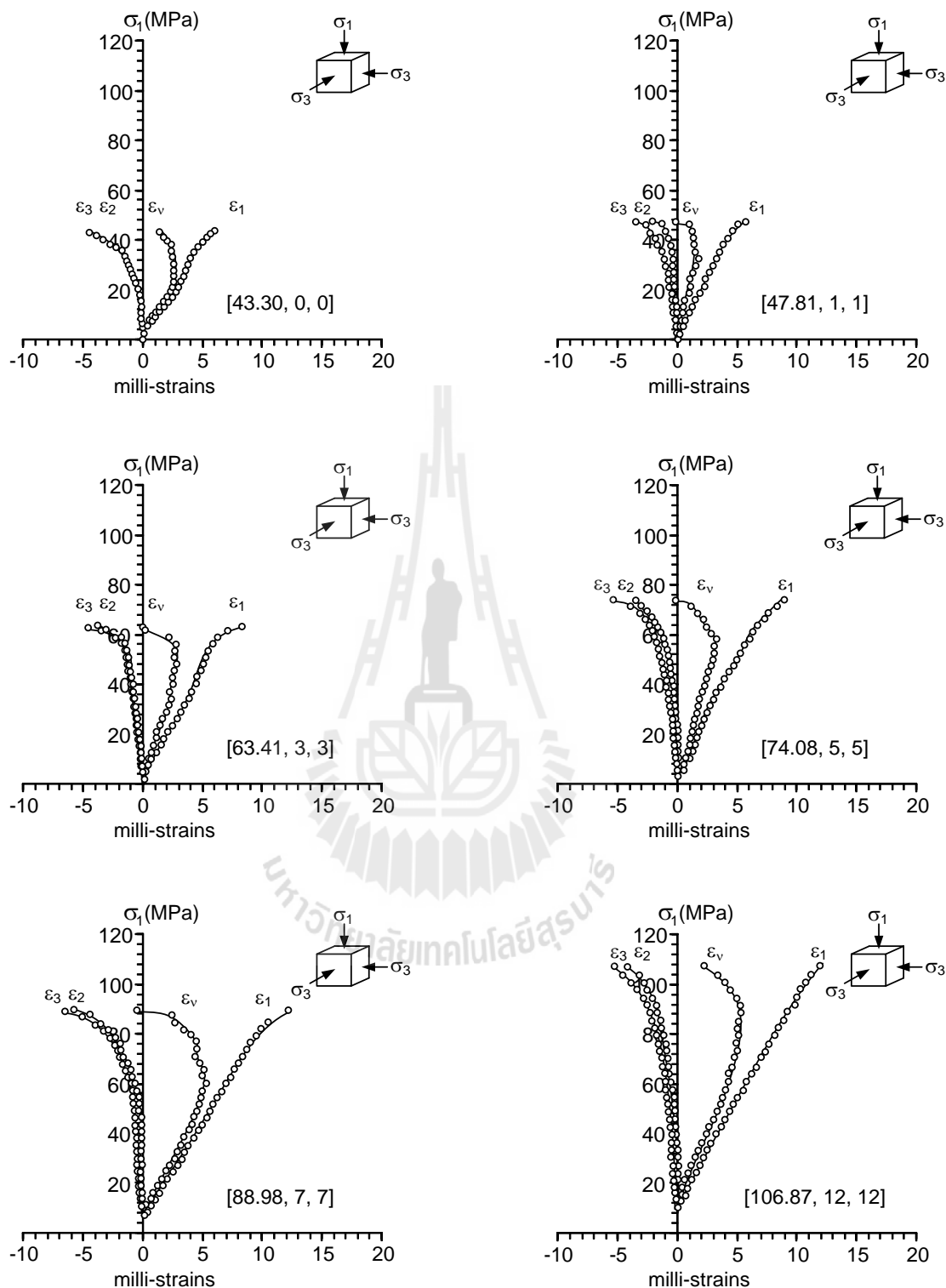


**Figure B.1** Stress-strain curves for intact specimens. Numbers in brackets indicate  $[\sigma_1, \sigma_3, \sigma_3]$  at failure in MPa.

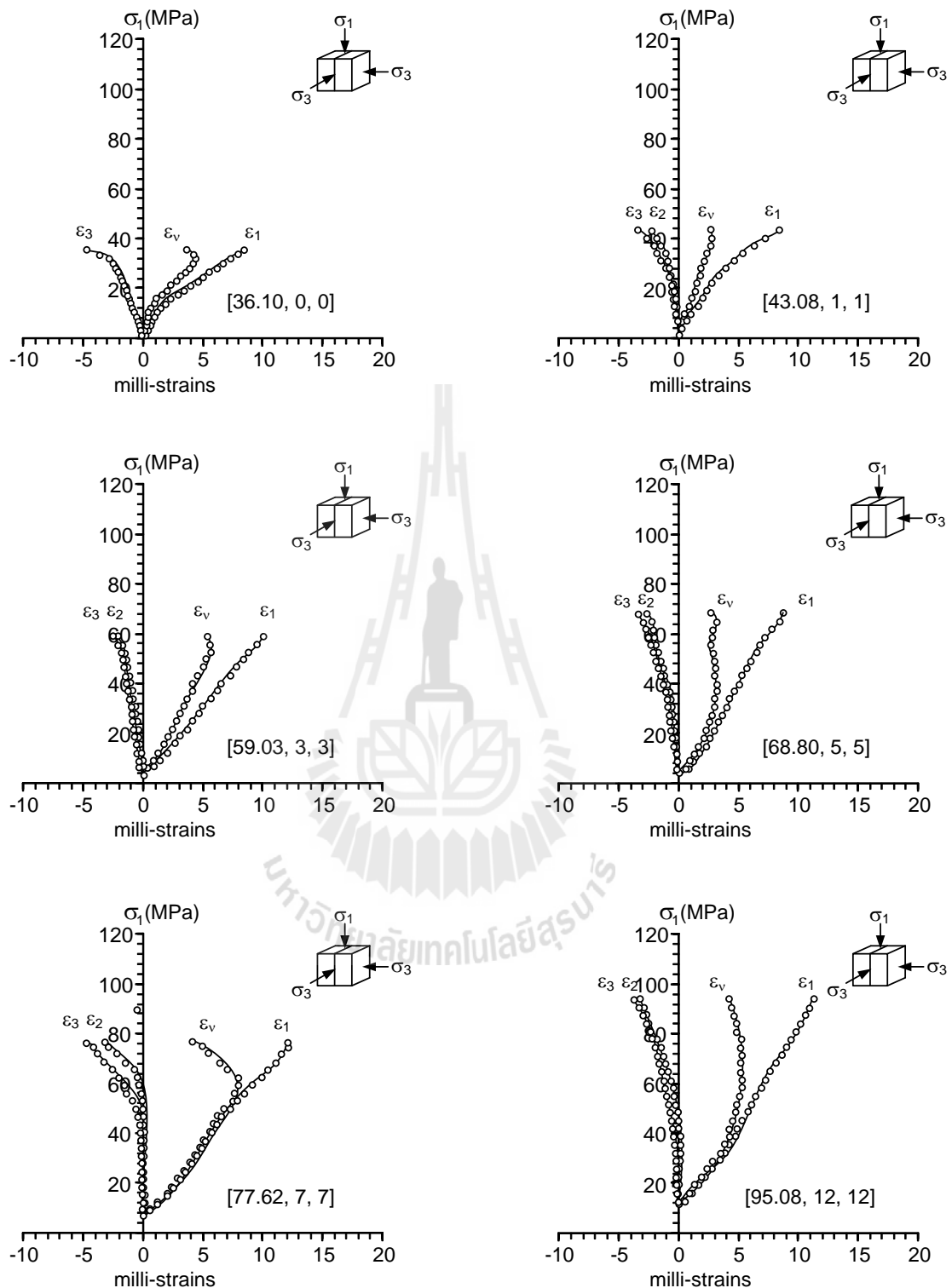


**Figure B.2** Stress-strain curves of 1 joint per set specimens for case B1. Numbers in brackets indicate  $[\sigma_1, \sigma_3, \sigma_3]$  at failure in MPa.

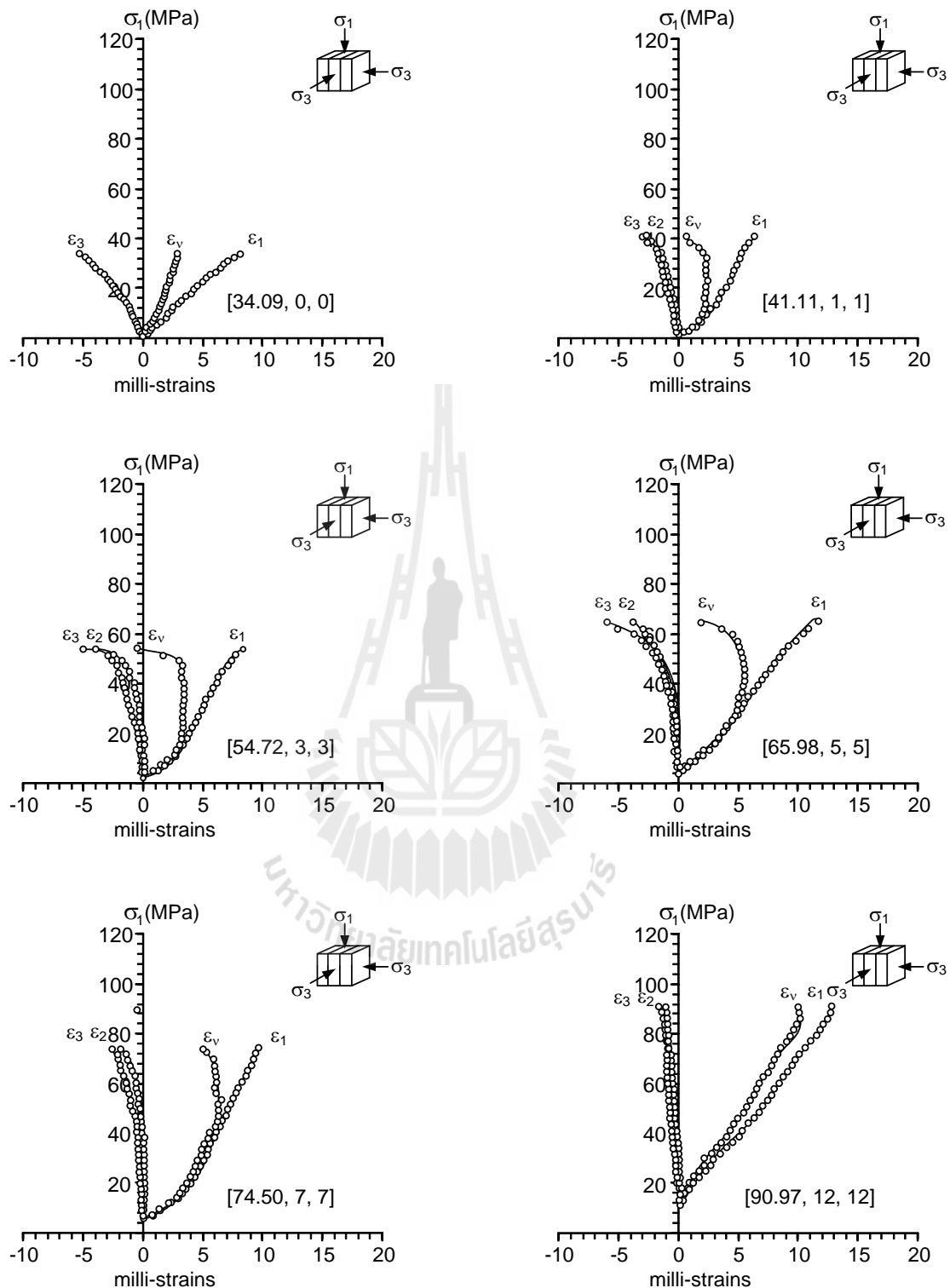


**Figure B.3** Stress-strain curves of 2 joints per set specimens for case B1. Numbers in brackets indicate  $[\sigma_1, \sigma_3, \sigma_3]$  at failure in MPa.

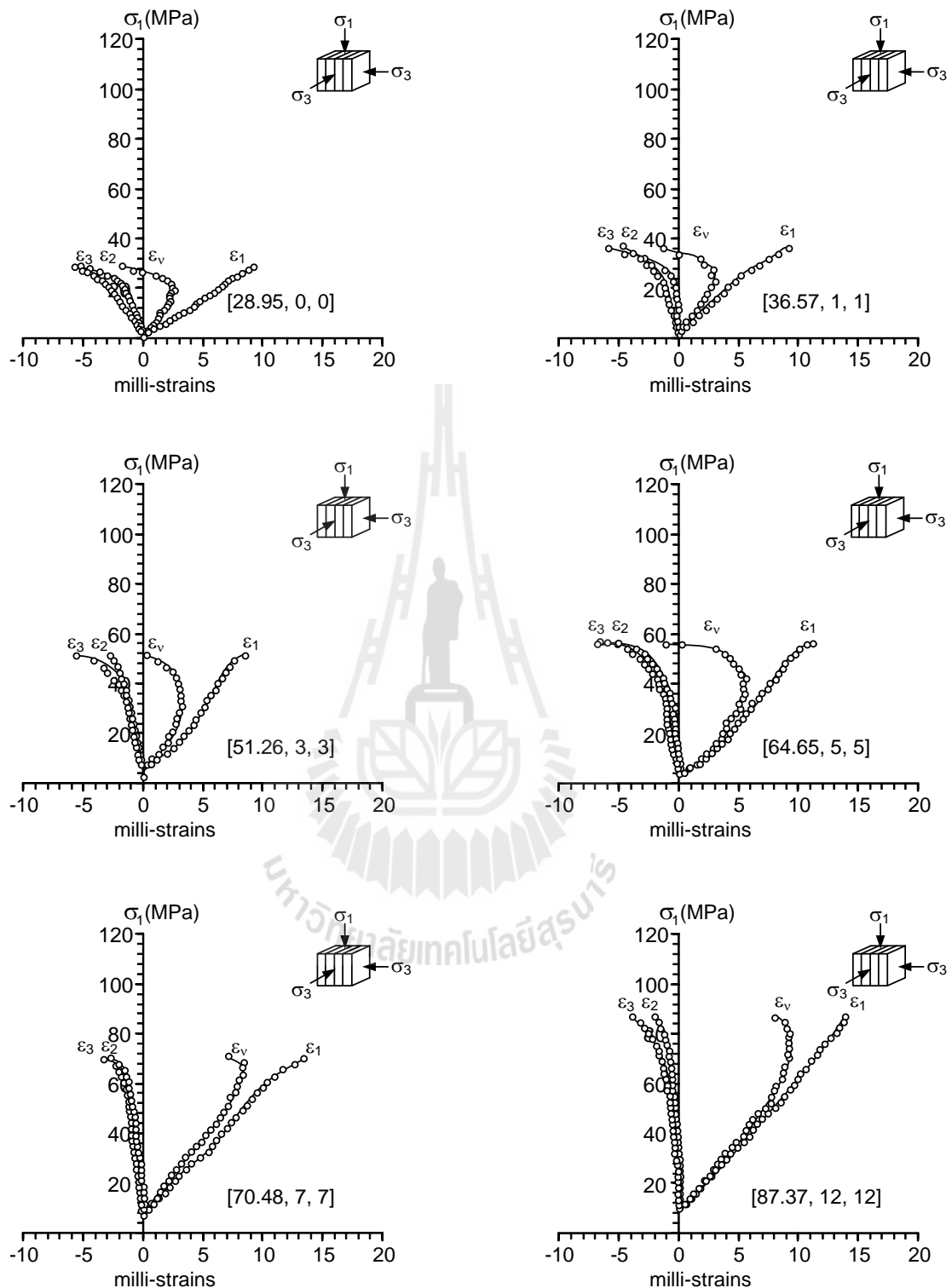


**Figure B.4** Stress-strain curves of 3 joints per set specimens for case B1. Numbers in brackets indicate  $[\sigma_1, \sigma_3, \sigma_3]$  at failure in MPa..

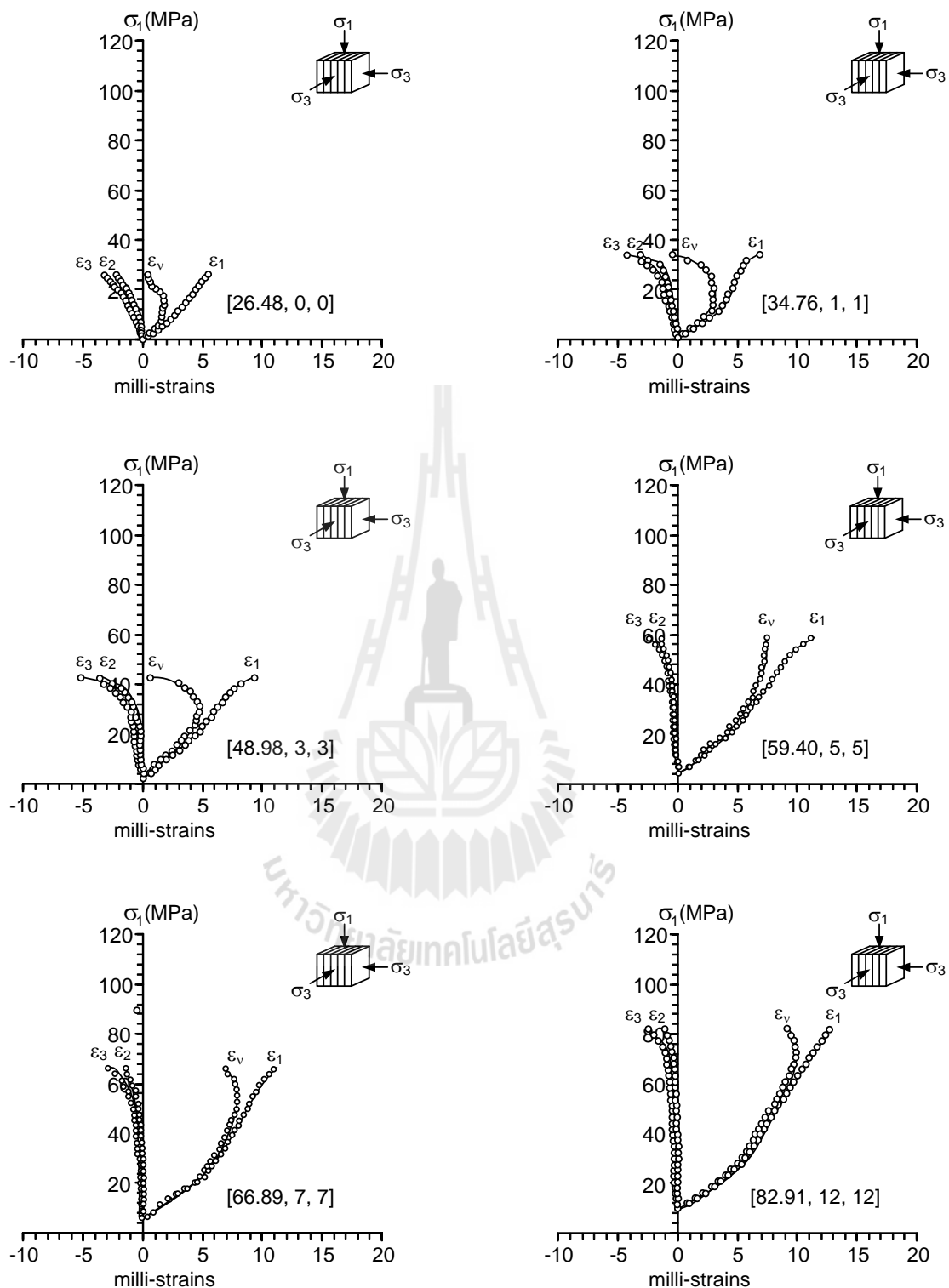


**Figure B.5** Stress-strain curves of 4 joints per set specimens for case B1. Numbers in brackets indicate  $[\sigma_1, \sigma_3, \sigma_3]$  at failure in MPa.

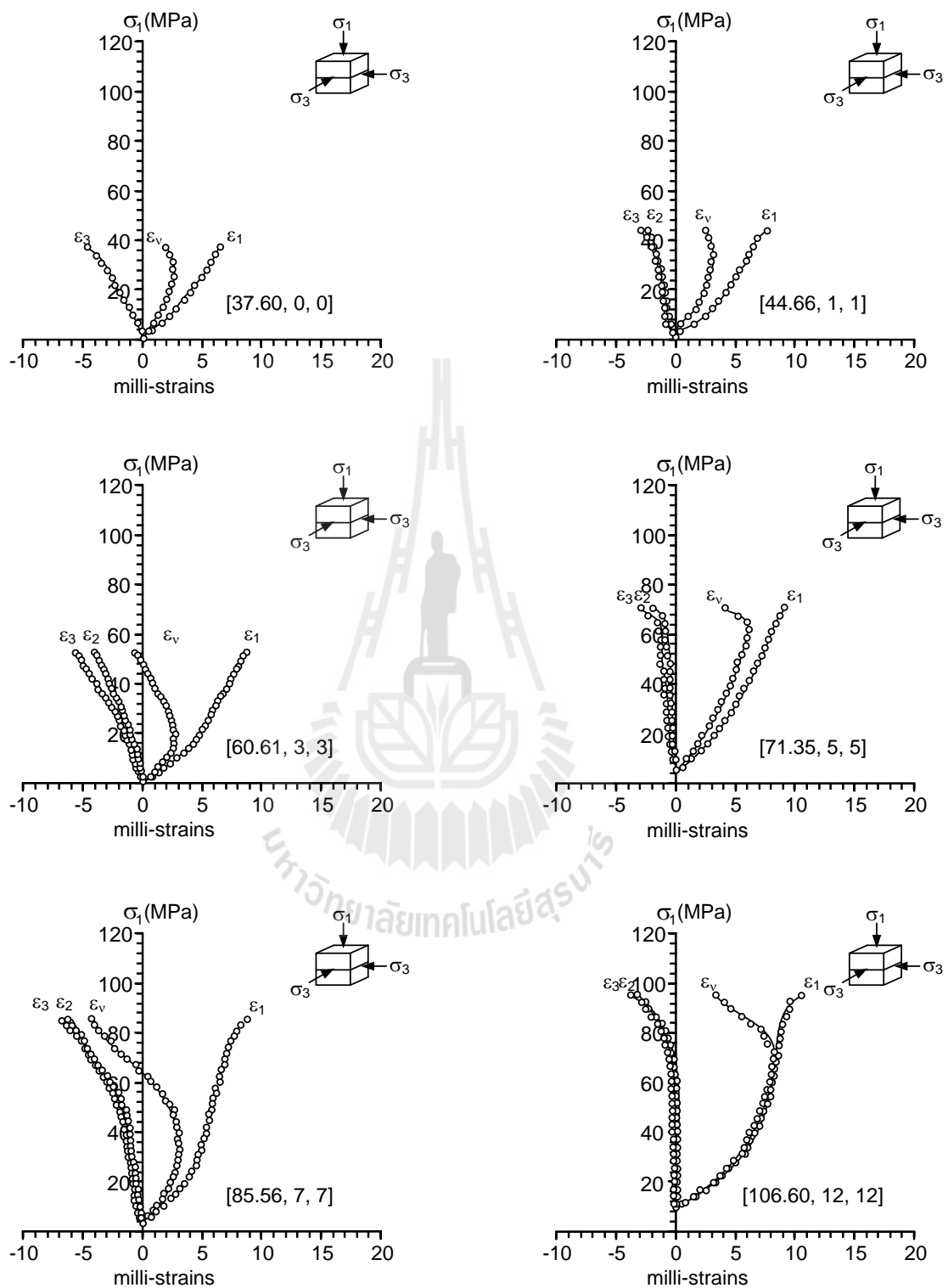


**Figure B.6** Stress-strain curves of 1 joint per set specimens for case B2. Numbers in brackets indicate  $[\sigma_1, \sigma_3, \sigma_3]$  at failure in MPa.

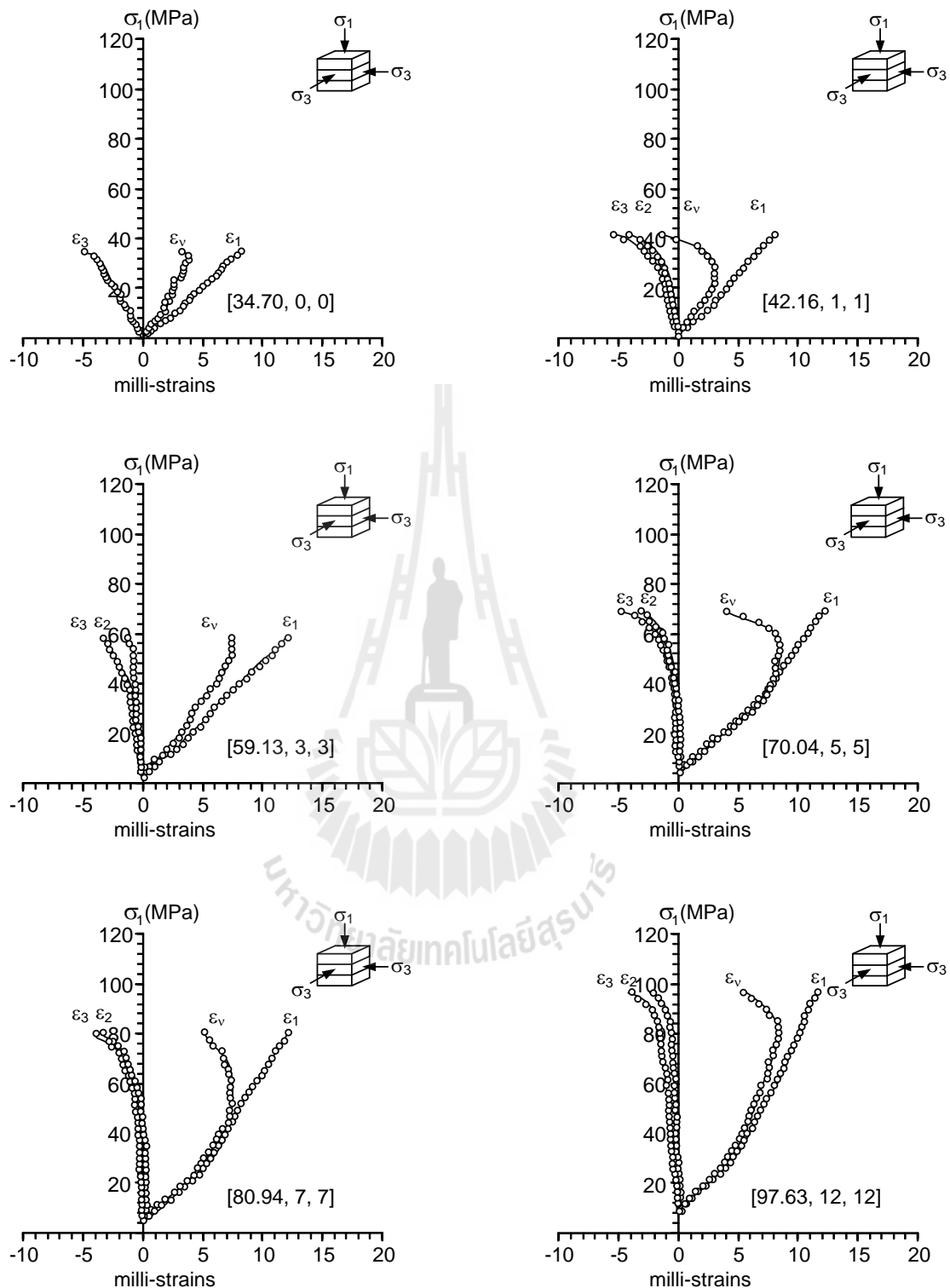


**Figure B.7** Stress-strain curves of 2 joints per set specimens for case B2. Numbers in brackets indicate  $[\sigma_1, \sigma_2, \sigma_3]$  at failure in MPa.

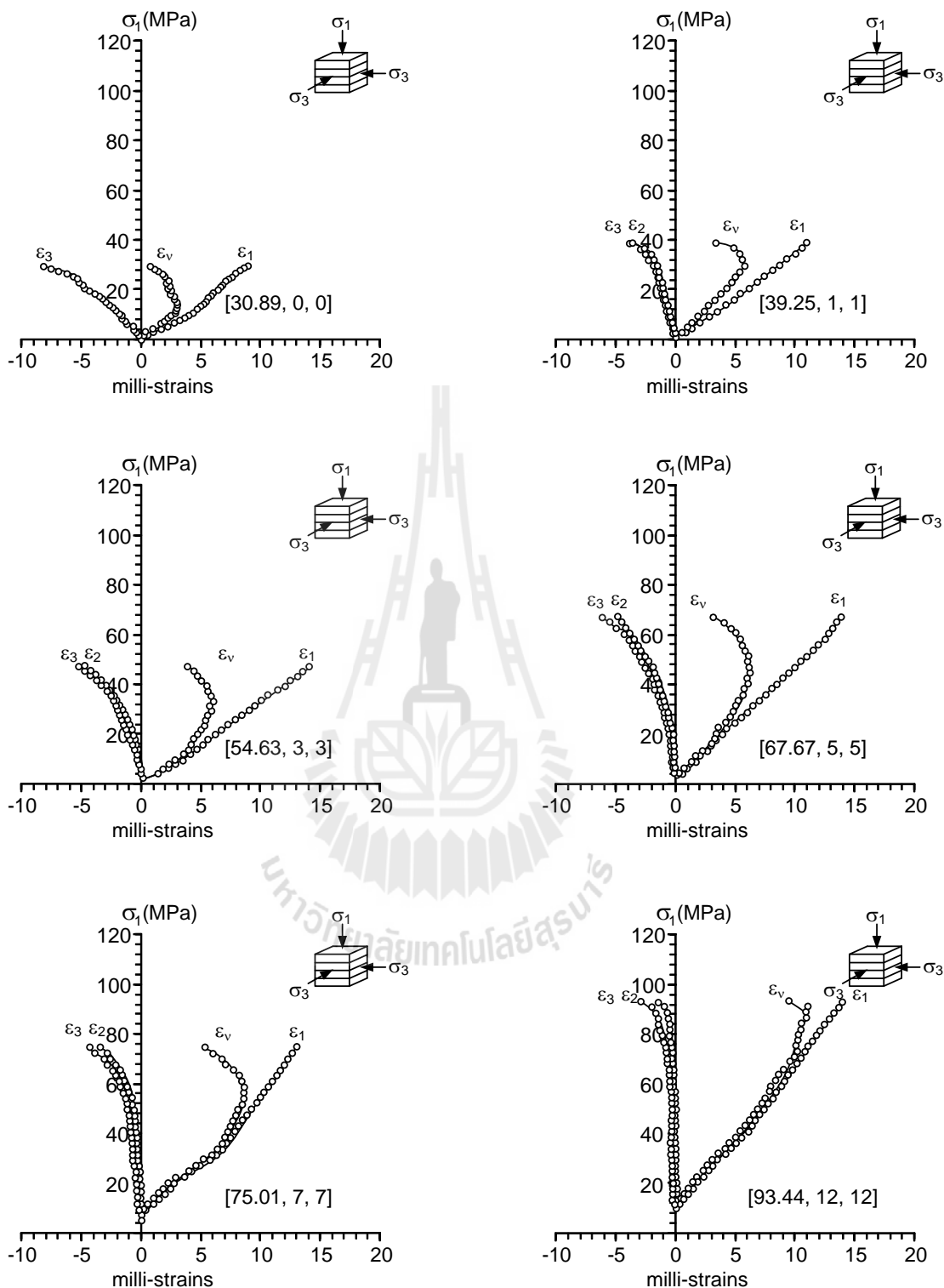


**Figure B.8** Stress-strain curves of 3 joints per set specimens for case B2. Numbers in brackets indicate  $[\sigma_1, \sigma_3, \sigma_3]$  at failure in MPa.

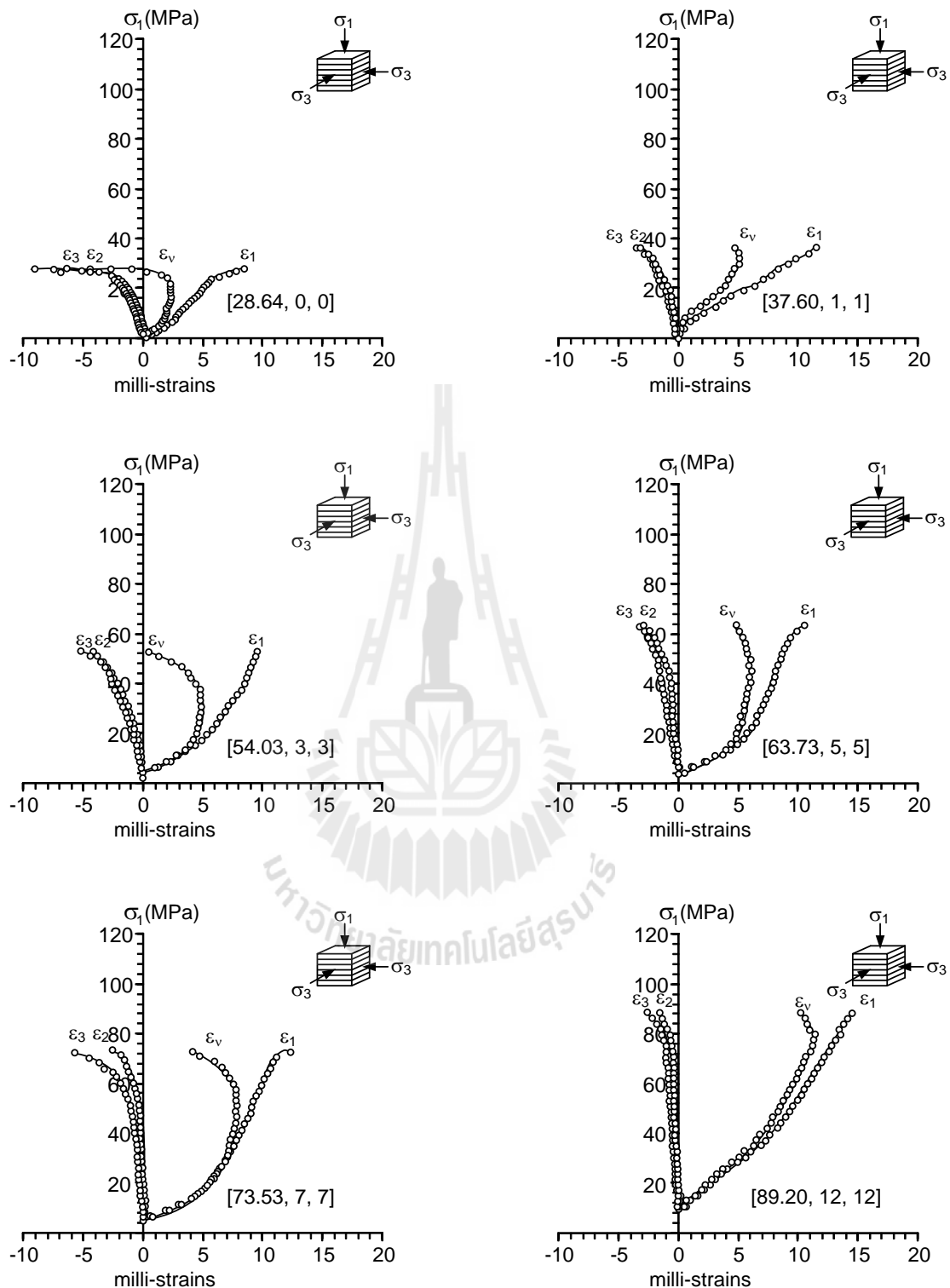


**Figure B.9** Stress-strain curves of 4 joints per set specimens for case B2. Numbers in brackets indicate  $[\sigma_1, \sigma_3, \sigma_3]$  at failure in MPa.

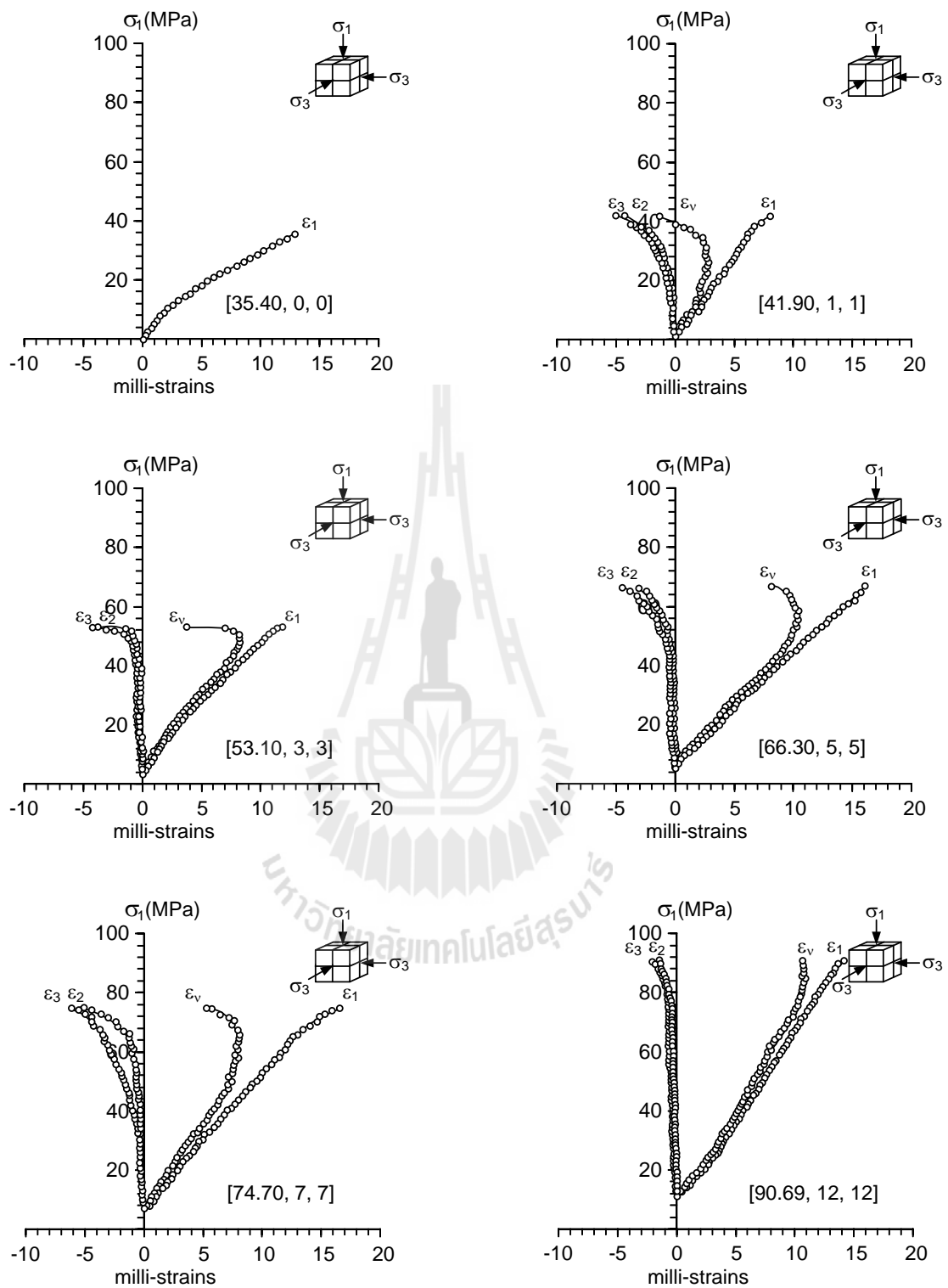


**Figure B.10** Stress-strain curves of 1 joint per set specimens for case C. Numbers in brackets indicate  $[\sigma_1, \sigma_3, \sigma_3]$  at failure in MPa.

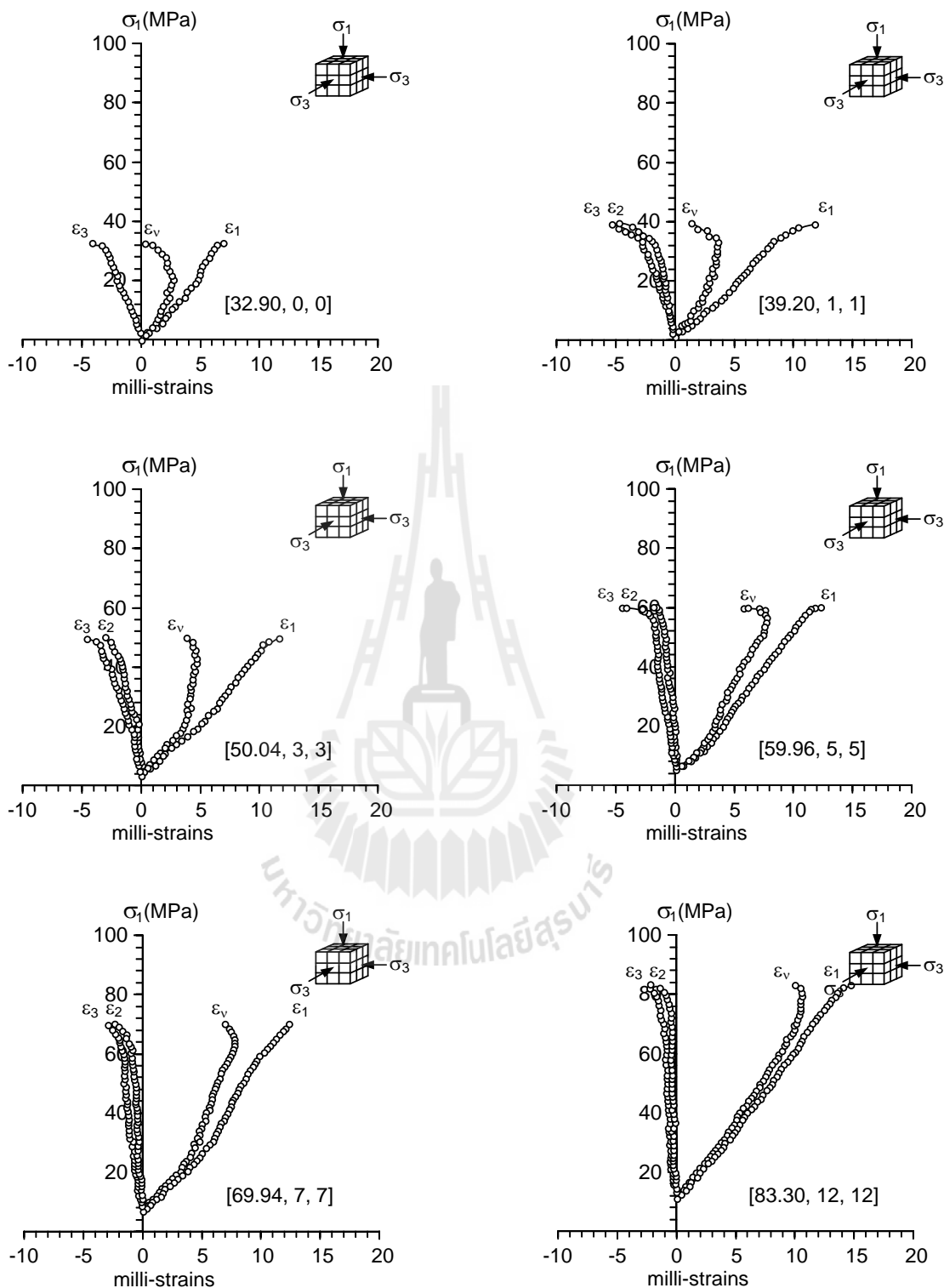


**Figure B.11** Stress-strain curves of 2 joints per set specimens for case C. Numbers in brackets indicate  $[\sigma_1, \sigma_3, \sigma_3]$  at failure in MPa.

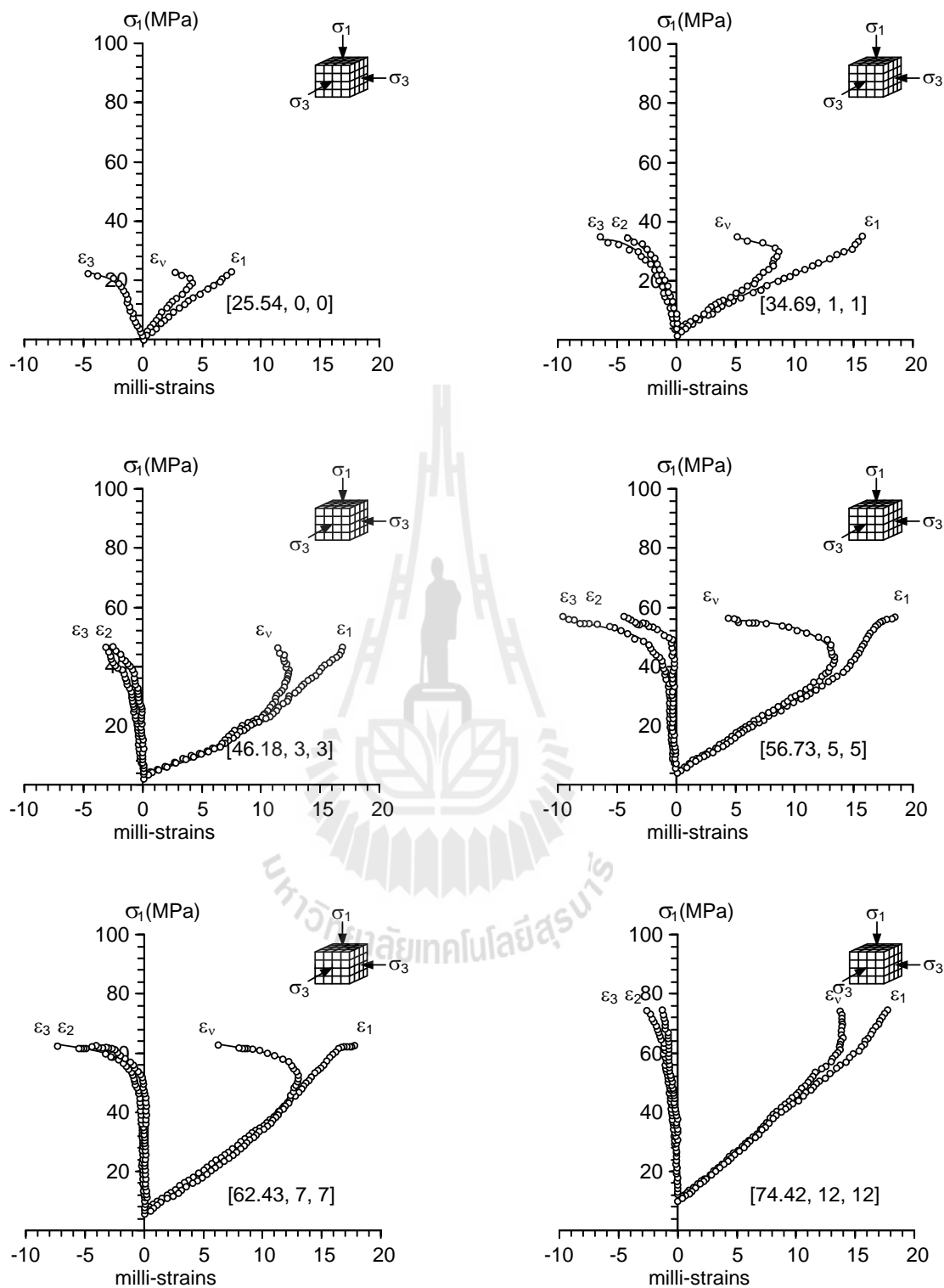


**Figure B.12** Stress-strain curves of 3 joints per set specimens for case C. Numbers in brackets indicate  $[\sigma_1, \sigma_3, \sigma_3]$  at failure in MPa.

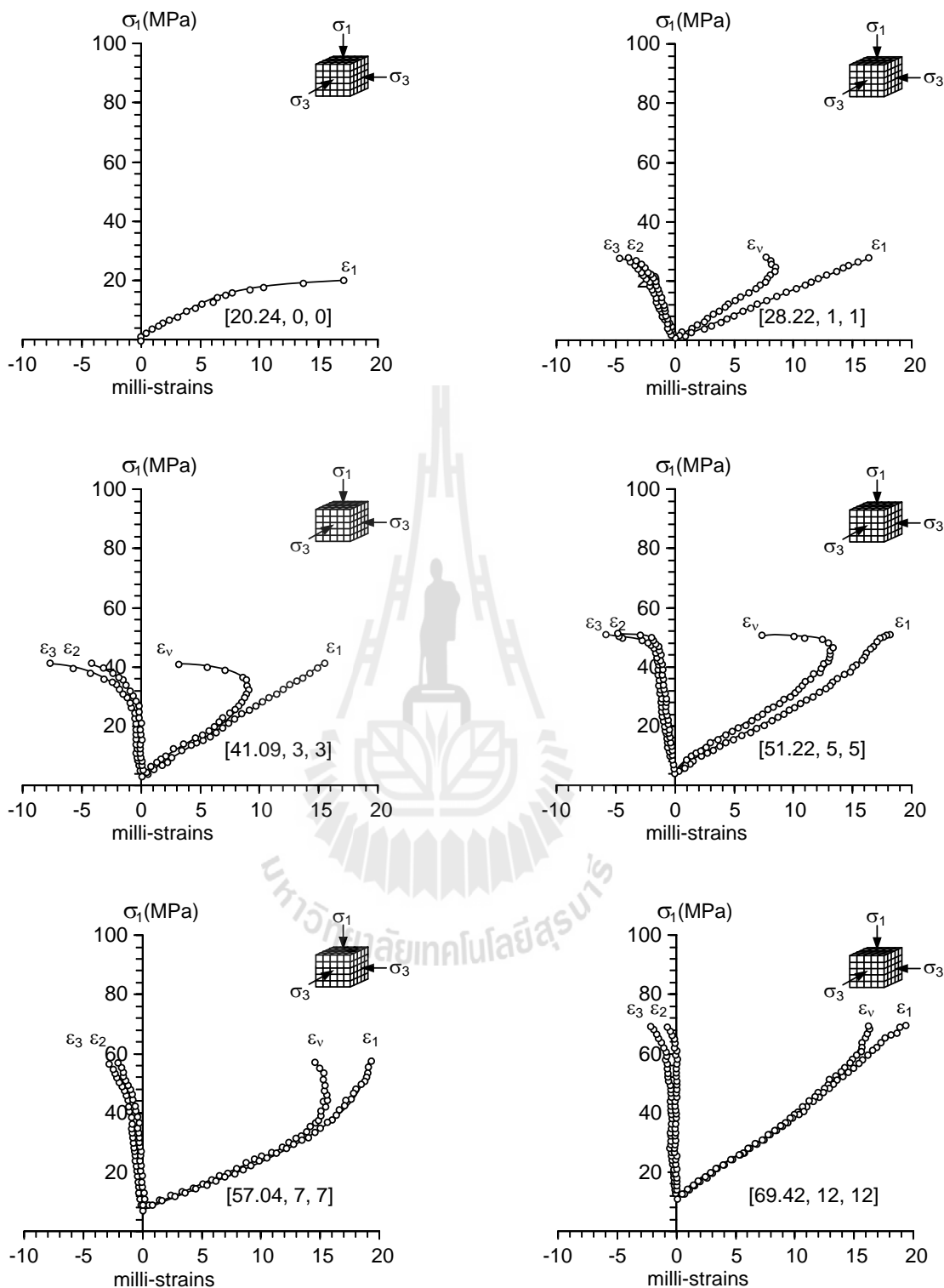


**Figure B.13** Stress-strain curves of 4 joints per set specimens for case C. Numbers in brackets indicate  $[\sigma_1, \sigma_3, \sigma_3]$  at failure in MPa.

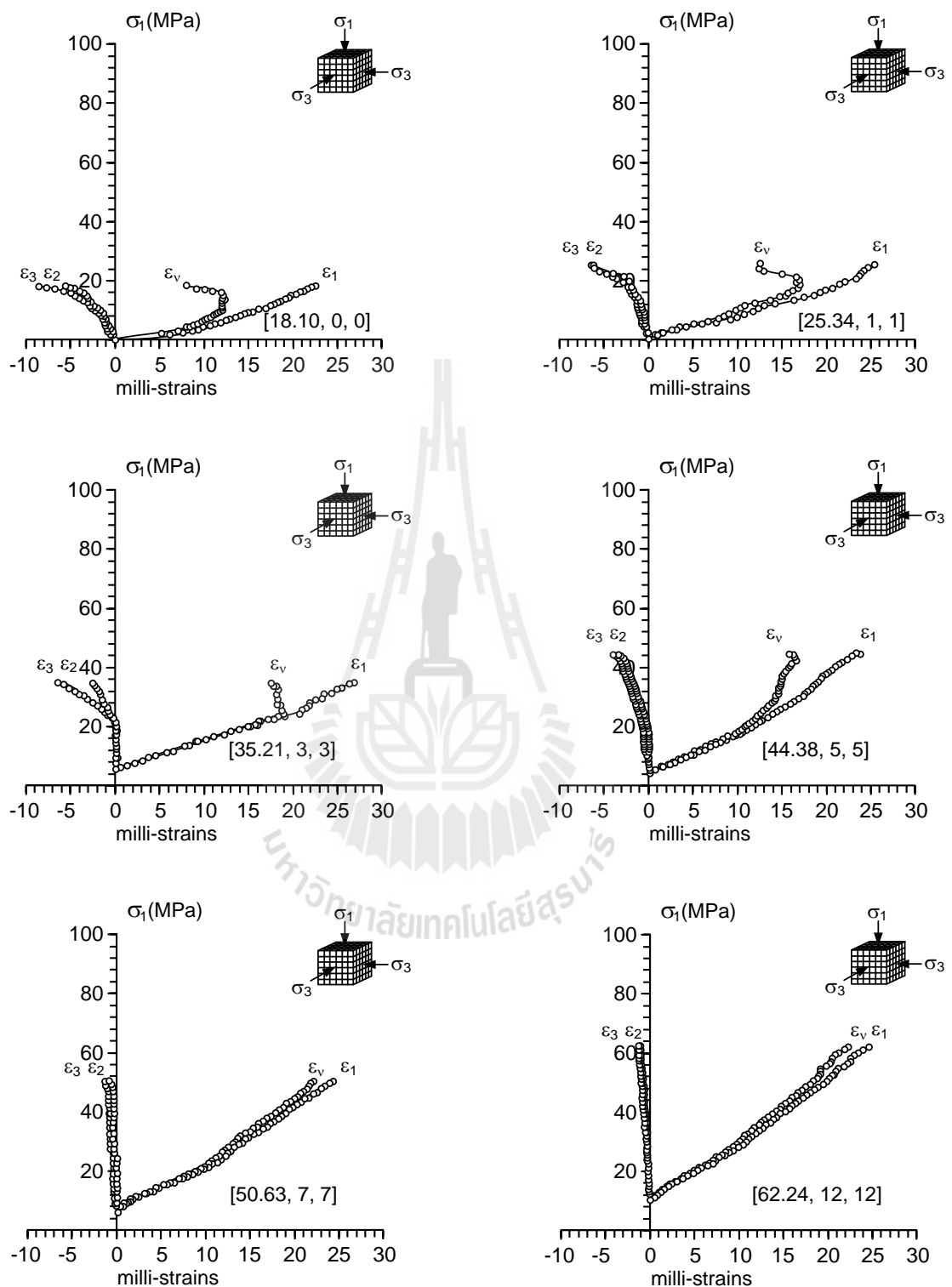


**Figure B.14** Stress-strain curves of 5 joints per set specimens for case C. Numbers in brackets indicate  $[\sigma_1, \sigma_3, \sigma_3]$  at failure in MPa.

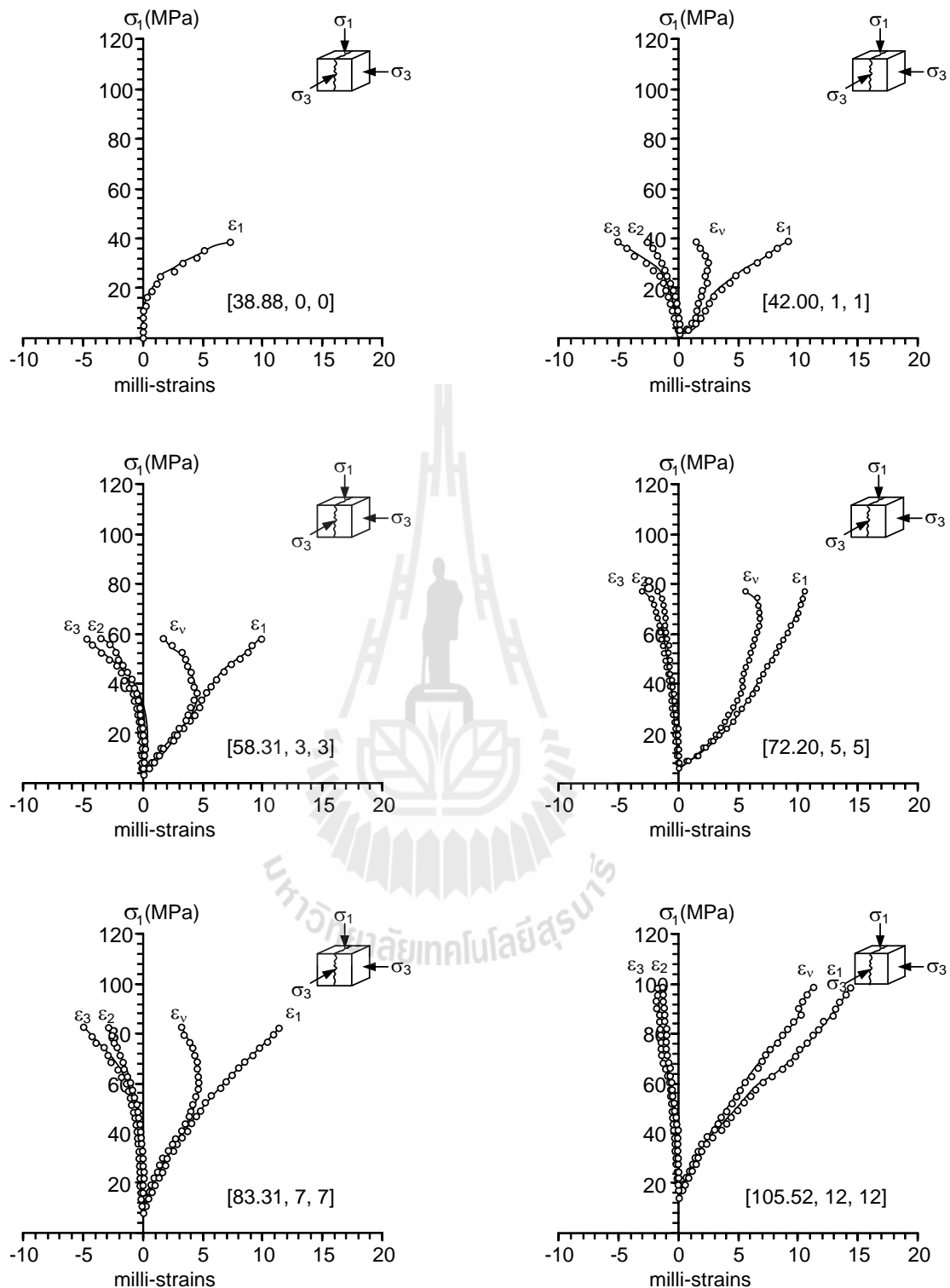


**Figure B.15** Stress-strain curves for case A1 with joints parallel to the major principal stress. Numbers in brackets indicate  $[\sigma_1, \sigma_3, \sigma_3]$  at failure in MPa.

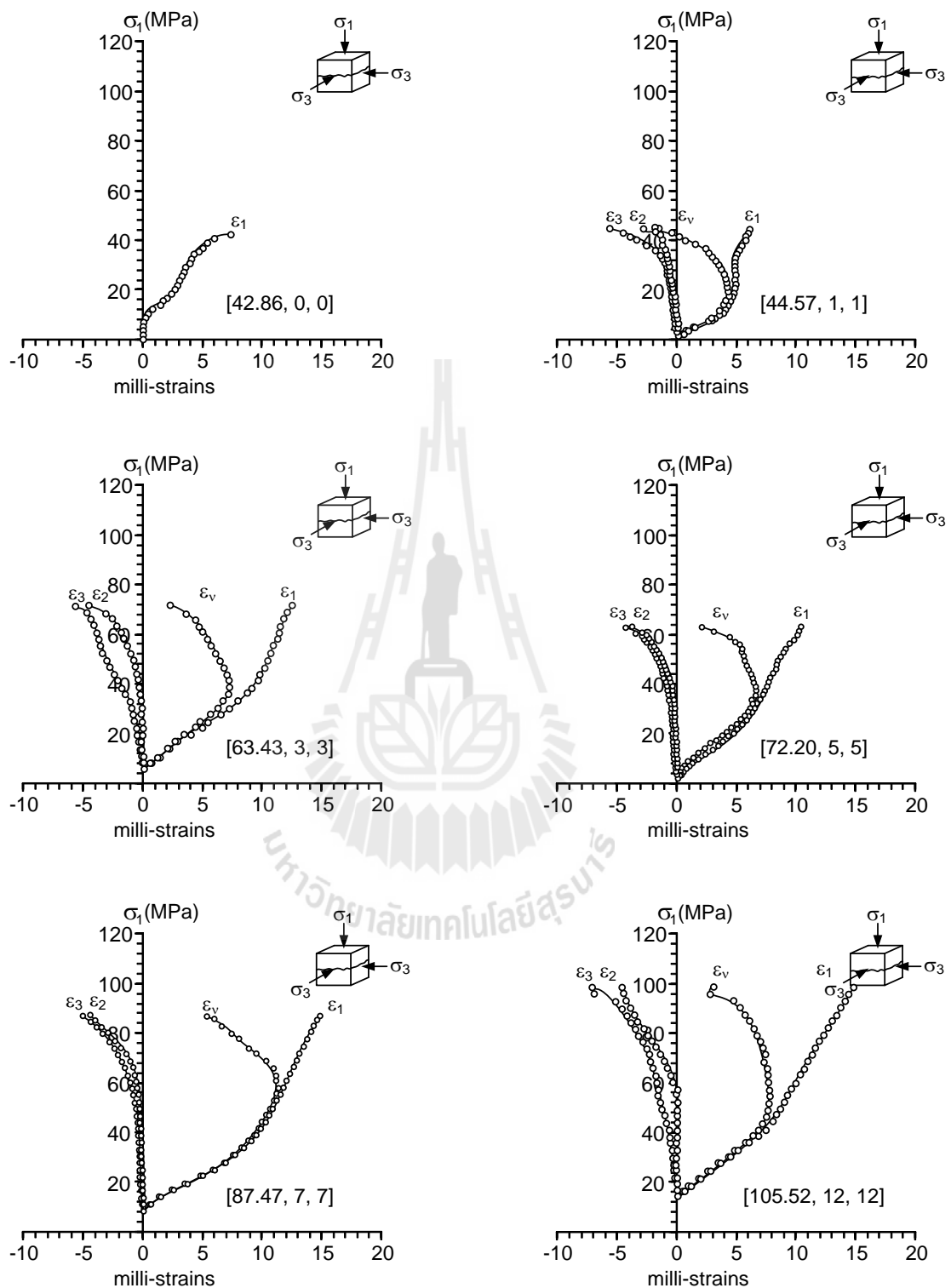


**Figure B.16** Stress-strain curves for case A2 with joints normal to the major principal stress. Numbers in brackets indicate  $[\sigma_1, \sigma_3, \sigma_3]$  at failure in MPa.

## **BIOGRAPHY**

Miss. Saisuree Thaweeboon was born on March 11, 1990 in Chaiyaphum province, Thailand. She received her Bachelor's Degree in Engineering (Geotechnology) from Suranaree University of Technology in 2011. For her post-graduate, she continued to study with Doctor of Philosophy Program in the Geological Engineering Program, Institute of Engineering, Suranaree university of Technology. During graduation, 2012-2014, she was a part time worker in position of research associate at the Geomechanics Research Unit, Institute of Engineering, Suranaree University of Technology.

